Quantum Critical Response at the Onset of Spin Density Wave Order in Two-dimensional Metals

Share Your Story

Quantum critical response at the onset of
spin density wave order in two-dimensional metals

Sean A. Hartnoll, Diego M. Hofman, Max A. Metlitski, and Subir Sachdev

Department of Physics, Harvard University, Cambridge MA 02138

(Dated: May 31, 2011)

Abstract

We study the frequency dependence of the electron self energy and the optical conductivity in a recently developed field theory of the spin density wave quantum phase transition in two-dimensional metals. We focus on the interplay between the Fermi surface 'hot spots' and the remainder of the 'cold' Fermi surface. Scattering of electrons off the fluctuations of the spin density wave order parameter, ϕ, is strongest at the hot spots; we compute the conductivity due to this scattering in a rainbow approximation. We point out the importance of composite operators, built out of products of the primary electron or ϕ fields: these have important effects also away from the hot spots. The simplest composite operator, ϕ^2, leads to non-Fermi liquid behavior on the entire Fermi surface. We also find an intermediate frequency window in which the cold electrons loose their quasiparticle form due to effectively one-dimensional scattering processes. The latter processes are part of umklapp scattering which leads to singular contributions to the optical conductivity at the lowest frequencies at zero temperature.

I. INTRODUCTION

Many experimental developments in the past few years point to the quantum criticality associated with the onset of spin density wave order in metals as a crucial phenomenon in the physics of modern correlated electron materials[1–3]; some recent experimental reports may be found in Refs. 4–7. It is also interesting that such a quantum critical point leads naturally to a mechanism for higher temperature superconductivity with d-wave-like spin-singlet pairing[8–13].

Theoretically, the problem of the quantum criticality of metals has been the focus of much study for several decades[14–18]. In recent work, it is has become clear that the quantum critical theories are strongly coupled in two spatial dimensions[19–21]. A $1/N$ expansion, where N is the number of fermion flavors, can be used to organize perturbation theory and derive renormalization group equations at low orders in $1/N$. However, there are new classes of infrared divergences that appear at higher orders from fermion excitations on the Fermi surface, and these are not suppressed by the powers of $1/N$ expected from counting fermion flavors. Nevertheless, much can be deduced about the nature of the strongly-coupled theory, assuming that the general framework of the field theory survives.

For the onset of spin density wave order in two-dimensional metals, the critical theory[17,21,22] is expressed in terms of fermions at special 'hot spots' on the Fermi surface, which are coupled to the fluctuations of a bosonic field, ϕ, representing the spin density wave order: an explicit action for this theory appears in Section II for the case of commensurate antiferromagnetic ordering at the wavevector (π, π) on the square lattice. We will restrict our attention to this commensurate case in the present paper. The hot spots are identified as points on the Fermi surface which are separated by the spin density wave ordering wavevector (see Fig. 1 below). The fermionic excitations at the hot spots lose their quasiparticle character from strong coupling to ϕ, justifying their prominent role in the critical theory.

The transport properties of metals near a spin density wave transition are also clearly of interest. The early theoretical work[23,24] concluded that these were unlikely to be dominated by the physics of the fermions near the hot spots. Instead, the cold fermions on the remainder of the Fermi surface would 'short-circuit' the electrical current, and so dominate the electrical conductivity. More recently, the quantum critical conductivity of the hot spot fermions has been considered[17] at frequencies or temperatures large enough so that the momentum dependence of the fermion self energy could be neglected. We will re-examine the quantum critical conductivity from ϕ scattering in the present paper, and find significant differences from the earlier results. We also note a recent study of the conductivity at non-zero temperatures on the ordered side of the critical point[25]: we will not address this regime here, and will limit our study to the quantum critical point.

It is important to note that the dichotomy between 'cold' and 'hot' regions of the Fermi surface is intrinsically a weak-coupling concept, and assumes that the fermion damping can be organized in terms of scattering from quanta of ϕ fluctuations. More generally, we should

consider the full set of composite operators of the field theory, made up of multiple primary fermion or ϕ operators, and determine how they relax the current of fermions at all points on the Fermi surface. An example of the importance of such composite operators appeared in the work of Pelissetto *et al.*[26], who examined the simpler problem of the onset of spin density wave order in a d-wave superconductor. Here the low energy fermionic excitations reside only at special 'nodal points' in the Brillouin zone, and these are not generically connected by the ordering wavevector. Thus, the analog of the 'hot spots' is absent in this problem, and one would initially conclude that the nodal fermionic excitations are not strongly scattered by the ϕ fluctuations. However, it was shown that a composite operator linked to the square of ϕ, which measured Ising-nematic ordering, did broaden the nodal fermions, so that the nodal quasiparticles were ultimately only marginally defined near the spin density wave quantum critical point. For this problem, the critical theory was ultimately under good analytic control, allowing accurate determination of the influence of composite operators.

This paper will describe various spectral functions of the spin density wave quantum critical point at zero temperature ($T = 0$). We will address the fermion self energy both on and off the hot spots, and the frequency dependent conductivity $\sigma(\Omega)$ *i.e.* the optical conductivity. However, we will not address the difficult issues associated with $T > 0$, and in particular frequencies with $\Omega < T$. The latter regime is clearly of great experimental importance, but requires an analysis of relaxational processes which we will not undertake. Such finite T transport has been addressed away from the critical point,[27–31] and we hope our critical-point results below at $T = 0$ will serve as a prelude to the corresponding analysis at $T > 0$.

We will begin in Section II by recalling the low energy theory of the spin density wave quantum critical point in two spatial dimensions. In the leading gradient expansion, the fermion energy disperses linearly as a function of wavevector, and so is particle-hole symmetric about the Fermi surface. As a consequence of this particle-hole symmetry and the ordering wavevector being (π, π) the effective action acquires an emergent $(SU(2))^4$ pseudospin symmetry.[21] An important point, reviewed in Section II, is that the electrical current transforms as a vector under this pseudospin symmetry, while the total momentum is a pseudospin scalar. Consequently, when we perturb the system electrically and create an electrical current, the resulting state has vanishing momentum, allowing the electrical current to relax to zero even in the absence of any impurities[32]. Thus umklapp scattering processes are implicitly included within our continuum theory. Provided we regulate the low energy theory in a manner which protects the pseudospin symmetry, the d.c. conductivity will be finite at $T > 0$. This is an attractive feature of the theory allowing, in principle, computation of a T-dependent resistivity which depends upon interactions alone in a non-Fermi liquid.

Section III will begin our computation of the conductivity of the fermions from interactions alone. We will consider electron scattering from ϕ fluctuations. We will do this within the framework of a conventional rainbow approximation, computing self energies and corresponding vertex corrections, while retaining full momentum and frequency dependence. We

3

find that at $T = 0$ the low frequency optical conductivity takes the form,

$$\sigma(\Omega) = C_0 \frac{i}{\Omega + i\epsilon} + C_1 + C_2(-i\Omega)^{r_0} \tag{1.1}$$

where $r_0 > 0$ is a computable exponent whose value depends only upon the Fermi surface geometry, and is specified in Fig. 7. The C_0 term in Eq. (1.1) is the non-dissipative Drude contribution, while the constant C_1 term is the first dissipative correction. These two terms have the same form as in a Fermi liquid with umklapps, and are dominated by the contribution of cold fermions away from the hot spot. Unlike in certain critical theories which do not posses a Fermi surface, the constant C_1 is non-universal. We will explicitly demonstrate that C_1 remains finite in the 'weak coupling' limit of the theory in Section II.

The C_2 term in Eq. (1.1) is the quantum-critical hot spot contribution to the optical conductivity, which includes the contributions of some umklapp processes. Vertex corrections lead to a positive exponent $r_0 > 0$, thus suppressing this term relative to the cold contribution. The result (1.1) is too small to explain the optical conductivity in the hole-doped cuprates[33,34], which has a negative exponent. Our theoretical results here are at variance with earlier treatments[17].

We note a recent numerical study of the optical conductivity near a spin density wave transition[35], which included only the first term in the set of rainbow vertex corrections which we have summed. In this approximation, our analysis shows that the singular term in Eq. (1.1) reduces to $\sigma(\Omega) \sim \log(1/\Omega)$, but the numerical study does not appear to have the dynamic range to observe this.

Section IV will turn our focus to scattering off composite operators, built out of products of the primary fields of the low energy theory of Section II. We will describe the general structure of the fermion self energy corrections due to such operators, and the corresponding contributions to the conductivity. We will also introduce a number of specific composite operators, whose fluctuations will be explored in the subsequent sections. The simplest is the square of the order parameter, ϕ^2, analogs of which were considered in Ref. 26. A second class of composite operators is associated with pairs of fermions: important among them is the Cooper pair operator and a $2k_F$ charge density wave (CDW) operator (which has an Ising-nematic component), fluctuations of which are enhanced near the quantum critical point[13,21]. We emphasize that all these operators are generated directly from our continuum theory in Eq. (2.1), and do not require reference to the underlying lattice model.

Section V will present our results on self energy of the fermions from composite operator scattering, focusing on the previously 'cold' regions of the Fermi surface away from the hot spots. We will find that scattering off the ϕ^2 operator leads to fermion self energy which behaves as $\Omega^{3/2}$, assuming leading order scaling dimensions from the low energy field theory. Thus this simplest composite operator is already sufficient to give non-Fermi liquid behavior over the entire Fermi surface.

Also notable will be the contribution from scattering in the $2k_F$ channel. Here, for

fermions in the vicinity of the hot spots, we find an intermediate energy window in which the Fermi surfaces may be regarded as flat, giving rise to effectively one-dimensional Luttinger liquid-like divergences, which destroy the cold fermionic quasiparticles. Whether such divergences sum up to give a power-law behavior of the electron Green's function, as in a true Luttinger liquid, or lead to an instability is subject to further investigation. At lowest energy, the one-dimensional divergences will be cut off by the Fermi surface curvature, which therefore controls the width of the intermediate frequency regime and the possible crossover to coherent Fermi liquid behavior. We further describe how processes saturating the Fermi surface curvature scale change the low energy scaling dimension of $2k_F$ operators.

Section VI will extend the computations of Section V to the electrical conductivity. For low-momentum scattering processes, the contributions to the optical conductivity are less singular than those to the self energy, because they do not lead to an appreciable degradation of the electrical current. However, this does not apply to the scattering off $2k_F$ fluctuations, which lead to umklapp processes. We estimate that such processes give rise to a power law optical conductivity as $\Omega \to 0$ (at $T = 0$),

$$\delta\sigma(\Omega) \sim (-i\Omega)^{-b_\kappa/(2+b_\kappa)}, \tag{1.2}$$

with a negative exponent controlled by the interplay of one-dimensional divergences (noted in Section V) and Fermi surface curvature. At leading order, we find $b_\kappa = 1$, but higher order renormalization group flows[21] are expected to renormalize this to smaller values, as we will discuss in Section V B. Such $2k_F$ umklapp contributions are a promising avenue for understanding the optical conductivity data,[33,34] given the negative exponent in Eq. (1.2).

II. LOW ENERGY THEORY

Our starting point will be the following (imaginary time) low energy effective field theory of fermionic excitations living at pairs of hot spots and interacting via bosonic fluctuations of a (π, π) spin density wave[21]

$$\begin{aligned}
\mathcal{L} &= \frac{N}{2c^2}(\partial_\tau \phi)^2 + \frac{N}{2}\left(\vec{\partial}\phi\right)^2 + \frac{Nu}{4}(\phi^2)^2 \\
&\quad + \sum_{a,\ell} \frac{1}{2}\Psi_a^{\dagger\ell}\left(\partial_\tau - i\vec{v}_a^\ell \cdot \vec{\partial}\right)\Psi_a^\ell + \sum_\ell \frac{\lambda}{2}\phi \cdot \left(\Psi_1^{\dagger\ell}\tau\Psi_2^\ell + \Psi_2^{\dagger\ell}\tau\Psi_1^\ell\right).
\end{aligned} \tag{2.1}$$

In this Lagrangian, ϕ is a three component boson and each Ψ_a^ℓ is a four component spinor. The mass of the boson has be tuned to zero. The label ℓ runs over the four pairs of hot spots while a runs over the two patches of each pair. The geometry of the Fermi surface and hot spots is shown in Fig. 1. The four components of the spinor may be labeled by the pair of two component indices $\{\sigma, \alpha\}$, where σ is a spin index and α is a particle-hole index. We

5

have suppressed these indices in the above Lagrangian. The Pauli matrices τ act on the spin indices. Also suppressed is a fermion flavor index running from 1 to N. All interactions are diagonal in flavor. The spatial derivatives $\vec{\partial}$ act in two-dimensional space with coordinates $\{x, y\}$ and $\vec{v}_a^\ell$ are the Fermi velocities of each hot spot. In terms of the fermions illustrated in Figs. 1 and 2, the fermions Ψ_a^ℓ are given by

$$\Psi_a^\ell = \begin{pmatrix} \psi_a^\ell \\ i\tau^2 \psi_a^{\ell\dagger} \end{pmatrix} \tag{2.2}$$

so that they satisfy the hermiticity condition

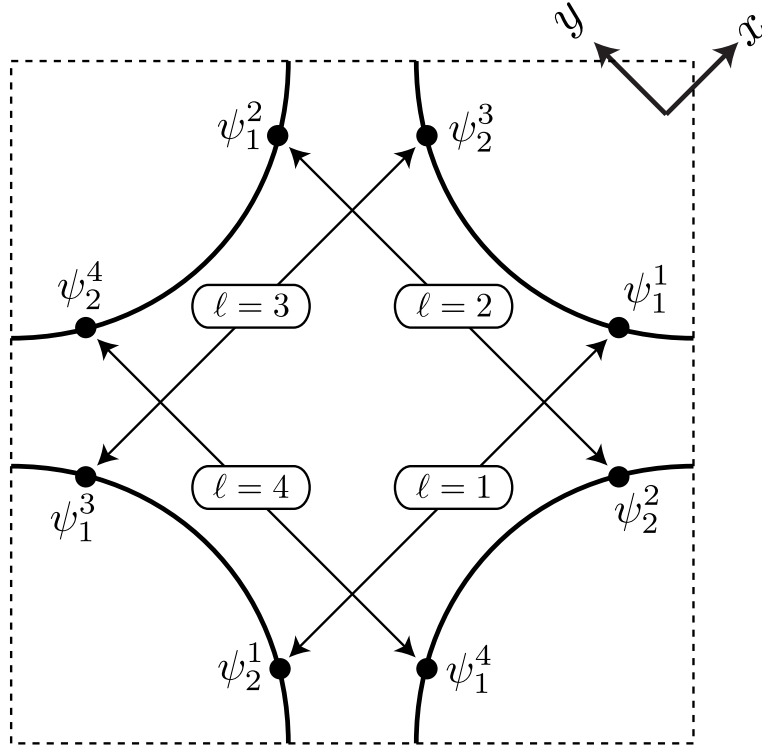$$i\tau^2 \begin{pmatrix} 0 & -1 \\ 1 & 0 \end{pmatrix} \Psi_a^\ell = \Psi_a^{\ell*}. \tag{2.3}$$

FIG. 1: The four pairs of hot spots and locations of the fermion fields Ψ_a^ℓ, related to the fields in the figure by Eq. (2.2).

The advantage of writing the action in terms of four component fermions is that it makes manifest an emergent $(SU(2))^4$ 'pseudospin' symmetry[21]. For each ℓ we have an $SU(2)$ symmetry with the generators T_ℓ^m acting as

$$SU(2)_\ell : \quad T_\ell^m \Psi_a^\ell = i\sigma^m \Psi_a^\ell , \tag{2.4}$$
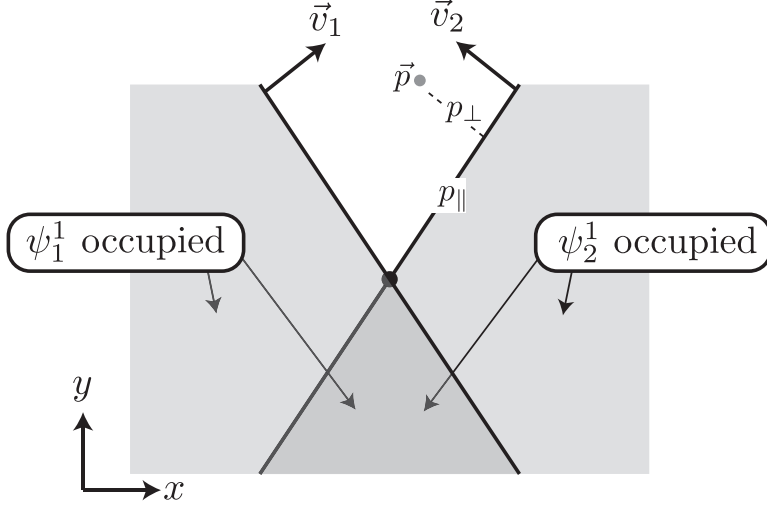
FIG. 2: (From Ref. 13) Configuration of the $\ell = 1$ pair of hot spots, with the momenta of the fermion fields measured from the common hot spot at $\vec{k} = 0$, indicated by the dark filled circle. The Fermi velocities $\vec{v}_{1,2}$ of the $\psi_{1,2}$ fermions are indicated. The momentum components of the $\psi_2^1(\vec{p})$ fermion parallel ($p_\parallel$) and orthogonal ($p_\perp$) to the Fermi surface are indicated.

and leaving all other fields invariant. Here σ^m are Pauli matrices acting on the particle-hole indices of the spinor. The symmetry therefore has the following charge densities and currents

$$J_{\ell\tau}^m = \frac{i}{2} \sum_a \Psi_a^{\dagger\ell} \sigma^m \Psi_a^\ell, \qquad \vec{J}_\ell^m = \frac{1}{2} \sum_a \vec{v}_a^\ell \Psi_a^{\dagger\ell} \sigma^m \Psi_a^\ell. \tag{2.5}$$

The diagonal subgroup of each $SU(2)$ describes the conservation of fermion number at each pair of hot spots. Higher order kinetic terms in the action describing e.g. the curvature of the Fermi surface will break the $SU(2)$ symmetries down to this subgroup. These and other symmetry breaking terms are irrelevant in the low energy scaling limit.

The Fermi velocities at one pair of hot spots can be parameterised by

$$\vec{v}_1^{\ell=1} = (v_x, v_y), \qquad \vec{v}_2^{\ell=1} = (-v_x, v_y). \tag{2.6}$$

The remaining velocities are given by 90 degree rotations

$$\vec{v}_a^\ell = R_{\pi/2}^{\ell-1} \vec{v}_a^{\ell=1}. \tag{2.7}$$

Later it will also be convenient to introduce the ratio and the modulus

$$\alpha \equiv \tan\varphi \equiv \frac{v_y}{v_x}, \qquad v = |\vec{v}|. \tag{2.8}$$

Here $0 < 2\varphi < \pi$ is the angle between the Fermi surfaces at the hot spot.

7

The fermion and boson propagators are constrained by both the pseudospin symmetry and by the form of the scaling limit. The symmetry requires the fermion propagators to take the form

$$\langle \Psi^{\ell}_{a\sigma\alpha}(x)\Psi^{\ell'\dagger}_{b\sigma'\beta}(x')\rangle = -\delta^{\ell\ell'}\delta_{ab}\delta_{\sigma\sigma'}\delta_{\alpha\beta}G^{\ell}_{a}(x-x')\,. \tag{2.9}$$

In the low energy scaling limit, the fermion and boson two point functions are characterised by the dynamical critical exponent z and anomalous dimensions η_{ψ} and η_{ϕ}. Thus

$$G^{-1}(\omega,\vec{p}) = p^{z/2-\eta_{\psi}}\widetilde{G}^{-1}\left(\frac{\omega}{p^z},\hat{p}\right)\,, \tag{2.10}$$

$$D^{-1}(\omega,\vec{p}) = p^{2-\eta_{\phi}}\widetilde{D}^{-1}\left(\frac{\omega}{p^z},\hat{p}\right)\,. \tag{2.11}$$

Here $p = |\vec{p}|$. Much of the interesting physics we will describe below is due to fermions that are within the scaling regime, but far from the hot spots. If $p_{\perp}$ is the distance to the Fermi surface and $p_{\parallel}$ the distance along the Fermi surface to the hot spot, then this condition requires $p_{\perp}, \omega^{1/z} \ll p_{\parallel}$. In this 'lukewarm' region one expects the quasiparticle form[1]

$$G(\omega,\vec{p}) = \frac{Z(p_{\parallel})}{i\omega - v_F(p_{\parallel})p_{\perp}} \qquad , \qquad (p_{\perp}, \omega^{1/z} \ll p_{\parallel})\,, \tag{2.12}$$

with

$$v_F(p_{\parallel}) \propto p_{\parallel}^{z-1}\,, \qquad Z(p_{\parallel}) \propto p_{\parallel}^{z/2+\eta_{\psi}}\,. \tag{2.13}$$

Working in the rainbow approximation and taking the limit $N \to \infty$ one finds that $z = 2$ and $\eta_{\psi} = \eta_{\phi} = 0$. The explicit forms of the correlators were obtained in Refs. 17,21. The boson has

$$D^{-1}(\omega,\vec{p}) = N\left(\gamma|\omega| + \vec{p}^{\,2}\right)\,, \tag{2.14}$$

with

$$\gamma = \frac{4\lambda^2}{2\pi v_x v_y}\,, \tag{2.15}$$

while the fermions have

$$G_a^{-1}(\omega,\vec{p}) = i\omega - \vec{v}_a\cdot\vec{p} + \frac{1}{N}\frac{3v\sin 2\varphi}{8}i\,\mathrm{sgn}(\omega)\left(\sqrt{\gamma|\omega| + (\hat{v}_{\bar{a}}\cdot\vec{p})^2} - |\hat{v}_{\bar{a}}\cdot\vec{p}|\right)\,. \tag{2.16}$$

Here, $\bar{1} = 2$ and $\bar{2} = 1$ and we have suppressed the hot spot index ℓ. In the expression (2.16) we have not explicitly written the real part of the self energy which renormalises the velocities v_x and v_y. Note that the tree level analytic term $i\omega$ in the propagator is suppressed at low energy compared to the dynamically generated self energy. We have kept the tree level term here as a UV regulator as will be discussed in more detail below. For future

---

[1] A possible violation of the quasiparticle form in Eqs. (2.12), (2.13) will be discussed in section V B.

reference, it will be convenient to introduce the momentum scale,

$$\Lambda = \frac{3v\gamma \sin 2\varphi}{16N} = \frac{3\lambda^2}{4\pi N v} \tag{2.17}$$

and the associated energy scale $\Lambda_\omega = \Lambda^2/\gamma$. Λ and Λ_ω are the momentum and energy scales at which the dynamically generated self energy becomes comparable to the tree level analytic term $i\omega$. The numerical factors in Eq. (2.17) are inserted for future convenience.

We may also represent Eq. (2.16) as

$$G^{-1}(\omega, \vec{p}) = i\omega - v p_\perp + \frac{1}{N}\frac{3v \sin 2\varphi}{8} i \, \mathrm{sgn}(\omega) \left(\sqrt{\gamma|\omega| + \left(\hat{v}_1 \times \hat{v}_2 \, p_\parallel \right)^2} - \left| \hat{v}_1 \times \hat{v}_2 \, p_\parallel \right| \right). \tag{2.18}$$

Here again $p_\perp = \hat{v} \cdot \vec{p}$ is the momentum in the direction orthogonal to the Fermi surface while $p_\parallel$ is the distance to the hot spot and is the momentum in the direction orthogonal to $\hat{v}$. Furthermore, assuming for concreteness that the propagator in question is for the Ψ_1 fermions, in the self energy we have approximated

$$\hat{v}_2 \cdot \vec{p} \quad \rightarrow \quad |\hat{v}_1 \times \hat{v}_2| \, p_\parallel = \sin 2\varphi \, p_\parallel \,. \tag{2.19}$$

In general $\hat{v}_2$ is not orthogonal to $\vec{v}_1$ and so this replacement is not exact. However, the dependence on the $\vec{v}_1$ component of the momentum in the self energy is subleading in powers of N in the full propagator compared to the tree-level $v p_\perp$ dependence in (2.18). Thus we can and have projected out the component of $\hat{v}_2$ parallel to $\hat{v}_1$ for the purposes of this paper, see e.g. the computations in Ref. 21.

The correlators (2.14) and (2.18) will be used at various points in the remainder of this paper. From them one can read off the constants of proportionality (2.13) in the lukewarm region. Note that in the present approximation, the lukewarm fermions have a Fermi liquid like ω^2 damping rate,

$$G(\omega, \vec{p}) = \frac{Z(p_\parallel)}{i\omega - v_F(p_\parallel) p_\perp - i a(p_\parallel)\omega^2 \mathrm{sgn}(\omega)} \quad , \quad (p_\perp, \sqrt{\gamma\omega} \ll p_\parallel) \,, \tag{2.20}$$

with $a(p_\parallel) \sim p_\parallel^{-2}$. We will demonstrate in Sec. V that scattering off composite operators qualitatively modifies the damping rate of cold (and hence also lukewarm) fermions. Such corrections, however, appear only at higher order in $1/N$.

We should note that the large N expansion used to obtain the propagators (2.14) and (2.18) breaks down both at sufficiently low energy scales and at higher loop order: The RG flow equations at leading nontrivial order in N flow to an $\alpha = 0$ IR fixed point, at which Fermi surfaces at each hot spot pair are parallel[21]. At sufficiently low energies the anomalous dimensions become order one and the large N expansion breaks down. The RG flow can be controlled only in the regime $1/\sqrt{N} \ll \alpha \ll 1$. In this regime all anomalous

dimensions acquire small nonzero corrections. In particular $z \neq 2$. At higher loop order the large N expansion breaks down for the reasons first identified in Ref. 19 for a 2+1 dimensional Fermi surface coupled to a gauge field. Loops involving fermions on the Fermi surface give extra powers of N that disrupt the naïve large N scaling of diagrams. We will essentially ignore this last complication; perhaps the expansion can be controlled using a generalization of the methods developed in Refs. 36–38. Alternatively, a strong coupling approach to metallic criticality may be possible using the holographic correspondence, along the lines of e.g. Refs. 39–41.

III.   HOT SPOT CONDUCTIVITY: RAINBOW APPROXIMATION

As discussed in Section I, we first consider the conductivity due to scattering off the primary field, ϕ. This scattering is strongest at the hot spots. As shown in Ref. 21, the hot spot theory remains strongly coupled even when one takes the number of fermion flavors $N \to \infty$. In this section, we treat the hot spot theory in the 'rainbow' approximation. Furthermore, we take the limit $N \to \infty$ in order to simplify the calculations. A similar approach was considered previously in Ref. 17. A key difference with Ref. 17 is that we take into account the rainbow corrections to the current vertex, which are necessary to satisfy the Ward identity associated with charge conservation.

The four $SU(2)$ currents of the theory (2.5) necessarily have orthogonal correlators

$$- \int d^3x \langle J_\mu^{\ell m}(z) J_\nu^{\ell' n}(0) \rangle e^{-i\vec{q}\vec{x}} e^{i\omega\tau} \equiv \delta^{mn} \delta^{\ell\ell'} \Pi_{\mu\nu}^\ell(\omega, \vec{q}) \,. \tag{3.1}$$

Here μ, ν are space-time indices. We focus on the electrical conductivity which is related to the $m = 3$ component of the $SU(2)$ current correlator (3.1) summed over all of the hot spots. (From here on, all the pseudospin indices m, n are set to 3, unless otherwise noted.) Specifically, the electrical conductivity at real frequency Ω and vanishing momentum is

$$\sigma_{ij}(\Omega) = \left. \frac{\sum_\ell \Pi_{ij}^\ell(\omega, 0)}{\omega} \right|_{i\omega = \Omega + i\epsilon} . \tag{3.2}$$

In relating the conductivity and current correlator in this way, we are neglecting the tadpole or 'diamagnetic' term, which gives rise to a δ-function at zero frequency in the real part of the conductivity and a $1/\Omega$ behavior in the imaginary part. Such a contribution is always present at zero temperature. Below, we will be interested in corrections to this behavior.

It will also be convenient for our purposes to define the current vertex $\Gamma_{\mu a}^\ell$

$$\int d^3z d^3x \langle J_\mu^\ell(z) \psi_{\sigma a}^{\ell'}(x) \psi_{\sigma' b}^{\dagger \ell'}(0) \rangle e^{-iqz} e^{-ipx} = \delta_{\sigma\sigma'} \delta_{ab} \delta^{\ell\ell'} \Gamma_{\mu a}^\ell(q, p) G_a^\ell(p) G_a^\ell(p+q) \tag{3.3}$$

Note that the correlator vanishes for $\ell \neq \ell'$ by pseudospin symmetry. The diagonal subgroup of the $SU(2)$ symmetry at each hot spot pair implies the following Ward identities,

$$-q_\tau \Pi^\ell_{\tau\nu}(q) + q_i \Pi^\ell_{i\nu}(q) = 0 \tag{3.4}$$

$$-q_\tau \Gamma^\ell_{\tau a}(q, p) + q_i \Gamma^\ell_{ia}(q, p) = G^\ell_a(p)^{-1} - G^\ell_a(p+q)^{-1} \tag{3.5}$$

In particular, the density-density correlation function at zero wavevector vanishes,

$$\Pi^\ell_{\tau\tau}(\omega, 0) = 0 \tag{3.6}$$

We concentrate below on the hot spot pair with $\ell = 1$. Observe that,

$$
\begin{aligned}
J^1_\tau &= i(\psi^{1\dagger}_1 \psi^1_1 + \psi^{1\dagger}_2 \psi^1_2) \\
J^1_x &= v_x(\psi^{1\dagger}_1 \psi^1_1 - \psi^{1\dagger}_2 \psi^1_2) \\
J^1_y &= v_y(\psi^{1\dagger}_1 \psi^1_1 + \psi^{1\dagger}_2 \psi^1_2)
\end{aligned}
\tag{3.7}
$$

We see that J^1_y is proportional to J^1_τ. Therefore, $\Pi^1_{yy}(\omega, 0) = 0$. Moreover, $\Pi^1_{xy}(\omega, 0) = 0$ by reflection symmetry, $x \to -x$. Thus, the only non-trivial element of the conductivity tensor at zero wavevector is Π^1_{xx}.

To compute Π^1_{xx}, we first evaluate the corresponding current vertex Γ^1_{xa}. For briefness, we drop the hot spot index below; $\ell = 1$ is assumed unless otherwise noted. It is convenient to define the symmetric and antisymmetric vertices $\Gamma^\pm_a$ as

$$\int d^3z d^3x \langle ((\psi^\dagger_1 \psi_1 \pm \psi^\dagger_2 \psi_2)(z) \psi_{\sigma a}(x) \psi^\dagger_{\sigma' b}(0) \rangle e^{-iqz} e^{-ipx} = \delta_{\sigma\sigma'} \delta_{ab} \Gamma^\pm_a(q, p) G_a(p) G_a(p+q) \tag{3.8}$$

Then, $\Gamma_{\tau a} = i\Gamma^+_a$, $\Gamma_{xa} = v_x \Gamma^-_a$ and $\Gamma_{ya} = v_y \Gamma^+_a$ and the Ward identity (3.5) reads,

$$(-iq_\tau + v_y q_y)\Gamma^+_a(q, p) + v_x q_x \Gamma^-_a(q, p) = G^{-1}_a(p) - G^{-1}_a(p+q) \tag{3.9}$$

Also, we may express Π_{xx} as,

$$\Pi_{xx}(q) = 2N v_x^2 \sum_a (-1)^{a+1} \int \frac{d^3p}{(2\pi)^3} \Gamma^-_a(q, p) G_a(p) G_a(p+q) \tag{3.10}$$

We will treat the fermion propagator and the current vertex in the rainbow approximation. The rainbow approximation for the boson and fermion propagators amounts to performing a self-consistent Hartree-Fock + RPA calculation, see Fig. 3, and gives the following integral equations,

$$(G^\ell_a(p))^{-1} = i\omega - \vec{v}^\ell_a \cdot \vec{p} - \Sigma^\ell_a(p) \tag{3.11}$$

11
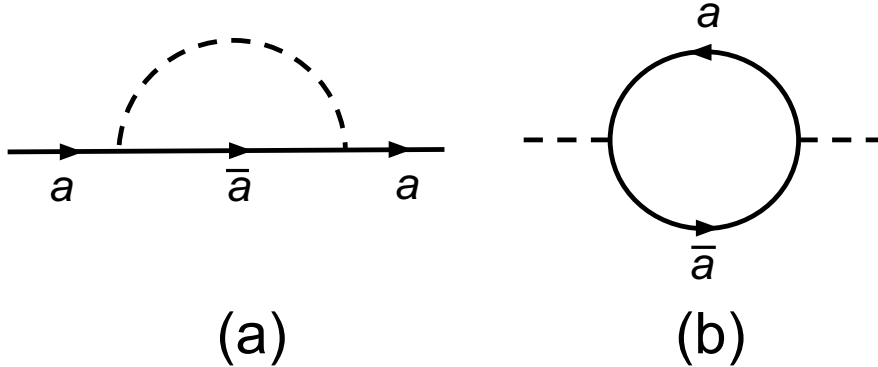
FIG. 3: (a) Fermion and (b) boson self-energies in the rainbow approximation. Solid lines are fermion Green's functions, while dashed lines are ϕ Green's functions. All internal lines are full self-consistent propagators. In this section we are dropping the hot-spot index ℓ, and so $\psi_1 \equiv \psi_1^1$ and $\psi_{\bar{1}} \equiv \psi_2^1$.

$$D^{-1}(q) = N\vec{q}^2 + \Pi(q) \tag{3.12}$$

$$\Sigma_a^\ell(p) = 3\lambda^2 \int \frac{d^3l}{(2\pi)^3} G_{\bar{a}}^\ell(p+l)D(l) \tag{3.13}$$

$$\Pi(q) = 2N\lambda^2 \sum_{\ell,a} \int \frac{d^3l}{(2\pi)^3} G_a^\ell(l+q)G_{\bar{a}}^\ell(l) \tag{3.14}$$

The solution to these integral equations in the limit $N \to \infty$ is given in Eqs. 2.14, 2.16.[17]

We would like to treat the current vertex at the same level of approximation as the boson and fermion propagators. This can be achieved by inserting the bare current vertex into every bare fermion propagator which appears when Eqs. (3.11)-(3.14) are iterated. The resulting dressed current vertex satisfies an integral equation which is diagramatically shown in Fig. 4. We note that the two 'Aslamazov-Larkin'-type diagrams in Figs. 4 c) and d) cancel with each other due to the pseudospin symmetry. Indeed, the triangle portion of the two diagrams involves the correlator $\langle J_\mu^\ell \phi\phi \rangle$. The current J_μ^ℓ transforms as a pseudospin vector, while the field ϕ transforms as a pseudospin scalar, therefore, $\langle J_\mu^\ell \phi\phi \rangle = 0$. Thus, the 'Aslamazov-Larkin' diagrams in the particle-hole Fig. 4 c) and particle-particle Fig. 4 d) channels cancel with each other and we are left only with the rainbow corrections in Fig. 4 b).

We note that the presence of umklapp processes in our theory is secretely hidden in the fact that the Aslamazov-Larkin diagrams cancel with each other and so can be ignored. Indeed, our theory allows for both types of scattering shown in Fig. 5. (For simplicity, we temporarily consider processes involving the hot spot pair $\ell = 1$ only.) The process in Fig. 5a) is a 'regular' scattering process, which conserves not only the electron momentum, but also the electron current. If only such processes were allowed, the optical conductivity
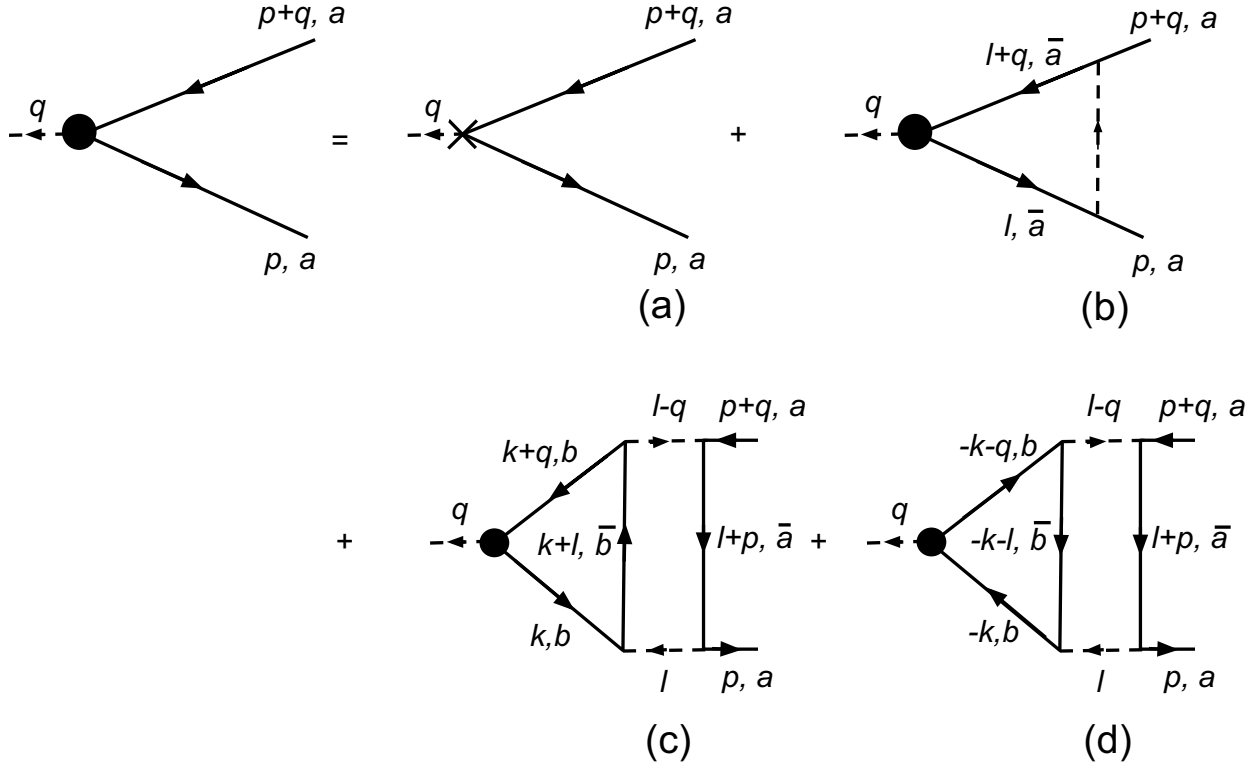
FIG. 4: Diagrams for the current vertex $\Gamma_a^{\pm}$ in the rainbow approximation. The cross denotes the bare vertex and the solid circle, the full vertex. The 'Aslamazov-Larkin' type diagrams in (c) and (d) cancel against each other due to pseudospin symmetry. As in Fig. 3, $\psi_1 \equiv \psi_1^1$ and $\psi_{\bar{1}} \equiv \psi_2^1$.

at finite frequency would vanish.[2] On the other hand, the processes in Fig. 5b) (see also Fig. 6) are 'umklapp' scattering processes, which flip the x component of the electron current - hence, a finite optical conductivity is expected. At the level of the rainbow approximation, the main difference between the two cases is the following. If only the regular processes in Fig. 5a) are allowed, then the index b of the Aslamazov-Larkin diagram in the particle-hole channel, Fig. 4 c), is constrained to be $b = a$, while in the particle-particle channel, Fig. 4 d), $b = \bar{a}$. Hence, there is no longer a cancellation between the two Aslamazov-Larkin diagrams. Instead, in the umklapp-free case, the Aslamazov-Larkin diagrams, Fig. 4 c),d), and the rainbow diagram, Fig. 4 b) would conspire to give a vanishing optical conductivity. On the other hand, in the case when umklapps are allowed, this conspiracy between the Aslamazov-Larkin and rainbow graphs is broken. The pseudospin symmetry technically simplifies the calculation, allowing one to ignore the Aslamazov-Larkin diagrams alltogether,

---

[2] In principle, the electron current is not strictly conserved by 'regular' scattering processes once a finite Fermi surface curvature is accounted for in the definition of the electrical current. However, the resulting corrections to the optical conductivity are expected to be of higher order than those due to umklapp processes and won't be considered in this section.

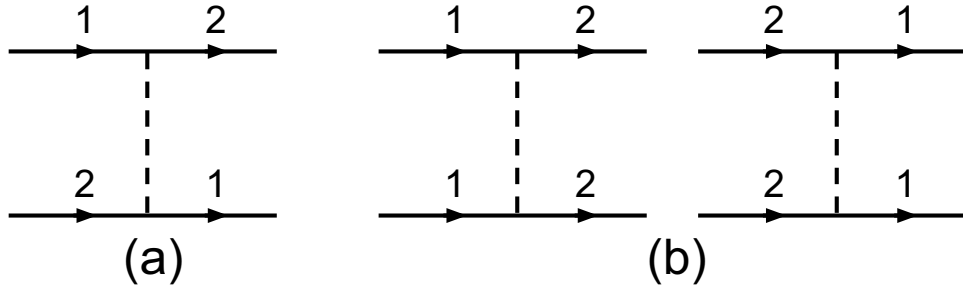and the remaining rainbow graphs give a finite optical conductivity as we will explicitly verify below.

FIG. 5: Scattering processes involving fermions from the hot spot pair $\ell = 1$. The diagram in (a) corresponds to 'regular' scattering, which conserves the current. The two diagrams in (b) correspond to 'umklapp' scattering, which conserves the lattice momentum but not the current. Note that $\psi_2 \equiv \psi_{\bar{1}}$.

Note, finally, that although for illustrative purposes we have limited the above discussion to hot spot pair $\ell = 1$ only, in fact, umklapp processes involving different pairs of hot spots also contribute to the optical conductivity. At the level of the rainbow approximation, all hot spot pairs contribute to the boson polarization in Fig. 3 b), and hence scattering between hot spots with different ℓ is accounted for in the fermion self energy Fig. 3 a). The umklapp nature of this scattering is again hidden in the fact that it contributes to the fermion self energy, but not directly to the current vertex corrections. Indeed, the rainbow diagrams in Fig. 4 b) involve only one pair of hot spots, while the Aslamazov-Larkin diagrams Figs. 4 c), d) cancel for fermions from any hot spot ℓ' running in the internal loop.

With the above remarks in mind, to obtain the current vertex we have to sum the series of rainbow diagrams in Fig. 4 b). This sum obeys the following integral equation,

$$
\Gamma_a^+(q,p) = 1 + 3\lambda^2 \int \frac{d^3l}{(2\pi)^3} G_{\bar{a}}(l) G_{\bar{a}}(l+q) D(l-p) \Gamma_{\bar{a}}^+(\omega, l)
$$

$$
\Gamma_a^-(q,p) = (-1)^{a+1} + 3\lambda^2 \int \frac{d^3l}{(2\pi)^3} G_{\bar{a}}(l) G_{\bar{a}}(l+q) D(l-p) \Gamma_{\bar{a}}^-(q, l) \tag{3.15}
$$

A detailed analysis of Eqs. (3.15) is performed in Appendix A. We summarise the results of this analysis below.

Let us set $q = (\omega, 0)$ and without loss of generality assume $\omega > 0$. It is convenient to change variables to $l_a = \hat{v}_a \cdot \vec{l}$. As shown in Appendix A, in the limit $N = \infty$, to determine $\Gamma_a^\pm(\omega, p)$ for all p it is sufficient to know its behavior for $p_a = 0$, i.e. we need to find the current vertex with external momentum on the Fermi surface. Moreover, introducing the
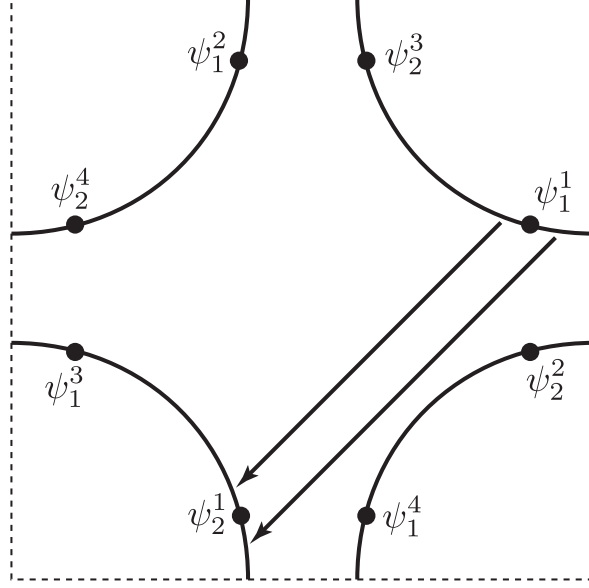
FIG. 6: Umklapp scattering processes in Fig. 5b. Such processes degrade the electric current and lead to a finite optical conductivity

variable $\nu = p_\tau + \omega$ we can restrict our attention to $0 < \nu < \omega$. Thus, definining,

$$\Gamma_a^+(\omega, \nu, p_a = 0, p_{\bar{a}} = p) \equiv \Gamma^+(\omega, \nu, p) \qquad (3.16)$$

$$\Gamma_a^-(\omega, \nu, p_a = 0, p_{\bar{a}} = p) \equiv (-1)^{a+1}\Gamma^-(\omega, \nu, p) \qquad (3.17)$$

we obtain, see Appendix A for details,

$$\Gamma^\pm(\omega, \nu, p) = 1 \pm 2\pi\gamma \sin 2\varphi \int \frac{dl}{2\pi} \int_0^\omega \frac{d\nu'}{2\pi} \frac{1}{\sqrt{\gamma\nu' + l^2} + \sqrt{\gamma(\omega - \nu') + l^2} - 2|l| + \frac{\gamma\omega}{2\Lambda}}$$

$$\frac{1}{(l - p\cos 2\varphi)^2 + \sin^2 2\varphi(\gamma|\nu' - \nu| + p^2)} \Gamma^\pm(\omega, \nu', l) \qquad (3.18)$$

where the UV momentum scale Λ is given by Eq. (2.17).

Let us check the consistency of Eq. (3.18) with the Ward identity. From Eq. (3.9) at $\vec{q} = 0$,

$$\Gamma_a^+(\omega, p) = 1 + \frac{3v \sin 2\varphi}{8N\omega} \left(\text{sgn}(p_\tau + \omega)(\sqrt{\gamma|p_\tau + \omega| + p_{\bar{a}}^2} - |p_{\bar{a}}|) - \text{sgn}(p_\tau)(\sqrt{\gamma|p_\tau| + p_{\bar{a}}^2} - |p_{\bar{a}}|) \right) \qquad (3.19)$$

which satisfies Eq. (3.18). Note that at low momentum $p \ll \Lambda$ and frequency $\omega \ll \Lambda_\omega$, the second term in Eq. (3.19) dominates over the bare vertex $\Gamma^{+,0} = 1$, so that $\Gamma^+(\omega, \nu, p)$ can

be written in the scaling form,

$$\Gamma^+(\omega, \nu, p) \propto \left(\frac{\omega}{\Lambda_\omega} \right)^{-1/2} \gamma^+ \left(\frac{\nu}{\omega}, \frac{p}{\sqrt{\gamma\omega}} \right) \tag{3.20}$$

with

$$\gamma^+(x, y) = \sqrt{x + y^2} + \sqrt{1 - x + y^2} - 2|y| \tag{3.21}$$

Observe that by summing the rainbow diagrams we have generated a large anomalous dimension for the vertex Γ^+.

We next proceed to discuss the vertex Γ^-. Unlike with Γ^+, one cannot extract Γ^- at $\vec{q} = 0$ from the Ward identity Eq. (3.9) without also knowing the low $\vec{q}$ behaviour of Γ^+. Hence, we must actually solve Eq. (3.18) for Γ^-. As shown in Appendix A, at low frequency and momentum Γ^- assumes the following scaling form,

$$\Gamma^-(\omega, \nu, p) \sim \left(\frac{\omega}{\Lambda_\omega} \right)^{r_0/2} \gamma^- \left(\frac{\nu}{\omega}, \frac{p}{\sqrt{\gamma\omega}} \right) \tag{3.22}$$

with the exponent r_0 given by

$$r_0 = \begin{cases} \dfrac{2\varphi}{\pi - 2\varphi}, & 0 < \varphi < \pi/4 \\[3mm] \dfrac{\pi - 2\varphi}{2\varphi}, & \pi/4 < \varphi < \pi/2 \end{cases} \tag{3.23}$$

Fig. 7 shows the behavior of the exponent r_0 as a function of φ. Note that $0 < r_0 \leq 1$. Hence, the vertex Γ^- acquires an anomalous dimension. Unlike Γ^+, which is enhanced at
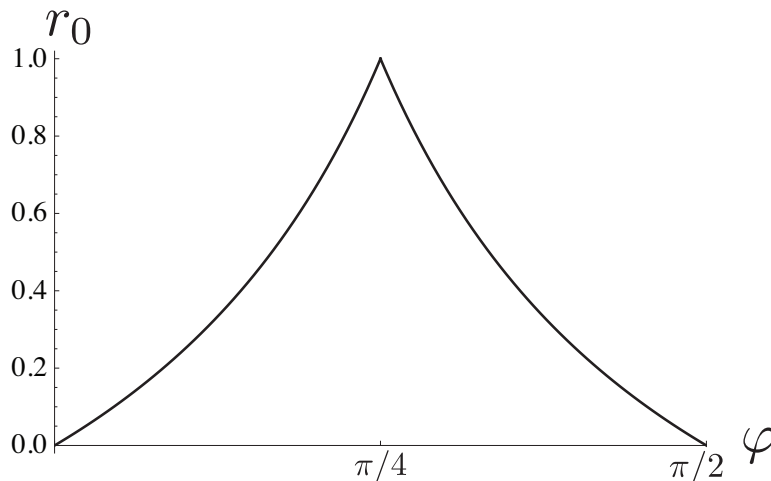

FIG. 7: The exponent r_0, Eq. (3.23), associated with the current vertex Γ^-, as a function of the angle 2φ between the Fermi surfaces.

low energy, Γ^- is suppressed. We briefly note that when $\varphi = \pi/4$, $r_0 = 1$, the scaling form (3.22) is modified by an additional factor $\log \Lambda_\omega/\omega$.

We have not been able to analytically determine the full form of the scaling function $\gamma^-(x, y)$ entering Eq. (3.22). However, we have extracted its asymptotic behavior for $y \to \infty$ (i.e. $p \gg \sqrt{\gamma\omega}$) We will shortly demonstrate that this asymptotic behavior controls the frequency dependence of the optical conductivity. As shown in Appendix A,

$$\gamma^-(x, y) = g_0 y^{r_0} + g_1(x) y^{r_0 - 2} + g_2 y^{r_2} + \cdots, \quad y \to \infty \tag{3.24}$$

Here,

$$r_2 = -2 - r_0 \tag{3.25}$$

The leading term in Eq. (3.24) ensures that Γ^- has a finite static limit, $\Gamma^-(p) = \lim_{\omega, \nu \to 0} \Gamma^-(\omega, \nu, p)$ with

$$\Gamma^-(p) \sim \left(\frac{p}{\Lambda}\right)^{r_0} \tag{3.26}$$

We have also kept two subleading terms in Eq. (3.24), which turn out to control the optical conductivity beyond the simple Drude response. Of particular interest is the last term in Eq. (3.24) with the exponent r_2, which as we will see, gives rise to the 'quantum critical' contribution to the optical conductivity. As will be discussed below, the relationship (3.25) between the exponents r_0 and r_2, which appears to come out accidentally in our calculations, is actually crucial for a consistent renormalization group (RG) interpretation of our results.

We now proceed from the vertex correction to conductivity itself. Starting with Eq. (3.10) and retracing the steps that led from (3.15) to (3.18), we obtain

$$\Pi_{xx}(\omega) = \frac{8N^2}{3\sin^2\varphi} \int \frac{dl}{2\pi} \int_0^\omega \frac{d\nu}{2\pi} \frac{1}{\sqrt{\gamma\nu + l^2} + \sqrt{\gamma(\omega - \nu) + l^2} - 2|l| + \frac{\gamma\omega}{2\Lambda}} \Gamma^-(\omega, \nu, l) \tag{3.27}$$

Substituting the scaling form (3.22) into (3.27) and cutting off the integral over l at $l \sim \Lambda$ we obtain,

$$\Pi_{xx}(\omega) \sim N^2 \omega \left(\frac{\omega}{\Lambda_\omega}\right)^{r_0/2} \int_0^{\sqrt{\Lambda_\omega/\omega}} dy \int_0^1 dx \frac{1}{\sqrt{x + y^2} + \sqrt{1 - x + y^2} - 2y} \gamma^-(x, y) \tag{3.28}$$

Now, as shown in Appendix A, for $\mu \gg 1$,

$$\int_0^\mu dy \int_0^1 dx \frac{1}{\sqrt{x + y^2} + \sqrt{1 - x + y^2} - 2y} \gamma^-(x, y) = a_0 \mu^{r_0 + 2} + a_1 \mu^{r_0} + a_2 \mu^{r_2 + 2} + \cdots \tag{3.29}$$

Hence,

$$\Pi_{xx} \sim N^2 \Lambda_\omega \left(a_0 + a_1 \frac{\omega}{\Lambda_\omega} + a_2 \left(\frac{\omega}{\Lambda_\omega}\right)^{(r_0 - r_2)/2}\right) \tag{3.30}$$

17

and the optical conductivity at real frequency Ω is given by

$$\sigma(\Omega) \sim N^2 \Lambda_\omega \left(a_0 \frac{i}{\Omega + i\epsilon} + a_1 \frac{1}{\Lambda_\omega} + a_2 \left(\frac{-i\Omega}{\Lambda_\omega} \right)^{(r_0 - r_2 - 2)/2} \right)$$

$$= N^2 \Lambda_\omega \left(a_0 \frac{i}{\Omega + i\epsilon} + a_1 \frac{1}{\Lambda_\omega} + a_2 \left(\frac{-i\Omega}{\Lambda_\omega} \right)^{r_0} \right) \tag{3.31}$$

where we've used Eq. (3.25) in the last step.

Let us discuss the three terms in Eq. (3.31). The term with the coefficient a_0 when added with the diamagnetic tadpole term renormalizes the total Drude weight. This term is clearly cut-off dependent and non-universal.

Next, consider the term with the coefficient a_1, which gives a constant contribution to the optical conductivity. It naively appears that the cut-off dependence cancels in this term. However, in reality, this term is non-universal. Indeed, we know that in a Fermi liquid with umklapps the real part of the optical conductivity tends to a constant as $\Omega \to 0$. Hence, we expect that umklapp scattering of Fermi liquid like quasiparticles away from the hot spots will renormalize the a_1 term rendering it non-universal. At a technical level this non-universality appears in our calculation in the following way. The cut-off dependence in Eq. (3.28) comes from two sources: i) the normalization of the current vertex, Eq. (3.22), ii) the cut-off on the integral over the momentum l along the Fermi surface. The argument given above indicates that we should not generally expect a universal cancellation between these two cut-offs in the a_1 term.

The final term with the coefficient a_2 in Eq. (3.31) is the critical hot spot contribution in the rainbow approximation. Unlike the first two terms in Eq. (3.31), which are present in a Fermi liquid, this term appears only at the critical point. Since $r_0 > 0$, this term is always suppressed compaired to the cold Fermi liquid contribution. In contrast, Chubukov *et al.*[17] found $r_0 = -1/2$ in the corresponding regime. There are two effects taken into account in our calculations that lead to the difference: i) the dependence of the fermion self energy on the momentum along the Fermi surface; ii) rainbow corrections to the current vertex.

It is interesting to discuss the a_2 term from the point of view of RG. Let $[J_x]$ be the scaling dimension of the current operator J_x. Then the current vertex $\Gamma(q, p)$ should have the dimension $[J_x] - 2[\psi]$. The dimension of the fermion operator $[\psi] = 3/2$ in the rainbow approximation (all dimensions are with respect to momentum). Hence, from Eq. (3.22), in the rainbow approximation,

$$[J_x] = 3 + r_0 \tag{3.32}$$

where we've used $z = 2$. Similarly, the quantum critical contribution to the optical conductivity $\sigma(\Omega)$ should have the dimension $2[J_x] - d - 2z = 2r_0$, which is precisely the scaling of the a_2 term in Eq. (3.31). Hence, our scaling forms for the conductivity and the current vertex have a consistent RG interpretation. Technically, this is based on the relation (3.25),

which seems to appear quite accidentally in our calculations.

Coming back to the constant a_1 'Fermi liquid' contribution to the conductivity, although this term is non-universal in the broad sense, it can still be calculated within our spin-fermion model if one treats the action (2.1) as a 'semi-microscopic' theory rather than an effective theory valid only in the infra-red scaling limit. This is only meaningful when the 'UV' scale of the theory Λ, Eq. (2.17), is much smaller then the Brillouin zone size. For this to be true, we must either send the coupling constant $\lambda \to 0$ or $N \to \infty$. In such a weak coupling limit, only the fermions within a distance Λ to the hot spot are strongly affected by the interactions with the spin density wave fluctuations and contribute to the constant term in the conductivity.

To extract the constant contribution in the rainbow approximation and in the limit $N \to \infty$, we have to solve the integral equation (3.18) for the current vertex Γ^- in the regime $p \sim \Lambda$ and then use Eq. (3.27) to determine the conductivity. The details of the calculation are presented in the Appendix B. Here we only quote the result

$$\mathrm{Re}\sigma_{ij}(\Omega) \to N^2 C_1(\varphi)\delta_{ij} \tag{3.33}$$

with the function $C_1(\varphi)$ shown in Fig. 8. Note that even though we have taken the 'weak-coupling' limit, the coupling constant λ does not enter the expression for C_1. Moreover, Eq. (3.33) is enhanced in N compared with the naively expected scaling $\sigma \sim N$. Note that the conductivity diverges in the nested limits $\varphi \to 0$, $\varphi \to \pi/2$.
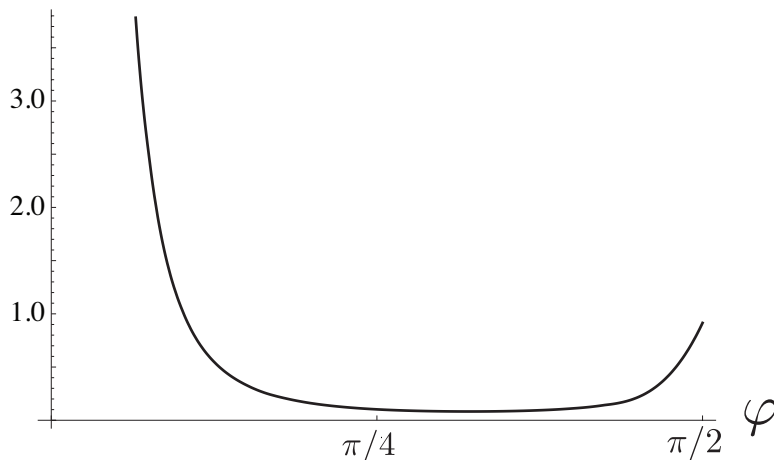

FIG. 8: The constant contribution to the conductivity as a function of the angle 2φ between the Fermi surfaces.

We conclude this section by reminding the reader that the 'Drude' pole (and associated delta function) in Eq. (3.31) should not be confused with the low frequency conductivity at $T > 0$. By setting $T = 0$ exactly in this paper we are effectively working in the limit $T \ll \Omega$, while the phenomenologically interesting d.c. conductivity is often $\Omega \ll T$. In the latter

limit, a delta function in the electrical conductivity follows from translational invariance if the electric current and momentum operators have nonvanishing overlap. In our quantum critical regime the electrical current lies in an $SU(2)$ pseudospin triplet, while the momentum is a pseudospin singlet. Therefore there can be no overlap and a finite quantum critical d.c. conductivity is expected at $T > 0$. A delta function will re-emerge due to the effect of irrelevant pseudospin symmetry breaking operators such as Fermi surface curvature terms. This delta function must then be resolved by additional physics such as impurity scattering or umklapp scattering beyond that already included in our theory[42,43].

IV.   SELF ENERGY, VERTEX CORRECTIONS AND 'COLD' CONDUCTIVITY

The anisotropic structure of criticality in our model – the existence of hot spots – means that as well as the quantum critical contribution to the conductivity, there is also the contribution of the 'cold' fermions. We have already encountered such a contribution in Sec. III. At the level of the approximation in Sec. III, the cold fermions are well-defined quasiparticles with a Fermi liquid like ω^2 damping rate, which give rise to a Drude peak in the optical conductivity, as well as a constant dissipative part at finite frequency.

In the remainder of this paper we will investigate the effects of scattering of the cold fermions by quantum critical modes living at the hot spots. Since the cold contribution in Sec. III was found to dominate over the critical hot spot contribution at low frequency, it is crucial to understand the extent to which hot modes can disrupt the cold Fermi liquid behavior. This issue is similarly important at finite temperature, where a cold Fermi liquid would contribute a T^{-2} temperature dependent DC conductivity, which is likely to short-circuit any phenomenologically interesting quantum critical temperature scaling of the conductivity[23,24].

In section V we will study the damping rate of cold fermions due to scattering by critical modes. We would like to see if it is possible to obtain a scattering rate that is stronger than the ω^2 result of Fermi liquid theory. The next question is the extent to which the scattering rate feeds through to the electrical conductivity. One must be wary of cancellations at low frequencies between the effects of self energy and vertex corrections to the conductivity[44]. This section studies the connection between self energy and conductivity in a general setting that is independent of the explicit form, e.g. (2.1), of the hot spot theory.

A.   Self energy and vertex correction cancellation

Before considering specific scattering processes, it is helpful to set up a general formalism describing the interaction of cold fermions with a (generically composite) operator $\mathcal{O}$ in the quantum critical theory. Since the momentum of critical fluctuations is small compared to the Fermi momentum of the cold fermions, it is sufficient at low energy to zoom into a patch

of the cold Fermi surface. In the simplest case of a zero momentum, neutral scalar operator $\mathcal{O}$ the interaction is effectively described by the coupling

$$S_1 = \lambda_1 \int d^3x \, \psi^\dagger(x)\psi(x)\mathcal{O}(x) \,. \tag{4.1}$$

We will see more concretely below how a local effective coupling emerges. In the patch, the cold fermions ψ have the usual inverse propagator

$$G_{\text{cold}}^{-1}(\omega, \vec{p}) = i\omega - v^\star p_\perp - \frac{p_\parallel^2}{2m^\star} \,. \tag{4.2}$$

Similarly to before, $p_\perp$ is the momentum perpendicular to the Fermi surface at the patch while $p_\parallel$ is the parallel momentum. In the patch the fermion has local Fermi velocity $v^\star$ and local Fermi surface curvature radius $m^\star v^*$. We are suppressing spin indices, their only effect is to add various factors of 2 below. The propagator for $\mathcal{O}$ is computed in the hot spot theory. In frequency space we will write

$$C(\omega, \vec{p}) = \int d\tau d^2x \, e^{i\omega\tau - i\vec{p}\cdot\vec{x}} \langle \mathcal{O}(\tau, \vec{x})\mathcal{O}(0,0)\rangle \,. \tag{4.3}$$

For the moment we will not need to make any assumptions about the form of this propagator.

As an example of how the local interaction (4.1) arises, consider the operator $\mathcal{O} = \phi^2$ of the critical theory (2.1). This is the relevant operator that drives the system away from criticality and will be an important example later in our paper. The coupling of this operator to two cold fermions is shown in figure 9. In figure 9 a cold fermion is scattered by a pair
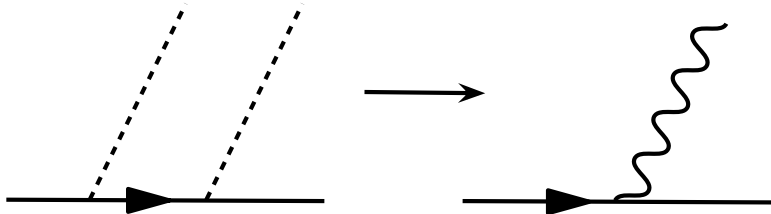

FIG. 9: Generating a local interaction between cold fermions and $\mathcal{O} = \phi^2$. As in Fig. 4, a full line is a fundamental fermion ψ, and a dashed line is a 'fundamental boson' ϕ. A wavy line represents a propagator for the operator $\mathcal{O}$. The intermediate fermion on the left hand graph is necessarily very off shell.

of hot bosons. Because the bosons are assumed to be hot, each bosonic scattering shifts the momentum of the fermion by the spin density wavevector. In the cold regions we are studying, away from the hot spots, this process takes the fermion far from the Fermi surface. Until being scattered back to the Fermi surface by the second boson, the fermion is hopelessly off shell. In the evaluation of figure 9 we can therefore approximate the propagators of these

off shell fermions by a constant. Thereby collapsing the two bosonic operators to a point, we obtain the local effective interaction (4.1) with the composite operator $\mathcal{O} = \phi^2$.

The three Feynman diagrams shown in figure 10 give the leading contribution to the conductivity due to the coupling λ_1 of (4.1). The current operator corresponding to the cold fermions (4.2) has components

$$J_\perp^{\text{cold}} = v^\star \psi^\dagger \psi \,, \qquad J_\parallel^{\text{cold}} = \frac{i}{m^\star} \psi^\dagger \partial_\parallel \psi \,. \tag{4.4}$$

Note that what is meant by the perpendicular and parallel directions, as well as the Fermi velocity, the curvature radius and indeed the coupling λ_1, is a function of the location of the patch on the Fermi surface.

We remark that in the present section we are neglecting the four-fermi interactions between the cold fermions. One result of such Fermi liquid interactions is to make the finite frequency current vertex $\vec{\Gamma}(\omega \to 0, \vec{p} = 0)$, relevant for the calculation of the optical conductivity, different from the Fermi velocity $\vec{v}^*$. As already shown in Sec. III this effect is parametrically strong for lukewarm fermions in the neighbourhood of the hot spot. However, the replacement $\vec{v}^* \to \vec{\Gamma}$ in the current vertex does not qualitatively modify our discussion below and we will not further consider the interplay between Fermi liquid and hot scattering.
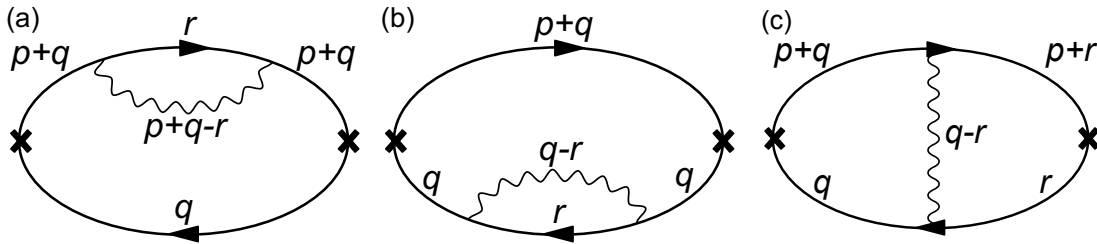

FIG. 10: The three leading order corrections in λ_1 to the conductivity due to cold fermions. The wavy lines denote propagators of the neutral bosonic quantum critical operator $\mathcal{O}$.

In the cold fermion current (4.4) the curvature term is down by a power of momentum compared to the Fermi velocity term. We can therefore drop the effects of curvature in a first computation. The first two graphs in figure 10, the self energy corrections, give the following contribution to the current correlator

$$\delta^{(a+b)} \Pi_{ij}^{\text{cold}}(\omega) = 2\lambda_1^2 \int \frac{d^3q}{(2\pi)^3} \frac{d^3r}{(2\pi)^3} v_i^\star v_j^\star G(q) G(r) G(p+q) \Big(G(p+q) C(p+q-r) + G(q) C(q-r) \Big) \,. \tag{4.5}$$

In this expression and in the following, the external 3-momentum is $p = (\omega, 0, 0)$. All the fermion propagators in this expression and the remainder of this section are those of the

22

cold fermions (4.2). The rightmost graph in figure 10, the vertex correction, gives

$$\delta^{(c)}\Pi_{ij}^{\text{cold}}(\omega) = 2\lambda_1^2 \int \frac{d^3q}{(2\pi)^3} \frac{d^3r}{(2\pi)^3} v_i^\star v_j^\star G(q)G(r)G(p+q)G(p+r)C(q-r)\,. \tag{4.6}$$

Using the following identity twice, where $p_\tau = \omega$ and the spatial components $\vec{p} = 0$,

$$G(q)G(p+q) = \frac{1}{i\omega}\Big(G(q) - G(p+q)\Big)\,, \tag{4.7}$$

it is easy to show that the self energy and vertex corrections are equal and opposite

$$\delta^{(a+b)}\Pi_{ij}^{\text{cold}}(\omega) = -\delta^{(c)}\Pi_{ij}^{\text{cold}}(\omega) = -\frac{2\lambda_1^2}{\omega^2} \int \frac{d^3q}{(2\pi)^3} \frac{d^3r}{(2\pi)^3} v_i^\star v_j^\star G(q)G(r)$$
$$\times \Big(C(p+q-r) + C(-p+q-r) - 2C(q-r)\Big)\,. \tag{4.8}$$

Therefore the total correction vanishes

$$\delta\Pi_{ij}^{\text{cold}}(\omega) = \delta^{(a+b)}\Pi_{ij}^{\text{cold}}(\omega) + \delta^{(c)}\Pi_{ij}^{\text{cold}}(\omega) = 0\,. \tag{4.9}$$

This cancellation is essentially the same as that observed in Ref. 44. The identity (4.7) integrates to a Ward identity relating vertex correction and self energy

$$\delta\Gamma(p,r) = \frac{i}{\omega}\Big(\Sigma(p+r) - \Sigma(r)\Big)\,. \tag{4.10}$$

Thus it is not surprising that the cancellation occurs in a range of different theories. The physics behind the cancellation is that, having neglected the effect of Fermi surface curvature in (4.4), the electrical current and charge density are proportional in each patch. Because the patches decouple at low energies, the current correlator is given by the density correlator summed over all patches. Conservation of particle number requires that the density correlator vanish at zero momentum. The vanishing of the current correlator $\Pi_{ij}^{\text{cold}}(\omega)$ then follows.

The fact that the leading order self energy correction does not contribute to the conductivity implies that non-Fermi liquid self energies will typically not translate into non-Fermi liquid response. At the end of this section we will obtain the leading nonzero answer for the conductivity, due to curvature terms in the current, and in the following sections we will explicitly evaluate the self energy and hence the conductivity due to scattering off specific low scaling dimension quantum critical modes. Before these discussions, however, we will describe in the following subsection one important circumstance in which vertex and self energy corrections reinforce each other rather than cancel. The non-cancellation occurs for similar reasons to those discussed in section III above, and will lead to interesting 'enhanced critical umklapp' modes that we discuss in detail below.

We conclude this section by noting that if we write the total current schematically as

$$J = J^{\text{cold}} + J^{\text{hot}}, \tag{4.11}$$

then in addition to the purely cold contribution to the conductivity $\langle J^{\text{cold}} J^{\text{cold}} \rangle$ considered above and the purely hot contribution $\langle J^{\text{hot}} J^{\text{hot}} \rangle$, there generally exists a cross-term $\langle J^{\text{cold}} J^{\text{hot}} \rangle$. The leading contribution in λ_1 to this cross-term is schematically shown in Fig. 11 and requires as an input from the critical theory the three point function $\langle J^{\text{hot}} \mathcal{O} \mathcal{O} \rangle$. For the simplest case when $\mathcal{O} = \phi^2$, this three point function in the critical theory vanishes by pseudospin symmetry and so the cross-term disappears. However, for the Cooper pair and charge density wave operators considered in the following section the three point function is generally finite and, in a full calculation, the cross-term cannot be neglected. Nevertheless, as a first pass, we will ignore the cross-term in the present paper.
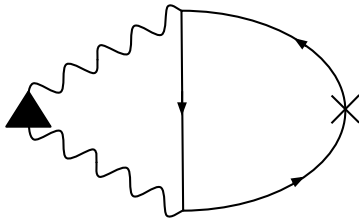

FIG. 11: The leading contribution to the cross-correlator of hot and cold fermion currents $\langle J^{\text{hot}} J^{\text{cold}} \rangle$. The triangle denotes the three point vertex $\langle J^{\text{hot}} \mathcal{O} \mathcal{O} \rangle$ in the critical theory.

B. Non-cancellation for scattering off neutral '$2k_F$' CDW modes

In this section we extend the considerations in section IV A to the interaction of cold fermions with other types of composite operators. Namely, we consider charge 2, zero momentum, Cooper pair operators and neutral, finite momentum, charge density wave operators. The fluctuations of both operators were found to be enhanced at the SDW critical point in Ref. 21.

Let us begin with the Cooper pair operator $\mathcal{O}$, which couples fermions with opposite Fermi momentum,

$$S_2 = \lambda_2 \int d^3x \left(\psi^\dagger(x) \widetilde{\psi}^\dagger(x) \mathcal{O}(x) + \widetilde{\psi}(x) \psi(x) \mathcal{O}^\dagger(x) \right). \tag{4.12}$$

Here we use ψ and $\widetilde{\psi}$ to denote cold fermion fields living in two antipodal patches of the Fermi surface. Note that the location of the antipodal patches on the Fermi surface can be arbitrary. We will shortly discuss how to generate the coupling (4.12) in the theory (2.1).

Next, consider the coupling of cold fermions to a generic CDW operator $\mathcal{O}$,

$$S_3 = \lambda_3 \int d^3x \left(\psi^\dagger(x)\widetilde{\psi}(x)\mathcal{O}(x) + \widetilde{\psi}^\dagger(x)\psi(x)\mathcal{O}^\dagger(x) \right). \tag{4.13}$$

Here ψ and $\widetilde{\psi}$ denote cold fermion fields in two patches separated by the wavevector $\vec{K}$ of $\mathcal{O}$. Generally, $\vec{K}$ only connects a finite number of points on the Fermi surface and so ψ and $\widetilde{\psi}$ must reside in the vicinity of these points. However, if the Fermi surface was nested with the wavevector $\vec{K}$, i.e. $\epsilon(\vec{k} + \vec{K}) = -\epsilon(\vec{k})$, ψ and $\widetilde{\psi}$ could reside anywhere on the Fermi surface.

The example of the CDW that will be of interest to us below is the operator $\mathcal{O} = \psi_2^{1\dagger}\psi_2^3$ of the critical theory (2.1). We call this a '$2k_F$' operator since it connects opposite hot spots $\ell = 1$ and $\ell = 3$, so that its wavevector $\vec{K} = -2\vec{K}_2^1 = -2\vec{K}_1^1$, with $\vec{K}_a^\ell$ - the momentum of the hot spot associated with fermion ψ_a^ℓ.[3] This operator was shown in Refs. 13,21 to condense at zero temperature, contributing to a modulated Ising-nematic order. Our full Fermi surface is generally not nested with respect to the wavevector $\vec{K}$, hence the operator $\mathcal{O}$ will only couple efficiently to the fermions in the vicinity of the hot spots. However, within the critical theory (2.1) the Fermi surface *is* nested with respect to $\vec{K}$ by virtue of the pseudospin symmetry. Indeed, Eq. (2.9) implies that $G_a^\ell(\omega, \vec{k}) = -G_a^\ell(-\omega, -\vec{k}) = -G_a^{-\ell}(-\omega, \vec{k})$, or measuring momenta in the full Brillouin zone

$$G(\omega, \vec{K}_a^\ell + \vec{k}) = -G(-\omega, -\vec{K}_a^\ell + \vec{k}). \tag{4.14}$$

Hence, if $\vec{k}$ is on the Fermi surface, so is $\vec{k} + \vec{K}$ and the Fermi surface is nested. Note that the nesting should not be confused with the Fermi surface being straight. Even though the bare theory (2.1) has a straight Fermi surface, the dressed Fermi surface possesses a finite curvature as discussed in Refs. 17,21. On the other hand, the nesting of the bare theory is protected by the pseudospin symmetry even when the effects of the interactions in the action (2.1) are taken into account. The nesting is destroyed only when we break the pseudospin symmetry by adding an explicit curvature term to the theory, which we schematically write as,

$$\delta L = \kappa_0 |\nabla \psi|^2. \tag{4.15}$$

The coupling constant κ_0 will generally have an RG flow,

$$\frac{d\kappa_0}{d\ell} = -b\kappa_0. \tag{4.16}$$

At tree level, $b = 1$, and so we expect the curvature to be an irrelevant perturbation to the critical theory. Nevertheless, for lukewarm fermions away from hot spots this irrelevancy is

---

[3] There is also an analogous operator connecting hot spots $\ell = 2$ and $\ell = 4$.

dangerous as it eventually destroys the nesting. Let us estimate the energy scale at which the effects of the perturbation (4.15) on lukewarm fermions a distance $k_\parallel$ from the hot spot kick in. From Eq. (2.10), in the absence of the curvature perturbation, the natural scale of the fermion propagator is $G^{-1} \sim k_\parallel^{z/2-\eta_\psi}$. Hence, from the flow (4.16), the curvature correction to G^{-1} scales as $\delta G^{-1} \sim \kappa_0 k_\parallel^{z/2-\eta_\psi+b}$. Assuming that lukewarm fermions remain well-defined quasiparticles, Eq. (2.12), on the Fermi surface $G^{-1} \sim (i\omega/k_\parallel^z)k_\parallel^{z/2-\eta_\psi}$. Hence, the curvature correction δG^{-1} becomes significant once $\omega \lesssim k_\parallel^{z+b}$. Therefore, there exists an energy window $k_\parallel^{z+b} \ll \omega \ll k_\parallel^z$ in which the lukewarm fermions can efficiently couple to the CDW operator $\mathcal{O}$.

With the above remarks in mind, let us see how the effective coupling (4.13) of the CDW operator $\mathcal{O} = \psi_2^{1\dagger}\psi_2^3$ to the lukewarm fermions can be generated in the theory (2.1). Via an intermediate fundamental boson ϕ the fermions in $\mathcal{O}$ can be coupled to fermions $\psi = \psi_1^3$ and $\widetilde{\psi} = \psi_1^1$. This coupling is illustrated in Fig. 12 below. Because we wish to consider scattering by hot operators in the critical theory, we demand that the pair of fermions constituting $\mathcal{O}$ be hot. The boson that connects the external cold (or lukewarm) fermions to the hot fermions is necessarily extremely off shell. Similarly to the off shell fermions in the previous subsection, we may replace its propagator by a constant. This then generates the local interaction (4.13), as is illustrated in figure 12. To be completely explicit, we could write
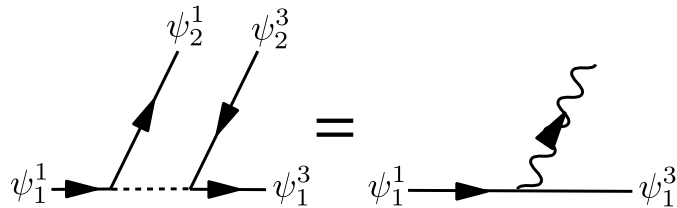

FIG. 12: Generating a local interaction of lukewarm fermions $\psi = \psi_1^3$ and $\widetilde{\psi} = \psi_1^1$ with the operator $\mathcal{O} = \psi_2^{1\dagger}\psi_2^3$. The intermediate 'fundamental' boson on the left hand side is necessarily very off shell. Wavy lines are propagators for the operator $\mathcal{O}$, as in Fig. 9.

this coupling as the four fermion interaction

$$S_{\text{umklapp}} \sim \int d^3x \psi_1^{3\dagger\text{cold}}\psi_1^{1\text{cold}}\psi_2^{1\dagger\text{hot}}\psi_2^{3\text{hot}} + \text{c.c.} . \tag{4.17}$$

We show this scattering process in Fig. 13. We see that in terms of the underlying microscopic fermions, this coupling does not conserve momentum and therefore describes umklapp scattering. We comment that numerical studies of the Hubbard model have also noted the importance of umklapp processes in the breakdown of Fermi liquid theory[47].

The same argument holds for the scattering off the Cooper pair operator $\mathcal{O} = \psi_2^1\psi_2^3$, leading to the interaction (4.12). All that is necessary is to reverse e.g. the arrows of ψ_1^3 and ψ_2^3 propagators in figure 12.
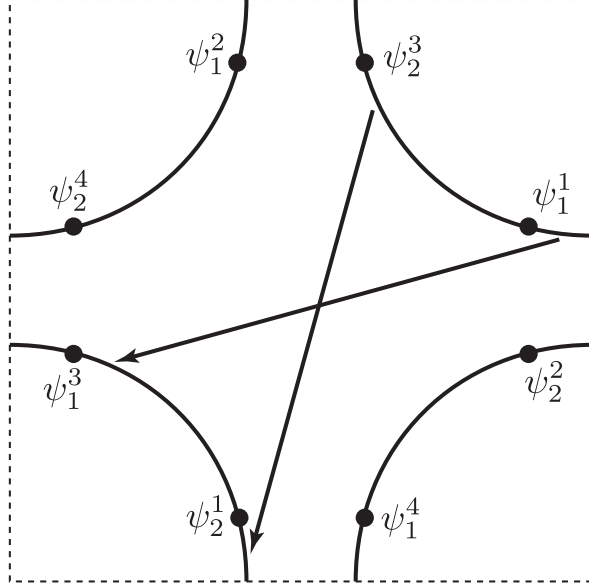
FIG. 13: The $2k_F$ operator generates the umklapp process shown here. The scattering is from the lukewarm regions near the hot spots, and conserves total momentum upto a reciprocal lattice vector. Note that this process arises after integrating out high energy degrees of freedom from the effective theory in Eq. (2.1).

We now proceed to the discussion of optical conductivity. Consider scattering off CDW fluctuations first. The diagrams describing the leading order corrections to the conductivity due to the interaction (4.13) are shown in figure 14. The wavy line now represents the two-point function of the CDW operator $C = \langle O O^\dagger \rangle$. The crucial fact to take into account
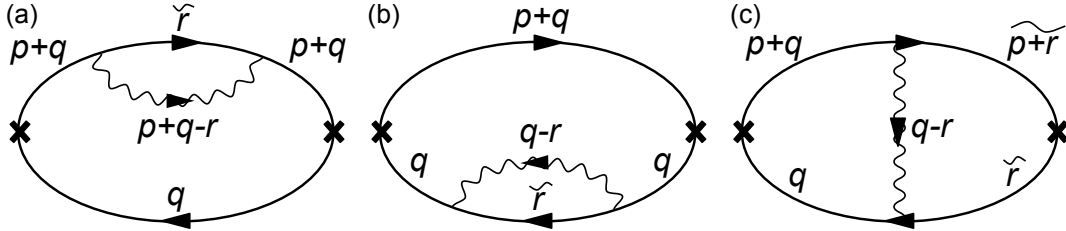

FIG. 14: The three leading order corrections in λ_3 to the conductivity due to cold fermions. Tildes over momenta indicate that the fermion propagator in question corresponds to the opposite patch. The hot operator $\mathcal{O}$ is now complex and so its propagators carry an arrow.

in evaluating these diagrams is that the Fermi velocity is pointing in opposite directions in the two patches separated by the ordering wavevector $\vec{K}$. This is a consequence of the relation (4.14). Therefore the current operator (neglecting as before the curvature term at low energies) should be written as

$$J_\perp^{\text{cold}} = v^\star \left(\psi^\dagger \psi - \widetilde{\psi}^\dagger \widetilde{\psi} \right). \tag{4.18}$$

Similarly to equations (4.5) and (4.6) previously, the graphs of figure 14 give

$$\delta^{(a+b)}\Pi_{ij}^{\text{cold}}(\omega) = 2\lambda_3^2 \int \frac{d^3q}{(2\pi)^3}\frac{d^3r}{(2\pi)^3}v_i^\star v_j^\star G(q)\widetilde{G}(r)G(p+q)\Big(G(p+q)C(p+q-r)+G(q)C(q-r)\Big).$$
(4.19)

and

$$\delta^{(c)}\Pi_{ij}^{\text{cold}}(\omega) = -2\lambda_3^2 \int \frac{d^3q}{(2\pi)^3}\frac{d^3r}{(2\pi)^3}v_i^\star v_j^\star G(q)\widetilde{G}(r)G(p+q)\widetilde{G}(p+r)C(q-r).$$
(4.20)

Recall that the external 3-momentum is $p = (\omega, 0, 0)$. The crucial minus sign difference with (4.6) is due to the minus sign in the current (4.18). Tilde indicates a Green's function for fermions on the opposite patch. The factors of 2 work out a little differently compared to section IV A: the Feynman diagrams have a reduced symmetry and we must be careful not to double count the patches. The extra minus sign means that upon using the identity (4.7), the self energy and vertex contributions add rather than cancel. The total result is

$$\delta\Pi_{ij}^{\text{cold}}(\omega) = \delta^{(a+b)}G_{ij}^{\text{cold}}(\omega) + \delta^{(c)}G_{ij}^{\text{cold}}(\omega)$$
(4.21)
$$= -\frac{4\lambda_3^2}{\omega^2} \int \frac{d^3q}{(2\pi)^3}\frac{d^3r}{(2\pi)^3}v_i^\star v_j^\star G(q)\widetilde{G}(r)\Big(C(p+q-r)+C(-p+q-r)-2C(q-r)\Big).$$

The absence of a cancellation means that the scattering off the CDW operator will directly influence the conductivity. We must, however, remember that due to the dangerously irrelevant curvature terms, such scattering is only efficient for lukewarm fermions in the neigbourhood of the hot spot. This issue will be discussed in more detail in sections V B and VI B, which will present a calculation of the fermion self energy and conductivity due to $2k_F$ scattering.

Finally we turn to the case of the interaction with the Cooper pair operator. As already noted, in contrast to the CDW case, such scattering is efficient everywhere on the Fermi surface. The diagrams giving the leading order correction to the conductivity are shown in figure 15. The fermions ψ and $\widetilde{\psi}$ now live in antipodal patches and therefore again have
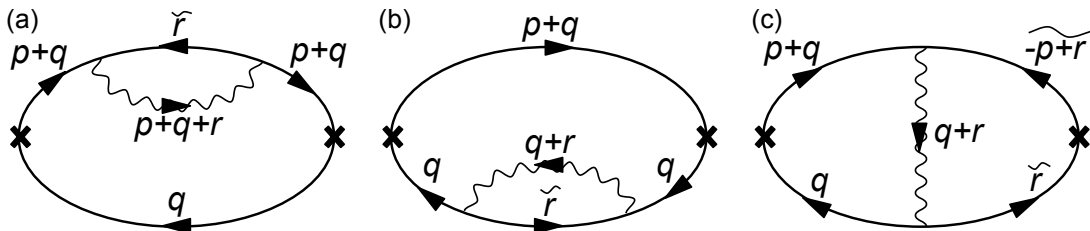

FIG. 15: The three leading order corrections in λ_2 to the conductivity due to cold fermions. A few fermionic arrows are reversed compared to figure 14.

opposite Fermi velocities. Thus, using the two patch current (4.18) we can evaluate these

graphs to obtain

$$\delta^{(a+b)}\Pi_{ij}^{\text{cold}}(\omega) = -2\lambda_2^2 \int \frac{d^3q}{(2\pi)^3} \frac{d^3r}{(2\pi)^3} v_i^\star v_j^\star G(q)\widetilde{G}(r)G(p+q)\Big(G(p+q)C(p+q+r)+G(q)C(q+r)\Big).$$
(4.22)

and

$$\delta^{(c)}\Pi_{ij}^{\text{cold}}(\omega) = 2\lambda_2^2 \int \frac{d^3q}{(2\pi)^3} \frac{d^3r}{(2\pi)^3} v_i^\star v_j^\star G(q)\widetilde{G}(r)G(p+q)\widetilde{G}(-p+r)C(q+r).$$
(4.23)

These expressions have various minus signs in different places compared to the previous corresponding formulae for the CDW case. These are seen to lead to a cancellation upon using the identity (4.7) and thus

$$\delta\Pi_{ij}^{\text{cold}}(\omega) = \delta^{(a+b)}\Pi_{ij}^{\text{cold}}(\omega) + \delta^{(c)}\Pi_{ij}^{\text{cold}}(\omega) = 0\,,$$
(4.24)

similar to the first case we considered. Analogous cancellations in the fluctuation conductivity of clean superconductors are noted in Refs. 48,49. Each term takes the form

$$\delta^{(a+b)}\Pi_{ij}^{\text{cold}}(\omega) = -\delta^{(c)}\Pi_{ij}^{\text{cold}}(\omega) = \frac{2\lambda_2^2}{\omega^2} \int \frac{d^3q}{(2\pi)^3} \frac{d^3r}{(2\pi)^3} v_i^\star v_j^\star G(q)\widetilde{G}(r)$$
$$\times \Big(C(p+q+r) + C(-p+q+r) - 2C(q+r)\Big).$$
(4.25)

The leading self energy correction due to Cooper pair scattering does not therefore directly push forward to the conductivity. Fermi surface curvature terms are needed to obtain a nonzero contribution to the conductivity, which will consequently be suppressed by powers of momentum.

C. Fermi surface curvature and leading corrections to the conductivity

We found in Section IV A that the leading order conductivity due to scattering off a neutral, zero momentum scalar operator $\mathcal{O}$ vanished due to a cancellation. To obtain the leading nonzero contribution we must keep the curvature terms in the cold fermion current operator (4.4). The relevant Feynman diagrams remain those of figure 10, except that now there will be extra powers of momentum at the current insertions. One can check that the contribution to the conductivity due to the cross term $\langle J_\perp^{\text{cold}} J_\parallel^{\text{cold}}\rangle$ again vanishes upon adding the three diagrams. In verifying the cancellation one must use the symmetries $C(\omega,\vec{p}) = C(\omega,-\vec{p})$ and $C(\omega,\vec{p}) = C(-\omega,\vec{p})$. These follow for neutral operators from parity symmetry. The contribution $\langle J_\parallel^{\text{cold}} J_\parallel^{\text{cold}}\rangle$ does not vanish however. Summing the

three diagrams gives the following result

$$\delta\Pi_{ij}^{\text{cold}}(\omega) = -\frac{\lambda_1^2}{m^{\star 2}\omega^2} \int \frac{d^3q}{(2\pi)^3}\frac{d^3r}{(2\pi)^3}(q_\parallel - r_\parallel)_i(q_\parallel - r_\parallel)_j G(q)G(r)$$
$$\times \Big(C(p+q-r) + C(-p+q-r) - 2C(q-r) \Big).$$

(4.26)

Note how in this expression we are taking $q_\parallel$ to be a vector whose direction in general changes with the patch on the Fermi surface. Here, and in (4.21) above, we should strictly also bear in mind that the couplings λ and Fermi velocities and curvatures also depend on the Fermi surface patch.

An analogous expression to (4.26) exists for scattering off charged operators. The expression follows immediately from (4.25). Because of the symmetry in the argument of the C correlators in (4.25) it is not necessary to use any symmetry property of C in this case. In section VI we will evaluate the integrals in (4.26) to obtain the corresponding scaling dependence of the conductivity. Before this, we turn to a computation of the self energy due to the scattering processes we are considering. The main results of this section have been the general formulae (4.21) and (4.26) for the conductivity resulting from scattering off $2k_F$ and zero momentum operators respectively.

V. SELF ENERGY FROM COMPOSITE OPERATORS

The cold fermion self energy acquired by scattering off one of the bosonic operators in the previous section, with any of the three couplings λ_i, is

$$\Sigma(q) \equiv \lambda_i^2 \int \frac{d^3r}{(2\pi)^3}G(r)C(q-r)\,.$$

(5.1)

The self energy gives a measure of the effect of scattering off hot modes prior to any cancellations that occur in computing the conductivity. In this section we compute the self energy due to various operators at the hot spots and then use these results in the following section to compute the corresponding conductivity. The self energy is of course also of interest in itself, especially insofar as one obtains deviations from Fermi liquid theory.

A. Self energy for charge and momentum preserving scattering

Consider first the case in which the operator $\mathcal{O}$ is a zero momentum neutral operator of the critical theory. Under scale transformations

$$\mathcal{O}(\tau, \vec{x}) \to s^\Delta \mathcal{O}(s^z\tau, s\vec{x})\,.$$

(5.2)

Here z is the dynamical critical exponent, which we keep arbitrary for the moment, and Δ is the scaling dimension of the operator $\mathcal{O}$. The most important example, on which we concentrate below, is the operator ϕ^2 of the critical theory (2.1). This operator perturbs the theory away from the critical point and determines the correlation length exponent ν via

$$\frac{1}{\nu} = z + 2 - \Delta \, . \tag{5.3}$$

At a mean field 'Hertz-Moriya-Millis'[14–16,18] level, $z = 2$, $\nu = 1/2$ and $\Delta = 2$. An important feature of our treatment here is that we can also think of z and Δ as free variables and thereby consider the dependence of physical quantities on z and Δ. Within the specific model of (2.1), the values of z and Δ are in principle determined from a difficult computation in the strongly interacting critical theory. The mean field values provide an estimate at best. In general, the scaling dimension Δ determines the scaling form of the correlator (4.3) to be

$$C(\omega, \vec{p}) = \frac{1}{\omega^{(z+2-2\Delta)/z}} \widetilde{C}\left(\frac{\vec{p}}{\omega^{1/z}}\right) \, . \tag{5.4}$$

Here we have kept only the singular contribution to C. The singular term is greater than the analytic terms at low energy if $z + 2 \geq 2\Delta$. The tilde over $\widetilde{C}$ is not related to opposite patches but indicates that $\widetilde{C}$ is dimensionless.

The self energy (5.1) can be written explicitly, using (4.2) and shifting integration variables, as

$$\Sigma(\omega, \vec{p}) = \lambda_1^2 \int \frac{dq_\tau d^2 q}{(2\pi)^3} \frac{C(q_\tau, \vec{q})}{i(\omega - q_\tau) - v^\star(p_\perp - q_\perp) - (p_\parallel - q_\parallel)^2/2m^\star} \, . \tag{5.5}$$

The main contribution to the self energy (5.1) comes from the regime $q_\tau \sim |\vec{q}|^z$ in which the critical fluctuations are on shell. Conservation of energy and momentum implies that the fermion can absorb the momentum of the critical fluctuations and stay on the Fermi surface only if $q_\tau \sim v^\star q_\perp + q_\parallel^2/2m^\star$. If $z > 1$ consistency with the critical regime then requires $q_\perp \sim \max(q_\parallel^2, q_\parallel^z) \ll q_\parallel$ and therefore the momentum of the critical fluctuations is nearly tangent to the Fermi surface. This condition is familiar from the study of quantum critical points or phases involving the interaction of the Fermi surface with a bosonic field carrying zero wavevector[45,46]. The difference in the present case is that the operator $\mathcal{O}$ is a composite of the 'elementary' critical excitations. We note that a condition $z < 3$ is necessary to ignore terms such as $q_\perp q_\parallel^2$ and $q_\parallel^3$ in the fermion dispersion. Thus the results that follow are valid for $1 < z < 3$.

The upshot of the previous paragraph is that in the regime when the boson is 'on shell' we can ignore the dependence of C on $q_\perp$. It is then easy to perform the integral over $q_\perp$ in

(5.5) to give

$$\Sigma(\omega, \vec{p}) = \frac{i\pi\lambda_1^2}{v^\star} \int \frac{dq_\tau dq_\parallel}{(2\pi)^3} \text{sgn}(q_\tau - \omega) C(q_\tau, q_\parallel) \tag{5.6}$$

$$= -\frac{i\lambda_1^2 \text{sgn}(\omega)}{(2\pi)^2 v^\star} \int_0^{|\omega|} dq_\tau \int_{-\infty}^\infty dq_\parallel C(q_\tau, q_\parallel). \tag{5.7}$$

To obtain the second line we used the fact that C is an even function of q_τ. The momentum dependence of the self energy has disappeared. Now using the scaling form (5.4) and changing variables to $q_\tau = |\omega|x$ and $q_\parallel = |\omega|^{1/z}y$ gives

$$\Sigma(\omega, \vec{p}) = -\frac{i\lambda_1^2 \text{sgn}(\omega)}{2\pi^2 v^\star} |\omega|^{(2\Delta-1)/z} \int_0^1 \frac{dx}{x^{(z+2-2\Delta)/z}} \int_0^{\Lambda/|\omega|^{1/z}} dy \widetilde{C}\left(\frac{y}{x^{1/z}}\right). \tag{5.8}$$

As in section III above, we introduced a cutoff on the momentum of the critical fluctuations along the Fermi surface. It is clear from the scaled integral (5.8) that the non-cutoff-sensitive contribution to the self energy scales like

$$\Sigma(\omega) = -i\frac{\lambda_1^2 c}{v^\star} \text{sgn}(\omega) |\omega|^\kappa, \tag{5.9}$$

with exponent

$$\kappa = \frac{2\Delta - 1}{z}. \tag{5.10}$$

In (5.9), c is a real number. As a quick check of this expression we can note that substituting $z = 3$ and $\Delta = 3/2$, as appropriate for the Hertz theory of a nematic transition with $\mathcal{O}(x)$ being the nematic order parameter, we recover the expected $\kappa = 2/3$. In general, if the exponent $\kappa > 1$, the fermionic excitations in the cold regions of the Fermi surface remain well-defined quasiparticles. However, the lifetime of these quasiparticles is generically different from the Fermi liquid $\Gamma \sim \omega^2$ form.

Returning to the example in our theory of $\mathcal{O} = \phi^2$, we can write in terms of the critical exponent (5.3)

$$\kappa = 2 + \frac{3}{z} - \frac{2}{\nu z}. \tag{5.11}$$

In Hertz-Moriya-Millis theory this implies $\kappa = \frac{3}{2}$. Therefore at this level the cold fermions acquire a non-Fermi liquid dissipation, albeit surviving as well-defined excitations. The fact that the low energy behavior of the propagator is not disrupted indicates that the effective λ_1 coupling is irrelevant in this case. We will give a more sophisticated characterisation of the relevancy or irrelevancy of our λ_i couplings in section VI C.

We can confirm the scaling (5.9) with $\kappa = \frac{3}{2}$ via an explicit calculation. Indeed, at one loop level, the correlation function of the ϕ^2 operator is given by Fig. 16. Using the RPA
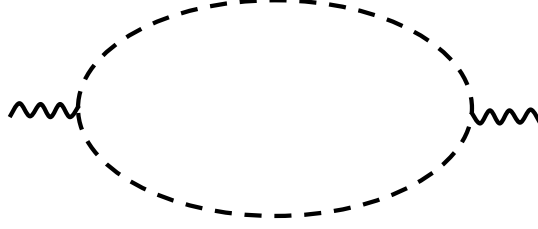
FIG. 16: The one loop contribution to the correlation function of the $\mathcal{O} = \phi^2$ operator.

propagator (2.14), we obtain (see Appendix C),

$$C_{\phi^2}(\omega, \vec{q}) = \frac{3}{2\pi^2 N^2 \gamma} \left(\log \frac{\Lambda^2}{\gamma|\omega| + \vec{q}^2} + X(\omega, \vec{q}) \right) , \qquad (5.12)$$

where

$$X(\omega, \vec{q}) = \frac{\gamma|\omega|}{\vec{q}^2} \log \left(\frac{\gamma|\omega|}{\gamma|\omega| + \vec{q}^2} \right) - \frac{1}{2} \text{Li}_2 \left(\frac{\vec{q}^2}{2\gamma|\omega| + \vec{q}^2} \right) + \frac{1}{2} \text{Li}_2 \left(\frac{-\vec{q}^2}{2\gamma|\omega| + \vec{q}^2} \right) . \qquad (5.13)$$

Upon substituting Eq. (5.12) into Eq. (5.7), we recover the expected scaling (5.9) with $\kappa = \frac{3}{2}$.

We have also performed a complete analysis of the correlation function C_{ϕ^2} of the ϕ^2 operator within the Hertz-Moriya-Millis theory. In Hertz theory, C_{ϕ^2} does not strictly satisfy the scaling form (5.4) due to the presence of a marginally irrelevant perturbation and the fact that the scaling dimension of the correlator C_{ϕ^2} is $2\Delta - z - 2 = 0$ in this case. A detailed calculation (see Appendix C) gives,

$$C_{\phi^2}(\omega, \vec{q}) \propto \left(\log \frac{\Lambda}{|\vec{q}|} \right)^{1/11} \left[1 + \frac{1}{22 \log \Lambda/|\vec{q}|} \left(-\log \left(1 + \frac{\gamma|\omega|}{\vec{q}^2} \right) + X(\omega, \vec{q}) + \text{const} \right) \right] + \text{const} , \qquad (5.14)$$

and from (5.7) we obtain,

$$\Sigma(\omega) \sim i \text{sgn}(\omega) |\omega|^{3/2} \left(\log \frac{\Lambda}{\omega} \right)^{-10/11} . \qquad (5.15)$$

We remind the reader that the spin density wave transition in two dimensions is not described by Hertz-Moriya-Millis theory. As shown in Ref. 21, the critical theory describing this transition is, in fact, strongly coupled and the exponents z and ν receive corrections from mean field values. Thus, the discussion of the correlator in Hertz theory is given above for illustrative purposes only, and in a full theory we expect to obtain the scaling form (5.9) for the self energy with the value of κ (5.11) renormalized compared to the Hertz result of $\kappa = \frac{3}{2}$.

We must also worry about the cutoff-dependent contribution to the integral (5.8). This

regime, $q_\parallel \sim \Lambda \gg q_\tau^{1/z}$, is most easily accessed by taking a step back to equation (5.7). At leading order we can ignore the frequency dependence of $C(q_\tau, q_\parallel)$. The contribution thus comes from exchanging static critical fluctuations with a large momentum and gives

$$\Sigma(\omega) = -\frac{i\lambda_1^2\omega}{2\pi^2 v^\star} \int_0^\Lambda dq_\parallel C(0, q_\parallel) \, . \tag{5.16}$$

This contribution simply renormalises the quasiparticle residue and Fermi velocity. We may also ask about the higher order frequency dependence of the self energy coming from the 'UV' part of the integral (5.7). In principle, the function $C(q_\tau, q_\parallel)$ need not have an analytic expansion in powers of q_τ for $q_\tau \ll |\vec{q}|^z$. Hence, one may obtain non trivial power law contributions to the quasiparticle width from this regime. For the Hertz-Moriya-Millis theory, the first subleading correction, as found in Appendix C, behaves as $q_\tau^2 \log|q_\tau|$, leading to $\Sigma(\omega) \sim \omega^3 \log\omega$, which is smaller than the contribution (5.9) from the $q_\tau \sim |\vec{q}|^z$ regime.

The main result of this subsection is the scaling form (5.9) for the self energy of cold electrons scattering off neutral and zero momentum quantum critical modes. In general the exponent κ is given by (5.10).

B. Self energy due to $2k_F$ scattering

In Section IV B we found that neutral hot operators carrying a net $2k_F$ momentum could scatter cold fermions without the self energy correction to the conductivity being cancelled by a vertex correction. In this subsection, we consider the self energy due to such a scattering process. Despite the absence of a cancellation, there are various obstacles potentially preventing interesting consequences of this scattering.

Firstly, as already discussed in Section IV B, this process cannot efficiently scatter most of the cold fermions due to the Fermi surface being non-nested. Only lukewarm fermions in the energy range $k_\parallel^{z+b} \ll \omega \ll k_\parallel^z$ are strongly affected by the scattering, with the exponent b determined by the RG flow (4.16) of the curvature perturbation (4.15). At tree level, $b = 1$.

Secondly, as we mentioned above, the simplest critical operator to which these considerations apply is $\mathcal{O} = \psi_2^{1\dagger}\psi_2^3$. At tree level, this operator has dimension $\Delta = 3$. Thus, with $z = 2$, the 'singular' self energy scales with a power $\Sigma \sim \omega^{5/2}$ in (5.9) which is even weaker than that due to the usual Fermi liquid interaction. Therefore, unless there are important renormalizations of the operator dimension and dynamical critical exponent, the hot $2k_F$ operator does not seem to significantly influence either the self energy or conductivity.

Nevertheless, it instructive to consider scattering in the $2k_F$ channel in the theory (2.1). As per the discussion above we will find that this process is dominated by scattering off lukewarm rather than hot fermions. Thus, the formalism in Sec. IV will not be directly appicable in this case. Even so, the interplay of the singular SDW interaction and the Fermi surface curvature will give rise to a number of new physical effects. We proceed to discuss

two such effects, the importance of effectively one-dimensional scattering and modification of the leading low energy scaling of certain observables due to curvature.
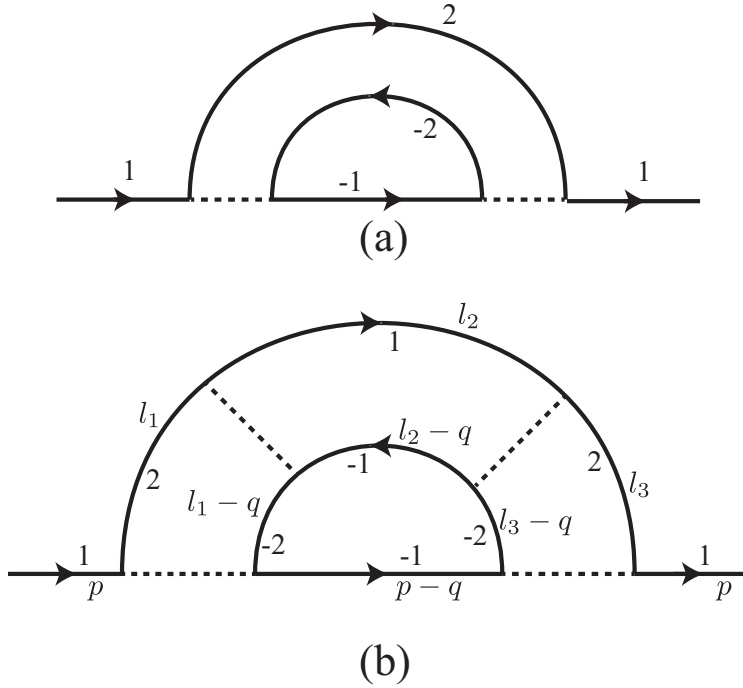
1. One-dimensional scattering

(a)

(b)

FIG. 17: Fermion self energy in the $2k_F$ channel. The scattering processes are those shown in Fig. 13; The 1 fermion refers to ψ_1^1, the 2 to ψ_2^1, the -1 to ψ_1^3 and the -2 to ψ_2^3. These fermions are also referred to as ψ_1, $\psi_{\bar{1}}$, ψ_{-1}, and $\psi_{-\bar{1}}$ respectively. The momentum labels in (b) correspond to the expression in Eq. (D1).

The two lowest order self energy diagrams in the $2k_F$ channel are shown in Fig. 17. The graph in Fig. 17a) is already taken into account in the rainbow approximation of Section III and gives rise to an ω^2 Fermi liquid like self energy for lukewarm fermions. We now turn our attention to the graph in Fig. 17b). We will consider the contribution to this graph from the region where all external and internal fermions are lukewarm. Thus, as a starting point we use the rainbow fermion propagators in the lukewarm region,

$$G_a(\omega, \vec{p}) = \frac{Z(\hat{v}_{\bar{a}} \cdot \vec{p})}{i\omega - v^*(\hat{v}_{\bar{a}} \cdot \vec{p})\hat{v}_a \cdot \vec{p}} \tag{5.17}$$

where $Z(l) = l/\Lambda$, $v^*(l) = |\vec{v}|l/\Lambda$ and Λ is given by Eq. (2.17). As shown in appendix D,

35

the resulting fermion self energy is

$$\Sigma(\omega, \vec{k}) \sim -\frac{i}{N}\frac{\omega}{k_\parallel}\log\left(\frac{k_\parallel^2}{\gamma|\omega|}\right) \tag{5.18}$$

This self energy is of non-Fermi liquid form and, in fact, implies that the fermionic quasi-particles are not well-defined even in the lukewarm region $\omega \ll k_\parallel^z$. It is interesting that Eq. (5.18) has the 'marginal Fermi liquid' form,[50] although it must be kept in mind that we have not determined whether this logarithm survives the resummation of higher order terms.

The origin of the infra-red divergence in Eq. (5.18) lies in the fact that at the level of the propagator (5.17) the Fermi surface is flat. Indeed, the self energy (5.18) comes from the region where the 2 and -2 fermions are off shell and can be integrated out to give an effective interaction between the 1 and -1 fermions, which has a singular dependence on the momenta along the Fermi surface of the latter. The resulting process, Fig. 18, is effectively one-dimensional - hence the logarithmic divergence familiar from one-dimensional physics. The prefactor of $1/k_\parallel$ in Eq. (5.18) comes from the $k_\parallel$ dependence of the effective interaction between the one-dimensional excitations.
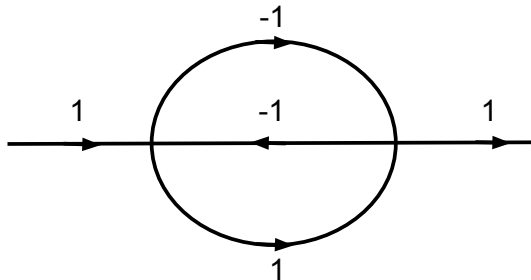

FIG. 18: Fermion self energy in the $2k_F$ channel. The 2 and -2 fermions in Fig. 17b) are assumed to be off shell and are integrated out. The resulting process is effectively one-dimensional. The interaction between the 1 and -1 fermions has a singular ($\sim 1/k_\parallel^2$) dependence upon their distance ($k_\parallel$) from the hot spot.

Clearly, the divergence in Eq. (5.18) will be cut off by the Fermi surface curvature. One source of curvature is the explicit perturbation κ_0 in the Lagrangian, Eq. (4.15). This perturbation is expected to give rise to a physical Fermi surface curvature $\kappa(k_\parallel) \sim \kappa_0 k_\parallel^{b-1}$ (here we are using the fact that the 'natural' scale of curvature $\kappa \sim k_\parallel^{-1}$). Still assuming the quasiparticle form in Eq. (2.12), following the argument in section IV B, the divergence (5.18) will be cut off below $\omega_\kappa(k_\parallel) \sim \kappa_0 k_\parallel^{z+b}$. However, even if $\kappa_0 = 0$ the Fermi surface of the theory (2.1) will dynamically develop a curvature. Indeed, we expect the Fermi surface

shape to be controlled by the RG flow of the variable α, related to the angle between the Fermi surfaces of fermions 1 and 2. If this flow has a stable fixed point at $\alpha = \alpha_*$,

$$\frac{d\alpha}{d\ell} = -b'(\alpha - \alpha^*) \tag{5.19}$$

then the physical Fermi surface curvature $\kappa(k_\parallel) \sim (\alpha - \alpha_*)k_\parallel^{b'-1}$ and we expect the one-dimensional divergence in Eq. (5.18) to be cut off at $\omega_\kappa(k_\parallel) \sim (\alpha - \alpha_*)k_\parallel^{z+b'}$. Hence, the curvature physics will be dominated by the smaller of the two correction-to-scaling exponents b and b'. Note that if $b_\kappa = \min(b, b') < 1$ the physical Fermi surface curvature diverges at the hot spot.

In Refs. 17,21 the one-loop RG flow of α was determined to be,

$$\frac{d\alpha}{d\ell} = -\frac{3}{\pi N}\frac{\alpha^2}{1+\alpha^2} \tag{5.20}$$

which has a fixed point at $\alpha^* = 0$. The flow towards the fixed-point is logarithmic, resulting in the Fermi surface shape,

$$k_y = \frac{3}{\pi N}k_x \log(\Lambda/|k_x|) \tag{5.21}$$

whose curvature $\kappa(k_y) \sim |k_y|^{-1}\log^{-2}(\Lambda/|k_y|)$. Hence, in this case we may write $b' \to 0^+$. However, it was found in Ref. 21 that all anomalous dimensions diverge in the limit $\alpha \to 0$ so we are not in a position to perform a careful analysis of the physics at the $\alpha^* = 0$ fixed point. Since the $1/N$ expansion in Refs. 17,21 is uncontrolled, it is quite possible that higher order calculations give a flow of the more conventional form (5.19) with $b' \neq 0$ and $\alpha^* \neq 0$.

We conclude that for lukewarm fermions there exists a window $k_\parallel^{b_\kappa+z} \ll \omega \ll k_\parallel^z$ in which the Fermi surfaces can be regarded as straight and effectively one-dimensional divergences of the form (5.18) appear.[4] In a truly one-dimensional system such logarithmic divergences sum up to a power-law giving rise to Luttinger-liquid physics. A more detailed analysis is needed to conclude whether an analogous phenomenon takes place in our system or if the divergences of the type (5.18) lead to an instability. In either case, the Green's function will not have the quasiparticle form (2.12) in the lukewarm region $\omega \ll k_\parallel^z$. Well-defined quasiparticles may reemerge at the lowest energies where the Fermi surface curvature plays a role, however, the behavior of the quasiparticle residue and Fermi velocity will differ from Eq. (2.13). Also, our estimate of the lower boundary of the intermediate energy window $\omega_\kappa \sim k_\parallel^{b_\kappa+z}$ was based on the assumption that fermionic quasiparticles are well defined in this window. As argued above this assumption is likely incorrect and a detailed understanding of the physics in this window is needed in order to estimate the energy scale at which curvature effects become important.

---

[4] If the one-loop flow of α, Eq. (5.20), is assumed, this window is only logarithmically wide.

In Section VI B below, we will discuss the contribution of these one-dimensional scatterings to the optical conductivity. Before doing this, we note that in addition to the 'one-dimensional' contribution to the self energy in Fig. 17 b), there is also a 'two-dimensional' contribution from the region where both the intermediate 1, -1 and 2,-2 are on shell. This contribution is not sensitive to whether the Fermi surface is curved, but is sensitive to whether it is nested. We will discuss this contribution in the remainder of the present section.

2. Low energy effects of Fermi surface curvature

As noted in section IV B, the explicit Fermi surface curvature perturbation, (4.15), generates a new energy scale $\omega \sim \kappa_0 k_\parallel^{z+b}$. At this scale the Fermi surface realizes that it is not nested with respect to the $2k_F$ wavevector and the BCS-like divergences in the particle-hole channel are cut off. Note that if the exponents b, b' in Eqs. (4.16), (5.19) satisfy $b < b'$, then this is also the energy scale at which the Fermi surface can no longer be treated as flat. Furthermore, it was enhancements at this scale that lead to the $2k_F$ instability in Refs. 13,21. In the remainder of this section we will look at the physics of $2k_F$ scattering in the regime where this curvature scale is being saturated. We will find that, while formally irrelevant as per the discussions of section IV B, the inclusion of curvature perturbation (4.15) leads to low energy scalings that are stronger than those arising from naïve dimensional analysis in the hot spot theory.

The basic object illustrating how curvature generates new energy scalings in the $2k_F$ channel is the propagator for the CDW operator $\psi_2^{1\dagger}\psi_2^3$. The tree level and leading corrected propagator for this density channel mode are shown in figure 19. Two vertex corrections
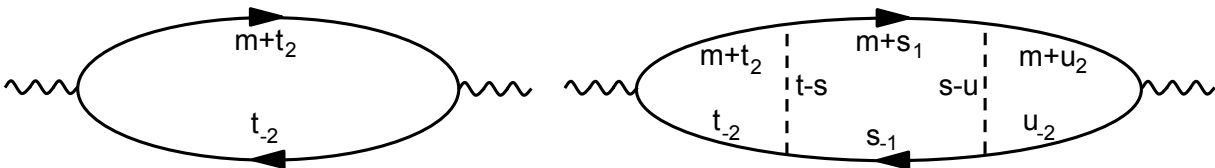

FIG. 19: Tree level (left) and leading correction (right) to the propagator for the operator $\psi_2^{1\dagger}\psi_2^3$. The subscripts show the hot spot involved. 1 and -1 correspond to the $a = 1$ hot spots of the $\ell = 1$ and $\ell = 3$ pair of hot spots, respectively. Similarly, 2 and -2 correspond to the $a = 2$ hot spots of the $\ell = 1$ and $\ell = 3$ pair.

are necessary because there is mixing between $\psi_2^{1\dagger}\psi_2^3$ and $\psi_1^{1\dagger}\psi_1^3$. These graphs are entirely analogous to those of figure 17 above. Here we are considering the density channel propagator as a quantity in its own right.

As in the previous subsection we can use the lukewarm inverse propagators following from (2.18) and (2.12). As we are now interested in saturating the scale at which curvature

terms violate Fermi surface nesting, we will include such a curvature explicitly in the fermion propagators

$$G_{\pm 2}^{-1}(q) = \mp v q_\perp + \frac{3\gamma v}{16N} \frac{i q_\tau}{|q_\parallel|} - \kappa q_\parallel^2 \,. \tag{5.22}$$

In this equation we are defining parallel and perpendicular with respect to the $\ell = 1, a = 2$ Fermi surface. We are being somewhat simpleminded here in just adding the irrelevant curvature coupling without systematically checking how this term backreacts on our previous results. The results of this subsection should be taken as a preliminary investigation into new scaling effects arising from the interplay of hot spot criticality with Fermi surface curvature.

Much of the interesting physics is already visible in the leading tree level term, left in Fig. 19. This diagram is evaluated in Appendix E. The difference relative to previous computations in this paper is that the curvature in (5.22) leads to a new low energy contribution due to fermions saturating the curvature scale. We focus on this contribution, which in fact gives the most singular terms at low energy and momenta

$$C^{(0)}(m) = -\frac{c_1}{2} \frac{(\gamma|m_\tau|)^{2/3}}{(c_2\kappa/v)^{2/3}} \sum_i \frac{3 + 2r^2 x_i + 4r x_i^2}{r^2 + 8r x_i + 12x_i^2} \log \frac{-x_i \kappa^2 (\gamma|m_\tau|)^{2/3}}{(c_2\kappa/v)^{2/3}} \,. \tag{5.23}$$

Here r is the ratio of momentum and energy

$$r = \frac{m_{\perp,2}}{(\gamma|m_\tau|)^{2/3}} \frac{c_2^{2/3}}{(\kappa/v)^{1/3}} \,, \tag{5.24}$$

and the x_i are the three roots of the polynomial

$$4x^3 + 4rx^2 + r^2 x + 1 = 0 \,. \tag{5.25}$$

The notation $m_{\perp,2}$ refers to the component of m perpendicular to the $\ell = 1, a = 2$ Fermi surface. The constants

$$c_1 = \frac{4N}{3\pi^2 \gamma v^2} \,, \qquad c_2 = \frac{16N}{3} \,. \tag{5.26}$$

The physical point here is that the scaling $m_\tau^{2/3}$ of the result (5.23) is both stronger than the dimensional analysis scaling for this dimension $\Delta = 3$ operator, which from (5.4) would be $C(m) \sim m_\tau$, and also weaker than the full BCS Fermi surface singularity $C(m) \sim \Lambda_\parallel^2 \log m_\tau$. This intermediate result is due to the interplay of Fermi surface curvature in the particle channel with the criticality of the lukewarm fermions. In particular the overall scaling power $m_\tau^{2/3}$ arises from the dimensionality of the operator together with the fact that, from (5.22), the curvature kicks in at the scale

$$\frac{v\gamma}{N} m_\tau \sim v m_\perp m_\parallel \sim \kappa m_\parallel^3 \,. \tag{5.27}$$

This tree level term does not capture, however, the physics of the enhancement of the

particle-hole channel that leads to a pairing instability[13,21]. These effects are contained in the vertex corrections of the right hand diagram in figure 19. This diagram is also studied in Appendix E. The most singular low energy terms, at leading order in singular logarithms, are found to be

$$C^{(1)}(m, \Lambda_\parallel) = \frac{c_1^3}{32} \frac{(\gamma |m_\tau|)^{2/3}}{(c_2 \kappa/v)^{2/3}} \log^2 \tilde{\Lambda}_\parallel^2 \log^2 \tilde{\kappa}^{8/3} \tilde{\Lambda}_\parallel^2 \tag{5.28}$$

$$\times \sum_i \left(\log(-x_i) x_i - \log(-y_i) \frac{3 + 2\bar{r}^2 y_i + 4\bar{r} y_i^2}{\bar{r}^2 + 8\bar{r} y_i + 12 y_i^2} \right) .$$

Here we introduced the analogous ratio to (5.24) for the $\ell = 1, a = 1$ Fermi surface

$$\bar{r} = \frac{m_{\perp,1}}{(\gamma |m_\tau|)^{2/3}} \frac{c_2^{2/3}}{(\kappa/v)^{1/3}} , \tag{5.29}$$

and the y_i are now the three roots of the polynomial

$$4y^3 + 4\bar{r} y^2 + \bar{r}^2 y + 1 = 0 . \tag{5.30}$$

Finally, we set

$$\tilde{\Lambda}_\parallel^2 = \frac{(c_2 \kappa/v)^{2/3}}{(\gamma |m_\tau|)^{2/3}} \Lambda_\parallel^2 , \qquad \tilde{\kappa}^2 = \gamma |m_\tau| \left(\frac{c_2 \kappa}{v} \right)^2 . \tag{5.31}$$

We must keep track of the dependence on the momentum cutoff $\Lambda_\parallel$. The above result describes the leading order singular behaviour in m_τ with the ratios $r, \bar{r}$ held fixed. As with the $2k_F$ vertex[21], the bosonic vertex corrections lead to singular logarithmic enhancements upon saturating the curvature scale (5.27). Here there are surviving overall powers of momentum that will then be evaluated at this scale, leading to the overall power of $m_\tau^{2/3}$. Note that (5.28) depends upon both momenta $m_{\perp,1}$ and $m_{\perp,2}$.

To summarize: the $2k_F$ propagator (5.28) contains two physical effects. The first is the $m_\tau^{2/3}$ (rather than m_τ) scaling, due the combination of hot spot scaling and saturation of the curvature scale, and the second is the presence of logarithmic enhancements due to both cut off BCS divergences and also vertex corrections.

We can now turn to the self energy (5.5) due to scattering off the enhanced $2k_F$ mode. As discussed above, curvature will restrict efficient scattering off this mode to be near the hot spot, so we take the intermediate fermion to be lukewarm rather than cold. Thus

$$\Sigma(q) = -\frac{\lambda_2^2}{\kappa^{2/3}} \int \frac{d^3 m}{(2\pi)^3} \frac{|m_\tau|^{2/3} \widetilde{C} \left(\frac{m_{\perp,1}}{\kappa^{1/3} m_\tau^{2/3}}, \frac{m_{\parallel,1}}{\kappa^{1/3} m_\tau^{2/3}} \right)}{\frac{\gamma v}{c_2} \frac{i(q_\tau - m_\tau)}{|q_\parallel - m_{\parallel,1}|} + v(q_\perp - m_{\perp,1}) - \kappa (q_\parallel - m_{\parallel,1})^2} . \tag{5.32}$$

We must be careful here to keep track of the different components of m relative to the ± 1 and ± 2 Fermi surfaces. The scaling of $\widetilde{C}$ suggested in (5.32) is violated by logarithmic terms

in (5.23) and (5.28). The above expression for the self energy is rather similar to the one we encountered previously in (5.4) and (5.5) with an effective $z = 3/2$ induced by Fermi surface curvature effects. The crucial difference however is that the fermion propagator in (5.32) is on the -1 Fermi surface, while it is contributing to the self energy of a fermion on the $+1$ Fermi surface. In particular the two fermions have opposite Fermi velocities. If we were to put both of the fermions precisely on their Fermi surfaces (i.e. $q_\perp = \pm q_\parallel^2$, respectively) the missing momentum gets sent through the critical mode and moves its momentum away from $2k_F$, thereby spoiling the enhancement we are looking for. Instead we can expect that the most efficient scattering will again occur upon saturating the curvature, i.e. when the external fermion has

$$\frac{q_\tau}{q_\parallel} \sim q_\perp \sim \kappa q_\parallel^2 \,. \tag{5.33}$$

Inspecting (5.32) we can now ask what scaling regime of the m energy and momenta will dominate the integral. The immediate choices are either to respect the scaling of the critical mode $\widetilde{C}$ for both components of the momentum, or to make the denominator have an overall scaling. The latter possibility in fact takes us back to the one-dimensionality of the previous subsection, so here we consider the former case. Thus we take

$$m_\tau = q_\tau x \,, \qquad m_{\perp,1} = q_\tau^{2/3} \kappa^{1/3} y \qquad m_{\parallel,1} = q_\tau^{2/3} \kappa^{1/3} z \,. \tag{5.34}$$

This implies that in the regime (5.33) $m_{\parallel,1} \ll q_\parallel$. We thereby obtain (taking $q_\tau > 0$ for simplicity)

$$\Sigma(q) = -\frac{\lambda_2^2}{\kappa^{1/3}} q_\tau^{2+1/2} \int \frac{dx\,dy\,dz}{(2\pi)^3} \frac{|x|^{2/3} \widetilde{C}\left(\frac{y}{x^{2/3}}, \frac{z}{x^{2/3}}\right)}{\frac{\gamma v}{c_2} i(1-x)\frac{q_\tau^{1/3}}{\kappa^{1/3}|q_\parallel|} + v\left(\frac{q_\perp}{\kappa^{1/3} q_\tau^{2/3}} - y\right) - \frac{\kappa^{2/3} q_\parallel^2}{q_\tau^{2/3}}} \,. \tag{5.35}$$

The denominator here is order one within the scaling regime and for external momenta satisfying (5.33).

To make sense of (5.35) we should recall that in our lukewarm regime the coupling $\lambda_2 \sim 1/q_\parallel^2$. This is because we collapsed a boson propagator (2.14) in generating the interaction (4.17). This collapsing involved taking $q_\parallel$ to be larger than the momenta running in the various loops that we computed to obtain (5.28). Thus the cutoff in (5.28) is $\Lambda_\parallel \sim q_\parallel$. Combined with the scaling regime we are considering, given by (5.33) and (5.34), we can see that this cutoff dependence on $q_\parallel$ will remove two of the four powers of $\log q_\tau$ that are violating the scaling of $\widetilde{C}$. Thus in fact the logarithmic enhancements in the propagator due to vertex corrections (as opposed to BCS logs) do not contribute to this observable. Putting

41

these facts together we can write schematically

$$\Sigma(\omega, \vec{q}) \sim -i\mathrm{sgn}(\omega)\frac{1}{\kappa^{1/3}}\frac{|\omega|^{2+1/3}}{q_{\parallel}^4}\log^2|\omega|\, F\left(\frac{q_{\parallel}}{(\omega/\kappa)^{1/3}}, \frac{q_{\perp}}{(\kappa\,\omega^2)^{1/3}}\right) \qquad (5.36)$$

$$\sim -i\mathrm{sgn}(\omega)\frac{|\omega|^2}{q_{\parallel}^3}\log^2|\omega|\, \widetilde{F}\left(\frac{q_{\parallel}}{(\omega/\kappa)^{1/3}}, \frac{q_{\perp}}{(\kappa\,\omega^2)^{1/3}}\right)\,. \qquad (5.37)$$

In the second line we have rescaled away the explicitly singular dependence on the curvature κ using $q_{\parallel} \sim (\omega/\kappa)^{1/3}$. This modifies the overall function: $F \to \widetilde{F}$. We are restricting ourselves to the regime (5.33) where the overall functions F and $\widetilde{F}$ are of order 1.

The self energy (5.37) is logarithmically stronger than the result of the rainbow approximation Eq. (2.20). It is also stronger than the naïve hot spot scaling $\Sigma \sim \omega^{5/2}/q_{\parallel}^4$ for scattering off the hot operator $\psi_2^{1\dagger}\psi_2^3$. Because of the instability in the $2k_F$ channel[13,21], resumming these logarithms presumably leads to a singularity below a critical frequency.

VI. CONDUCTIVITY FROM COMPOSITE OPERATORS

A. Conductivity due to neutral zero momentum operators

We are now in a position to compute the contribution to the conductivity of the various processes we have discussed. Consider first the conductivity due to scattering off neutral and zero momentum operators. We have derived the formula (4.26) as giving the leading low energy contribution to the current-current correlator in this case. As a warmup and for later use we can first compute the (ultimately cancelled) contribution due to self energy corrections (4.8). Using (5.1), this can be written in terms of the self energy as

$$\delta^{(a+b)}\Pi_{ij}^{\mathrm{cold}}(\omega) = \frac{2}{\omega^2}\int\frac{d^3q}{(2\pi)^3}v_i^{\star}v_j^{\star}G(q)\Big(\Sigma(p+q) + \Sigma(-p+q) - 2\Sigma(q)\Big)\,. \qquad (6.1)$$

Using the propagator for the cold fermions (4.2) and the singular contribution to the self energy (5.9), we first perform the integral over $q_{\perp}$, and then pick out the non-analytic term in the integral over q_{τ} to obtain

$$\delta^{(a+b)}\Pi_{ij}^{\mathrm{cold}}(\omega) = -\frac{4\,c\,|\omega|^{\kappa-1}}{\kappa+1}\int\frac{dq_{\parallel}}{(2\pi)^2}\frac{\lambda_1^2\,v_i^{\star}v_j^{\star}}{v^{\star\,2}}\,. \qquad (6.2)$$

Here $q_{\parallel}$ should be thought of as the integral along the different patches on the Fermi surface. Continuing to real time, it is then clear from the definition of the electrical conductivity in (3.2) that this contribution to the conductivity would have scaled as

$$\delta^{(a+b)}\sigma(\Omega) \sim \lambda_1^2\Lambda_{\parallel}\Omega^{\kappa-2}\,. \qquad (6.3)$$

For general κ this contribution contains both real and imaginary parts. Here $\Lambda_{\parallel}$ is a UV cutoff on the $q_{\parallel}$ integral in (6.2). We can estimate its value as the Fermi momentum $\Lambda_{\parallel} \sim m^{\star} v^{\star}$.

As we saw above, the actual leading contribution to the conductivity is (4.26) while the contribution we have just discussed gets cancelled. It is easy to see what the effect of the extra two insertions of momenta along the Fermi surface in (4.26) will be without doing any additional integrals. The momenta appear as $q_{\parallel}^2$ in (5.7). Upon moving to dimensionless variables as in equation (5.8) and below, the effect of these two extra powers of momentum will be to shift the exponent $\kappa \to \kappa + 2/z$ in what was previously the self energy. Then, following the same manipulations as we have above, we can conclude that the leading nonzero conductivity due to cold fermions scattering off neutral zero momentum operators is

$$\delta\sigma(\Omega) \sim \frac{\lambda_1^2}{v^{\star} m^{\star}} \Omega^{\kappa + 2/z - 2} . \tag{6.4}$$

Here we used the estimate $\Lambda_{\parallel} \sim m^{\star} v^{\star}$. Returning once again to the simplest example $\mathcal{O} = \phi^2$, at the level of Hertz-Moriya-Millis theory, our previous observation that $\kappa = \frac{3}{2}$ implies that $\delta\sigma(\Omega) \sim \Omega^{1/2}$. This is a weak low frequency dependence, comparable to the hot contribution to the conductivity (3.31). Presumably operators which are higher order polynomials in fields and derivatives have increasingly higher values of κ and are thereby increasingly irrelevant. Scattering off the $\mathcal{O} = \phi^2$ operator becomes more significant if z and Δ are renormalised such that z becomes larger and Δ smaller than the Hertz-Moriya-Millis values. At present a controlled computation of z and Δ in the theory is not available. Given z and Δ our formulae for the conductivities are presumably reliable so long as our effective interactions do not destroy the cold fermion quasiparticles. This is potentially compatible with non-Fermi liquid behavior of optical conductivity.

A check of the formulae (6.3) and (6.4) comes from comparing with Ref. 44. The theory studied in that paper had $\kappa = 2/3$ and $z = 3$. It was found that the individual self energy and vertex corrections to the conductivity scaled as $\Omega^{-4/3}$, while the total conductivity scaled as $\Omega^{-2/3}$. These results are in agreement with our expressions.

Also following Ref. 44 it is tempting to note that the leading scaling behavior (6.4) can be obtained somewhat naïvely from a modified Drude formula. Introduce the scattering rate

$$\frac{1}{\tau} \sim \text{Im}\Sigma(\Omega) \sim \Omega^{\kappa} . \tag{6.5}$$

The transport scattering rate involves the usual extra factor of $1 - \cos\theta$, with θ the angle between the initial and final fermion wavevectors. At low momenta and with the boson on shell as above $1 - \cos\theta \sim p^2/k_F^2 \sim \Omega^{2/z}$. Thus the transport scattering rate is

$$\frac{1}{\tau_{\text{tr.}}} \sim \Omega^{\kappa + 2/z} . \tag{6.6}$$

Now write down a generalized Drude formula

$$\operatorname{Re} \sigma(\Omega) \sim \frac{\tau_{\text{tr.}}^{-1}}{\Omega^2 + \tau_{\text{tr.}}^{-2}} \,. \tag{6.7}$$

As long as $\kappa + 2/z > 1$, at low frequency we may drop $\tau_{\text{tr.}}^{-2}$ in the denominator of Eq. (6.7). Using (6.6) the leading answer is then

$$\operatorname{Re} \delta\sigma(\Omega) \sim \Omega^{\kappa + 2/z - 2} \,, \tag{6.8}$$

in agreement with our previous (6.4).

It is further tempting, in the formulation of the previous paragraph, to take the $\Omega \to 0$ limit of the Drude formula (6.7) and further exchange the frequency dependence of the transport scattering rate (6.6) for temperature dependence. Doing this one would obtain a resistivity $\rho \sim T^{\kappa + 2/z}$. For the case $\mathcal{O} = \phi^2$ at a mean field level this translates into the weak resistivity $\rho \sim T^{5/2}$. This reasoning is however unlikely to be correct: it does not account for the key physics of how the delta function in the conductivity at $\Omega = 0$ is resolved through the umklapp scattering which is implicitly included in our theory (2.1), because pseudospin symmetry has played no role.

Before moving on, it is instructive to rewrite our result (6.4) as

$$\delta\sigma(\Omega) \sim \Omega^{(2\Delta + 1)/z - 2} \,. \tag{6.9}$$

This expression shows how a moderately large renormalised value of z enhances the effect of scattering off composite hot bosonic modes. In particular at large values of z the cancellation between self energy and vertex corrections becomes increasingly insignificant. This observation does not immediately appear to be related to the $z = \infty$ non Fermi liquids recently discussed holographically and otherwise[51,52]. We can note that $\Delta \sim z/2$ at large z will give a linear in temperature resistivity according to the simple discussion of the previous paragraph. While the usual unitarity bound on operator dimensions at a fixed point requires a full conformal symmetry, at least in some holographic settings the dimensions of scalar operators (in two spatial dimensions) are bounded by $\Delta \geq z/2$. This follows from adapting the finite action argument of Ref. 53 to the case[54] of a general z. These holographic setups do not include the spatial anisotropy for the critical theory we are studying in this paper.

B. Conductivity due to $2k_F$ modes

1. One-dimensional contribution

In section IV B we observed that there was no cancellation between vertex and self energy corrections for scattering off hot $2k_F$ CDW fluctuations. However, as discussed in section V B

in our theory the self energy in the $2k_F$ channel, Fig. 17b), is actually not dominated by the hot contribution, so the formalism in section IV B is not directly applicable. Nevertheless, as a first estimate we will ignore vertex corrections in the computation of the conductivity here. Then, similarly to the previous subsection,

$$\delta\Pi_{ij}(\omega) = \frac{1}{\omega^2}Nv_iv_j \int \frac{d^3k}{(2\pi)^3} Z^2(k_\parallel)G(k)(\Sigma(k+\omega) + \Sigma(k-\omega) - 2\Sigma(k)). \qquad (6.10)$$

Using the self energy, Eq. (5.18), we compute the integral above as in Eq. (6.1) to estimate,[5]

$$\delta\Pi(\omega) \sim \frac{1}{\gamma}\int dk_\parallel k_\parallel \log\frac{k_\parallel^2}{\gamma|\omega|}. \qquad (6.11)$$

The integral over the momentum $k_\parallel$ along the Fermi surface in Eq. (6.11) will be cut-off by the Fermi surface curvature. As estimated in section V B, curvature effects set in once $\omega \lesssim k_\parallel^{z+b_\kappa}$. Hence, setting $z = 2$ and ignoring logarithmic corrections,

$$\delta\sigma(\Omega) \sim (-i\Omega)^{-b_\kappa/(2+b_\kappa)}. \qquad (6.12)$$

Note that Eq. (6.12) holds as $\Omega \to 0$ (at $T = 0$); the energy scale set by the curvature, $\omega_\kappa(k_\parallel) \sim k_\parallel^{b_\kappa+z} \to 0$ as $k_\parallel \to 0$, and so the one-dimensional contribution appears at the lowest energy scales.

Clearly Eq. (6.12) is sensitive to the exponent b_κ, which controls the physical Fermi surface curvature. As discussed in section V B our understanding of this exponent is rather limited. If one assumes the one-loop flow of α, Eq. (5.20), then $b_\kappa \to 0^+$ and the correction in Eq. (6.12) is expected to be only logarithmic.

One should ask if vertex corrections strongly modify the result in Eq. (6.12). This question is particularly pressing due to the one-dimensional nature of the self energy divergence (5.18), which translates into the conductivity (6.12). In a purely one-dimensional system away from half-filling, at leading order in energy the electrical current would be proportional to the conserved electron momentum and so the finite frequency conductivity would vanish. Indeed, the simplified process in Fig. 18 naively looks like a forward-scattering process, which cannot contribute to the conductivity. However, unlike in a purely one-dimensional system, the intermediate 1 and -1 fermions in Fig. 18 possess a coordinate along the Fermi surface. The physical 'on shell' current vertex $Z(k_\parallel)\Gamma(\omega,k_\parallel)$ depends on this coordinate and hence we don't expect the cancellation between the self energy and vertex corrections to occur. Note that in the calculation leading to (6.12) we've used the bare current vertex $\Gamma_i(\omega,k_\parallel) = v_i$.

---

[5] Strictly speaking Eq. (5.18) represents only the self energy on the Fermi surface. However, inclusion of the dependence on momentum perpendicular to the Fermi surface does not qualitatively modify the result (6.11).

In principle, a systematic analysis of the current vertex which takes into account both the one-dimensional divergences in Section V B and the rainbow graphs in Section III is needed. Such an analysis is, however, outside the scope of this paper.

2. 'Enhanced critical umklapp'

With similar caveats to the discussion immediately above, we can estimate the contribution to the conductivity from the $2k_F$ channel when fermion loops are saturating the Fermi surface curvature scale. Using our result (5.37) of $\Sigma(\omega) \sim \omega^2/q_\parallel^3 \log^2 |\omega|$ and repeating the arguments of the previous subsection, or directly using the scaling (5.33), leads to

$$\delta\sigma(\Omega) \sim v^2 \log^2 \Omega \int^{\Omega^{1/3}} \frac{Z(q_\parallel)^2}{q_\parallel^3} dq_\parallel \sim v^2 \log^3 \Omega \,. \tag{6.13}$$

This is a stronger than Fermi liquid conductivity. To accurately describe this contribution we would have to consider the effect of resumming logarithms, and also the effects of Fermi surface curvature on the vertex correction computation in Section III.

C. Conductivity due to fluctuating critical modes

As well as the diagrams we have been considering, studies of quantum critical response (e.g. Ref. 44) or fluctuating superconductivity response (e.g. Ref. 49) also consider Aslamazov-Larkin type diagrams in which two separate fermion loops are connected via a pair of bosons. This graph is higher order in the couplings λ_i. We have seen above that in the mean field Hertz-Moriya-Millis level these couplings appear to in fact be irrelevant. Therefore we expect such higher order graphs to be suppressed in our low frequency $T = 0$ computations. However, because the parameters z and Δ will get renormalised, it is of interest to see what scaling is obtained from these graphs in general and whether there are cases in which this contribution can dominate. For instance in Ref. 44 such fluctuating criticality contributions were found to scale equally to the vertex and self energy corrections we have considered so far. At the end of this subsection we will give a scaling argument showing that the condition for the λ_i couplings to be relevant is that $\Delta < \frac{3}{2}$, independently of z. Let us first see this emerge from an explicit computation.

We can consider first the case of neutral and zero momentum critical operators. The two Feynman diagrams we are interested in are shown in figure 20. These two contributions can be written, using the leading order momentum-independent term in the currents (4.4),

$$\delta^{(d+e)}\Pi_{ij}^{\text{cold}}(\omega) \propto \lambda_1^4 \int \frac{d^3q}{(2\pi)^3} \frac{d^3r}{(2\pi)^3} \frac{d^3s}{(2\pi)^3} v_i^\star v_j^\star G(p+q) G(q) G(p+s) G(s) G(q+r)$$

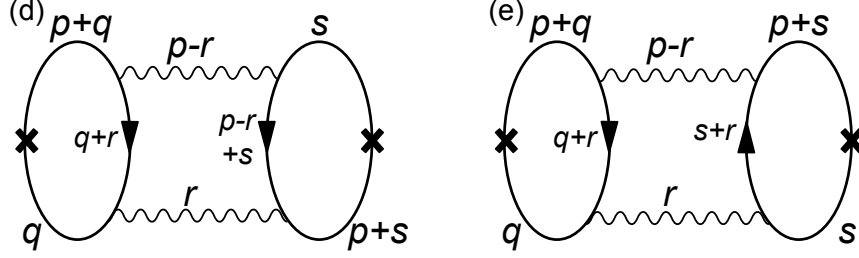$$\times C(r) C(p-r) \Big(G(p-r+s) + G(r+s) \Big) \,. \tag{6.14}$$

FIG. 20: The two diagrams describing the contribution to the conductivity of the cold fermions due to critical fluctuations. The wavy lines denote propagators of the neutral bosonic quantum critical operator $\mathcal{O}$.

We will not keep track of numerical prefactors in this subsection. As above, we must recall that the spatial components of the external momentum p vanish, so that $p = (\omega, 0, 0)$. This allows us to use the identity (4.7) twice on the first four Green's functions in the above equation. Relabeling momentum integrals then shows that the two diagrams precisely cancel, so that

$$\delta^{(d+e)}\Pi_{ij}^{\text{cold}}(\omega) = 0 \,. \tag{6.15}$$

An analogous cancellation was observed in Ref. 44. In order to obtain a nonzero contribution we will need to include the momentum-dependent term in the current, the second term in (4.4), as we did in section IV C for the vertex and self energy corrections which also cancelled. As in section IV C one finds that the cross term $\langle J_\perp^{\text{cold}} J_\parallel^{\text{cold}} \rangle$ also gives a vanishing contribution (upon using evenness of $C(r)$) while the term $\langle J_\parallel^{\text{cold}} J_\parallel^{\text{cold}} \rangle$ gives the nonvanishing answer

$$\delta^{(d+e)}\Pi_{ij}^{\text{cold}}(\omega) \propto -\frac{1}{\omega^2}\frac{\lambda_1^4}{m^{\star 2}} \int \frac{d^3q}{(2\pi)^3}\frac{d^3r}{(2\pi)^3}\frac{d^3s}{(2\pi)^3}(r_\parallel)_i(r_\parallel)_j C(r)C(p-r)$$
$$\times G(s)G(q)G(q+r)\Big(G(s+r) - G(s+r-p)\Big). \tag{6.16}$$

Before evaluating this expression we turn to the case of finite momentum critical modes, which once again is seen to exhibit no cancellation.

The two diagrams describing critical fluctuations of modes carrying momentum $2k_F$ are shown in figure 21. To properly account for the two opposite patches of the Fermi surface involved, we must again use the expression (4.18) for the current. As before, the relative minus sign in the contribution to the current from the two patches is crucial. The diagrams in the figure evaluate to

$$\delta^{(d+e)}\Pi_{ij}^{\text{cold}}(\omega) \propto \lambda_2^4 \int \frac{d^3q}{(2\pi)^3}\frac{d^3r}{(2\pi)^3}\frac{d^3s}{(2\pi)^3} v_i^\star v_j^\star G(p+q)G(q)\widetilde{G}(q+r)$$
$$\times C(-r)C(p-r)\Big(\widetilde{G}(p+s)\widetilde{G}(s)G(p-r+s) - G(p+s)G(s)\widetilde{G}(r+s)\Big). \tag{6.17}$$
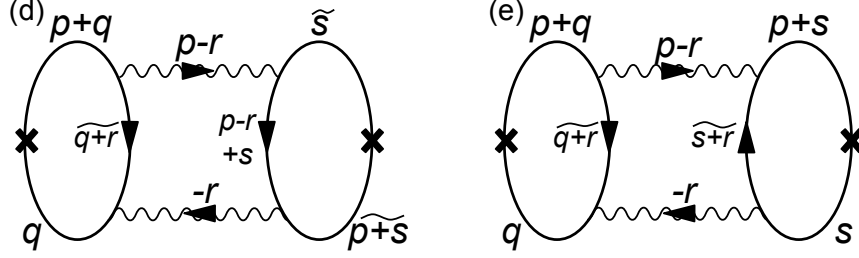
47

FIG. 21: The two diagrams describing the contribution to the conductivity of the cold fermions due to neutral critical fluctuations carrying momentum $2k_F$. Tildes over momenta indicate that the fermion propagator in question corresponds to the opposite patch. The hot operator $\mathcal{O}$ is now complex and so its propagators carry an arrow.

Performing the same operations as outlined above for zero momentum critical operators, we find that the terms now add rather than cancel. The result can be expressed as

$$
\delta^{(d+e)}\Pi_{ij}^{\text{cold}}(\omega) \propto \frac{\lambda_2^4}{\omega^2} \int \frac{d^3q}{(2\pi)^3} \frac{d^3r}{(2\pi)^3} \frac{d^3s}{(2\pi)^3} v_i^\star v_j^\star C(-r) C(p-r) G(q) G(s)
$$
$$
\times \left(\widetilde{G}(s+r) - \widetilde{G}(s+r-p) \right) \left(\widetilde{G}(q+r) - \widetilde{G}(q+r-p) \right) . \tag{6.18}
$$

Finally, we can consider fluctuations of zero momentum but charged critical modes. The two relevant diagrams are shown in figure 22. While we will not write out the expressions
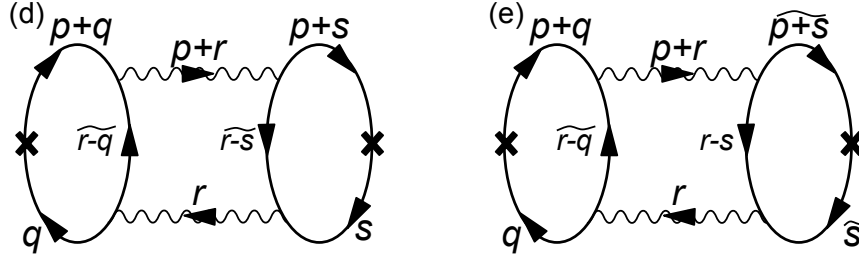

FIG. 22: The two diagrams describing the contribution to the conductivity of the cold fermions due to charged Cooperon-like critical fluctuations.

explicitly in this case, one can easily check that there is again a cancellation between the two diagrams. Therefore curvature terms in the current operator must be included and an expression similar to (6.16) is obtained for the current correlator.

We can now evaluate the momentum integrals to obtain the frequency scaling of these contributions to the conductivity. We will only evaluate the neutral and zero momentum case. Using the cold fermion Green's function (4.2), the scaling form (5.4) for the critical modes, and taking the critical modes to have momentum tangent to the Fermi surface as per the discussion in the paragraph below equation (5.5) above, it is easy to perform the

$\{q_\perp, q_\tau, s_\perp, s_\tau, r_\perp\}$ integrals in (6.16) to obtain

$$\delta^{(d+e)}\Pi_{ij}^{\text{cold}}(\omega) \propto \frac{i}{\omega^2} \frac{\lambda_1^4}{v^{\star 4} m^{\star 2}} \int \frac{dr_\parallel ds_\parallel dq_\parallel}{(2\pi)^3} \frac{(r_\parallel)_i (r_\parallel)_j}{r_\parallel(s_\parallel - q_\parallel)/m^\star v^\star + i\omega/v^\star} \times$$
$$\int_0^\omega \frac{dr_\tau}{r_\tau^{(2-2\Delta)/z}(\omega - r_\tau)^{(2-2\Delta)/z}} \widetilde{C}\left(\frac{r_\parallel}{r_\tau^{1/z}}\right) \widetilde{C}\left(\frac{r_\parallel}{(\omega - r_\tau)^{1/z}}\right) . \tag{6.19}$$

This expression is not yet ready to be put in a scaling form because of the curvature terms that have survived in the denominator of the last term in the first line. However, we can now symmetrise in $q_\parallel$ and $s_\parallel$ and then perform the $s_\parallel$ integral which is convergent. Then setting $r_\tau = \omega x$ and $r_\parallel = \omega^{1/z} y$ we obtain

$$\delta^{(d+e)}\Pi_{ij}^{\text{cold}}(\omega) \propto -\frac{\omega^{(4\Delta-2)/z}}{\omega} \frac{\lambda_1^4}{v^{\star 3} m^\star} \int \frac{dy dq_\parallel}{(2\pi)^2} \frac{y_i y_j}{y} \times$$
$$\int_0^1 \frac{dx}{[x(1-x)]^{(2-2\Delta)/z}} \widetilde{C}\left(\frac{y}{x^{1/z}}\right) \widetilde{C}\left(\frac{y}{(1-x)^{1/z}}\right) . \tag{6.20}$$

Taking the frequency scaling from the above formulae and using the expression for the conductivity (3.2) we obtain the singular (i.e. scaling) conductivity due to fluctuating critical modes

$$\delta^{(d+e)}\sigma(\Omega) \sim \Omega^{(4\Delta-2)/z-2} . \tag{6.21}$$

Comparing with our previous result (6.9) for the self energy and vertex contribution, we see that the fluctuating criticality contribution dominates if $\Delta \leq \frac{3}{2}$, independently of z. In particular when $\Delta = \frac{3}{2}$, the two contributions are equal, in agreement with the results of Ref. 44. While, as above, for $\mathcal{O} = \phi^2$ this contribution is not strong with the mean field values of exponents, that is $z = 2, \Delta = 2$, it is interesting to note in passing that if the dimension of this operator was renormalized down to the holographically motivated 'bound' we mentioned above, $\Delta = z/2 = 1$, then we would obtain a conductivity $\sigma = \Omega^{-1}$.

The condition $\Delta \leq \frac{3}{2}$ for the effective λ_i couplings to be relevant, and hence strong at low energies, can be derived from the following scaling argument. Exchange of a critical boson generates an effective four fermion interaction. The total cold fermion action is

$$S_\psi \sim \int d^3x \left[\psi^2\left(-i\omega + v^\star k_\perp + k_\parallel^2/2m^\star\right) + \lambda^2 \psi^4 \omega^{-(z+2-2\Delta)/z} \widetilde{C}\left(k_\parallel/\omega^{1/z}\right)\right] . \tag{6.22}$$

We are being schematic here, as we only wish to keep track of power counting. The natural scaling to consider, given this action, is

$$t \to s^z t, \quad x_\parallel \to s x_\parallel, \quad x_\perp \to s^2 x_\perp . \tag{6.23}$$

From the quadratic term we see that the fermion field ψ has dimension $(z+1)/2$ under this scaling action. The effective coupling after scaling is thus easily seen to be $\lambda^2 s^{3-2\Delta}$. At low

energies, $s \to \infty$, the interaction therefore becomes relevant if $\Delta \leq \frac{3}{2}$.

VII. CONCLUSIONS

We have analyzed the fermion spectrum and the optical conductivity at the quantum critical point describing the onset of spin density wave order in a two-dimensional metal. We focused on the universal character of the results as described by a recently developed low energy theory[21].

An appealing property of this low energy theory is that it has a finite d.c. conductivity at non-zero temperatures. This is a consequence of an emergent pseudospin symmetry which decouples the electrical current from the conserved momentum; umklapp processes are implicitly included in our continuum theory. Consequently there is no delta function in the conductivity at $\omega = 0$, and the d.c. conductivity is dominated by interactions among low energy excitations, leading to hopes of a universal non-Fermi liquid behavior. In other continuum theories of fermions at non-zero density, there is inevitably a strong delta function at $\omega = 0$ even at non-zero temperatures, and its resolution depends sensitively upon how terms beyond those in the leading critical theory will relax the momentum.

Going beyond our low energy critical theory, there are, of course, corrections which violate the emergent pseudospin symmetry. Some of these terms would, by themselves, induce a weak delta function at $\omega = 0$, but there are other (also formally irrelevant) umklapp terms which would broaden the delta function at non-zero temperatures. We did not examine the delicate interplay between various irrelevant terms for the zero frequency conductivity.

Here, we limited ourselves to the simpler problem of the zero temperature optical conductivity. In the leading rainbow approximation of fermions scattering off fluctuations of ϕ, the spin density wave order parameter, we found that the optical conductivity was suppressed relative to contribution expected from naive scaling arguments or previous computations[17]; these results appeared in Section III.

Next, we examined the influence of composite operators[26] on the optical conductivity: we found particularly strong effects from an operator representing $2k_F$ density fluctuations with an Ising-nematic character[13,21]. Scattering generated from this operator, which arises at higher orders in our low energy theory, leads to the umklapp process shown in Fig. 13. While analyzing this process, we have encountered an intermediate energy window for fermions in the hot spot vicinity, where Luttinger-liquid like one-dimensional divergences appear. We estimate that electrons in this window may give rise to a large optical conductivity, as summarized in Section VI B. Furthermore, we found that in the $2k_F$ channel, BCS-like divergences cut off at the Fermi surface curvature scale lead to a more singular low energy scaling of the density wave correlator than would follow from simple power counting in the hot spot scaling theory.

We also studied the nature of the electron spectral functions around the Fermi surface.

There is strong non-Fermi liquid damping of the quasiparticles at the hot spots, as was already discussed in earlier work[21]. Here we showed that non-Fermi liquid behavior is present at all locations on the Fermi surface, arising from scattering off composite operators. Such results appear in Section V.

Further progress on the difficult issues left open by our analysis will likely require new approaches. More complete solutions of simpler problems involving Fermi surface reconstruction would be useful. A holographic realization of a field theory like that in Eq. (2.1) would be valuable. Our analysis indicates that it would be best to work in a holographic setting in which the pseudospin symmetry is explicitly realized. This would ensure there are no zero frequency delta function contributions to the conductivity at non-zero temperatures. Such delta functions are a ubiquitous feature of existing holographic studies of fermion systems at non-zero density, which are often ignored without justification.

Appendix A: Current vertex in the rainbow approximation

In this appendix we present the details of the analysis of the integral equations (3.15) for the current vertex.

Let us set $q = (\omega, 0)$ and without loss of generality assume $\omega > 0$. It is convenient to change variables to $l_a = \hat{v}_a \cdot \vec{l}$. Then Eq. (3.15) for the current vertex Γ^- becomes,

$$
\begin{aligned}
\Gamma_a^-(\omega, p) = {} & (-1)^{a+1} + \frac{3\pi v^2 \gamma}{4N} \int \frac{dl_\tau dl_a dl_{\bar{a}}}{(2\pi)^3} \left(il_\tau + \frac{3iv \sin 2\varphi}{8N} \mathrm{sgn}(l_\tau)(\sqrt{\gamma|l_\tau| + l_a^2} - |l_a|) - vl_{\bar{a}} \right)^{-1} \\
& \times \left(i(l_\tau + \omega) + \frac{3iv \sin 2\varphi}{8N} \mathrm{sgn}(l_\tau + \omega)(\sqrt{\gamma|l_\tau + \omega| + l_a^2} - |l_a|) - vl_{\bar{a}} \right)^{-1} \\
& \times \left(\gamma|l_\tau - p_\tau| + \csc^2 2\varphi((l_a - p_a)^2 + (l_{\bar{a}} - p_{\bar{a}})^2 + 2(l_a - p_a)(l_{\bar{a}} - p_{\bar{a}})\cos 2\varphi) \right)^{-1} \Gamma_{\bar{a}}^-(\omega, l)
\end{aligned}
$$

$$(A1)$$

Let us perform the integral over $l_{\bar{a}}$ in Eq. (A1). In the $N \to \infty$ limit, the main contribution comes from the poles of the fermion propagators. Since these have $l_{\bar{a}} \sim O(1/N)$, we will set

$l_{\bar{a}}$ to zero in the rest of Eq. (A1),

$$
\begin{aligned}
\Gamma_a^-(\omega, p) &= (-1)^{a+1} + 2\pi\gamma\sin 2\varphi \int \frac{dl_a}{2\pi} \int_{-\omega}^0 \frac{dl_\tau}{2\pi} \frac{1}{\sqrt{\gamma|l_\tau + \omega| + l_a^2} + \sqrt{\gamma|l_\tau| + l_a^2} - 2|l_a| + \frac{\gamma\omega}{2\Lambda}} \\
&\quad \times \frac{1}{(l_a - p_a - p_{\bar{a}}\cos 2\varphi)^2 + \sin^2 2\varphi(\gamma|l_\tau - p_\tau| + p_{\bar{a}}^2)} \Gamma_{\bar{a}}^-(\omega, l_\tau, l_a, l_{\bar{a}} = 0)
\end{aligned}
\tag{A2}
$$

where the UV momentum scale Λ is given by Eq. (2.17). Hence, to determine $\Gamma_a^-(\omega, p)$ for all p it is sufficient to know its behavior for $p_a = 0$, i.e. we need to find the current vertex with external momentum on the Fermi surface. Moreover, introducing the variable $\nu = p_\tau + \omega$ we can restrict our attention to $0 < \nu < \omega$. Thus,

$$
\Gamma_a^-(\omega, \nu, p_a = 0, p_{\bar{a}} = p) = (-1)^{a+1} \Gamma^-(\omega, \nu, p)
\tag{A3}
$$

where Γ^- satisfies,

$$
\begin{aligned}
\Gamma^-(\omega, \nu, p) &= 1 - 2\pi\gamma\sin 2\varphi \int \frac{dl}{2\pi} \int_0^\omega \frac{d\nu'}{2\pi} \frac{1}{\sqrt{\gamma\nu' + l^2} + \sqrt{\gamma(\omega - \nu') + l^2} - 2|l| + \frac{\gamma\omega}{2\Lambda}} \\
&\quad \frac{1}{(l - p\cos 2\varphi)^2 + \sin^2 2\varphi(\gamma|\nu' - \nu| + p^2)} \Gamma^-(\omega, \nu', l)
\end{aligned}
\tag{A4}
$$

We note that repeating the same steps for Γ_a^+ gives,

$$
\Gamma_a^+(\omega, \nu, p_a = 0, p_{\bar{a}} = p) = \Gamma^+(\omega, \nu, p)
\tag{A5}
$$

with

$$
\begin{aligned}
\Gamma^+(\omega, \nu, p) &= 1 + 2\pi\gamma\sin 2\varphi \int \frac{dl}{2\pi} \int_0^\omega \frac{d\nu'}{2\pi} \frac{1}{\sqrt{\gamma\nu' + l^2} + \sqrt{\gamma(\omega - \nu') + l^2} - 2|l| + \frac{\gamma\omega}{2\Lambda}} \\
&\quad \frac{1}{(l - p\cos 2\varphi)^2 + \sin^2 2\varphi(\gamma|\nu' - \nu| + p^2)} \Gamma^+(\omega, \nu', l)
\end{aligned}
\tag{A6}
$$

We now proceed to study the vertex Γ^-. At low momentum and frequency, we may drop the term $\frac{\gamma\omega}{2\Lambda}$ in the kernel of Eq. (A4) (this term originates from the analytic part of the fermion propagators). Then,

$$
\begin{aligned}
\Gamma^-(\omega, \nu, p) &= 1 - 2\pi\gamma\sin 2\varphi \int \frac{dl}{2\pi} \int_0^\omega \frac{d\nu'}{2\pi} \frac{1}{\sqrt{\gamma\nu' + l^2} + \sqrt{\gamma(\omega - \nu') + l^2} - 2|l|} \\
&\quad \frac{1}{(l - p\cos 2\varphi)^2 + \sin^2 2\varphi(\gamma|\nu' - \nu| + p^2)} \Gamma^-(\omega, \nu', l)
\end{aligned}
\tag{A7}
$$

The integral in Eq. (A7) now requires regularization and should be cut-off at $l \sim \Lambda$.

Let us begin by determining $\Gamma^-(p) = \lim_{\omega,\nu\to 0}\Gamma^-(\omega,\nu,p)$. Expanding the kernel of Eq. (A7) for $\omega \to 0$ and performing the integral over ν' we obtain,

$$\Gamma^-(p) = 1 - \frac{\sin 2\varphi}{\pi}\int dl\frac{|l|}{(l-p\cos 2\varphi)^2 + \sin^2 2\varphi p^2}\Gamma^-(l) \tag{A8}$$

We expect that

$$\Gamma^-(p) \sim |p|^{r_0}, \quad |p| \ll \Lambda \tag{A9}$$

Note that the power r_0 cannot be negative. Indeed, if $r_0 < 0$ then for $p \to 0$ we may neglect the constant 1 in Eq. (A8). Assuming that $\Gamma^-(l) > 0$ for all l, this leads to a contradiction. Hence, $r_0 > 0$, which means,

$$\frac{\sin 2\varphi}{\pi}\int dl\frac{\Gamma^-(l)}{|l|} = 1 \tag{A10}$$

i.e.,

$$\Gamma^-(p) = -\frac{\sin 2\varphi}{\pi}\int dl\left(\frac{|l|}{(l-p\cos 2\varphi)^2 + \sin^2 2\varphi p^2} - \frac{1}{|l|}\right)\Gamma^-(l) \tag{A11}$$

We can now substitute the scaling form (A9) into Eq. (A11). The integral converges in the UV for $r_0 < 2$. Evaluating,

$$I(r) = \frac{\sin 2\varphi}{\pi}\int dy\left(\frac{|y|}{(y-\cos 2\varphi)^2 + \sin^2 2\varphi} - \frac{1}{|y|}\right)y^r = -\frac{\cos((\pi/2 - 2\varphi)(r+1))}{\sin \pi r/2} \tag{A12}$$

we obtain the condition,

$$I(r_0) = -1 \tag{A13}$$

which after some algebra may be rewritten as,

$$\cos(\varphi(r_0 + 1))\cos((\pi/2 - \varphi)(r_0 + 1)) = 0 \tag{A14}$$

giving

$$r_0 = -1 + \frac{\pi}{2\varphi}(2n - 1), \quad \text{or} \quad r_0 = -1 + \frac{\pi}{\pi - 2\varphi}(2n - 1), \quad n \in \mathbb{Z} \tag{A15}$$

We expect that the IR behavior of Γ^- will be dominated by the smallest positive exponent r_0; the other values of r_0 give corrections to scaling. Hence,

$$r_0 = \begin{cases} \frac{2\varphi}{\pi - 2\varphi}, & 0 < \varphi < \pi/4 \\ \frac{\pi - 2\varphi}{2\varphi}, & \pi/4 < \varphi < \pi/2 \end{cases} \tag{A16}$$

We note that Eq. (A7) is invariant under $\varphi \to \pi/2 - \varphi$, so below we only consider $0 < \varphi < \pi/4$. Fig. 7 shows the behavior of the exponent r_0 as a function of φ. Note that $0 < r_0 \le 1$. We also briefly point out that at the special value $\varphi = \pi/4$, $r_0 = 1$ and we expect a logarithmic correction $\Gamma^-(p) \sim |p|\log(\Lambda/|p|)$ to Eq. (A9).

Next, we come back to discuss the frequency dependence of Γ^-. We expect Γ^- to obey the following scaling form for $\omega \ll \Lambda_\omega$, $p \ll \Lambda$,

$$\Gamma^-(\omega, \nu, p) = C(\omega/\Lambda_\omega)\gamma^- \left(\frac{\nu}{\omega}, \frac{p}{\sqrt{\gamma\omega}}\right) \tag{A17}$$

For $p \gg \sqrt{\gamma\omega}$, we expect to recover the behavior (A9), hence,

$$\gamma^-(x, y) \sim y^{r_0}, \quad y \to \infty \tag{A18}$$

and consequently $C(\omega/\Lambda_\omega) \sim \left(\frac{\omega}{\Lambda_\omega}\right)^{r_0/2}$, i.e,

$$\Gamma^-(\omega, \nu, p) \sim \left(\frac{\omega}{\Lambda_\omega}\right)^{r_0/2} \gamma^- \left(\frac{\nu}{\omega}, \frac{p}{\sqrt{\gamma\omega}}\right) \tag{A19}$$

Hence, the vertex Γ^- aquires an anomalous dimension. Unlike, Γ^+, which is enhanced at low energy, Γ^- is suppressed.

To determine γ^- let us improve the UV convergence properties of the kernel in Eq. (A7).

$$\Gamma^-(\omega, \nu, p) = 1 - 2\pi\gamma \sin 2\varphi \int \frac{dl}{2\pi} \int_0^\omega \frac{d\nu'}{2\pi} \frac{2}{\gamma\omega\sqrt{\gamma\omega + l^2}}\Gamma^-(\omega, \nu', l)$$

$$- 2\pi\gamma \sin 2\varphi \int \frac{dl}{2\pi} \int_0^\omega \frac{d\nu'}{2\pi} \left(\frac{1}{(\sqrt{\gamma\nu' + l^2} + \sqrt{\gamma(\omega - \nu') + l^2} - 2|l|)}\right.$$

$$\times \left. \frac{1}{(l - p\cos 2\varphi)^2 + \sin^2 2\varphi(\gamma|\nu' - \nu| + p^2)} - \frac{2}{\gamma\omega\sqrt{\gamma\omega + l^2}}\right)\Gamma^-(\omega, \nu', l) \tag{A20}$$

We can now replace Γ^- in the second integral above by its scaling form (A17). The integral over l will converge as $r_0 < 2$. Note that the term $\frac{2}{\gamma\omega\sqrt{\gamma\omega + l^2}}$ that we have added and subtracted from the kernel is somewhat arbitrary; we could have used any ν and p independent term with the same UV behavior. Thus, we obtain,

$$\gamma^-(x, y) = 1 - \int_0^\infty dy' \int_0^1 dx' K(x, y; x', y')\gamma^-(x', y') \tag{A21}$$

with the kernel,

$$K(x, y; x', y') = \frac{\sin 2\varphi}{2\pi} \left(\frac{1}{\sqrt{x' + y'^2} + \sqrt{(1 - x') + y'^2} - 2y'} \right.$$

$$\times \left(\frac{1}{(y' - y\cos 2\varphi)^2 + \sin^2 2\varphi(|x' - x| + y^2)} + \frac{1}{(y' + y\cos 2\varphi)^2 + \sin^2 2\varphi(|x' - x| + y^2)} \right)$$

$$\left. - \frac{4}{\sqrt{1 + y'^2}} \right) \tag{A22}$$

and

$$C = 1 - \frac{4\pi \sin 2\varphi}{\omega} \int \frac{dl}{2\pi} \int_0^\omega \frac{d\nu'}{2\pi} \frac{1}{\sqrt{\gamma\omega + l^2}} \Gamma^-(\omega, \nu', l) \tag{A23}$$

Although we don't have an explicit analytic solution of Eq. (A21), by studying the behavior of $\gamma^-(x, y)$ for $y \gg 1$ we will obtain the 'sum rule' (3.29) that will allow us to compute the optical conductivity. We expect that in the above limit $\gamma^-(x, y)$ can be expanded as a power series in y. We, therefore, write

$$\gamma^-(x, y) = g_0(x)y^{r_0} + g_1(x)y^{r_1} + g_2(x)y^{r_2} + \ldots, \quad y \gg 1 \tag{A24}$$

We have already determined the exponent r_0 (Eq. (A16)) of the leading term in the above expansion; we now turn to the analysis of the subleading terms. Let us introduce a scale μ such that $1 \ll \mu \ll y$. We will divide the integration range in Eq. (A21) into two intervals $y' < \mu$ and $y' > \mu$. For $y' < \mu \ll y$ we expand the kernel (A22) in powers of y^{-2},

$$K = K_<^0 + K_<^2 + \cdots \tag{A25}$$

$$K_<^0(x, y; x', y') = -\frac{2\sin 2\varphi}{\pi} \frac{1}{\sqrt{1 + y'^2}} \tag{A26}$$

$$K_<^2(x, y; x', y') = \frac{\sin 2\varphi}{\pi} \frac{1}{\sqrt{x' + y'^2} + \sqrt{(1 - x') + y'^2} - 2y'} y^{-2} \tag{A27}$$

In the opposite range, $y' > \mu \gg 1$, we expand the kernel (A22) in powers of y^{-2} and $(y')^{-2}$,

$$K = K_>^0 + K_>^2 + \cdots \tag{A28}$$

$$K_>^0(x,y;x',y') = \frac{\sin 2\varphi}{\pi}\left(\frac{y'}{(y'-y\cos 2\varphi)^2 + y^2\sin^2 2\varphi} + \frac{y'}{(y'+y\cos 2\varphi)^2 + y^2\sin^2 2\varphi} - \frac{2}{y'}\right)$$

$$K_>^2(x,y;x',y') =$$
$$\frac{(x'^2 + (1-x')^2)\sin 2\varphi}{4\pi}\left(\frac{1}{(y'-y\cos 2\varphi)^2 + y^2\sin^2 2\varphi} + \frac{1}{(y'+y\cos 2\varphi)^2 + y^2\sin^2 2\varphi}\right)\frac{1}{y'}$$
$$-\frac{|x-x'|\sin^3 2\varphi}{\pi}\left(\frac{y'}{((y'-y\cos 2\varphi)^2 + y^2\sin^2 2\varphi)^2} + \frac{y'}{((y'+y\cos 2\varphi)^2 + y^2\sin^2 2\varphi)^2}\right)$$
$$+\frac{\sin 2\varphi}{\pi}\frac{1}{y'^3} \tag{A29}$$

Note that in the range $y' > \mu \gg 1$ we can use the expansion (A24). Hence, to the present order,

$$g_0(x)y^{r_0} + g_1(x)y^{r_1} + g_2(x)y^{r_2} = 1 - \int_0^\mu dy' \int_0^1 dx' K_<^0(x,y;x',y')\gamma^-(x',y')$$
$$- \int_0^\mu dy' \int_0^1 dx' K_<^2(x,y;x',y')\gamma^-(x',y')$$
$$- \int_\mu^\infty dy' \int_0^1 dx' K_>^0(x,y;x',y')(g_0(x')y'^{r_0} + g_1(x')y'^{r_1} + g_2(x')y'^{r_2})$$
$$- \int_\mu^\infty dy' \int_0^1 dx' K_>^2(x,y;x',y')g_0(x')y'^{r_0} \tag{A30}$$

Now, for $-4 < r < 2$, and $y \gg \mu$,

$$\int_\mu^\infty dy' K_>^0(x,y;x',y')y'^r = I(r)y^r + \frac{2\sin 2\varphi}{\pi}\frac{\mu^r}{r} - \frac{2\sin 2\varphi}{\pi}\frac{\mu^{r+2}}{r+2}y^{-2} + O(\mu^{r+4}y^{-4}) \tag{A31}$$

with $I(r)$ given by Eq. (A12). Likewise, for $-2 < r < 2$ and $y \gg \mu$,

$$\int_\mu^\infty dy' K_>^2(x,y;x',y')y'^r = \frac{1}{4}(x'^2 + (1-x')^2)\left(I(r-2)y^{r-2} - \frac{2\sin 2\varphi}{\pi}\frac{\mu^r}{r}y^{-2}\right)$$
$$- |x-x'|J(r)y^{r-2} - \frac{\sin 2\varphi}{\pi}\frac{\mu^{r-2}}{r-2} + O(\mu^{r+2}y^{-4}) \tag{A32}$$

with

$$J(r) = \frac{1}{2\sin \pi r/2}(r\sin 2\varphi \cos((\pi/2 - 2\varphi)r) + \cos 2\varphi \sin((\pi/2 - 2\varphi)r) \tag{A33}$$

We see that the integration over the range $0 < y' < \mu$ on the right-hand-side of Eq. (A21) gives a series of terms y^{-2m} with integer $m \geq 0$. The integration over the range $y' > \mu$ also gives such a contribution, but in addition produces a series of terms y^{r-2m} with integer

$m \geq 0$ and r - one of the exponents in the expansion (A24). Hence, we conclude that all exponents appearing in the expansion (A24) are either 'primary' exponents satisfying

$$I(r) = -1 \tag{A34}$$

or 'descendant' exponents of the form $r - 2m$ with r - a primary exponent and an integer $m \geq 1$. Note that terms of the form y^{-2m}, with integer $m \geq 0$ do not appear in the expansion (A24), as these produce terms of the form $y^{-2m} \log y$ upon convolution with $K_>^0$.

As already discussed, the solutions to Eq. (A34) take the form (A15). We have already determined the largest primary exponent r_0, Eq. (A16), hence, we only admit solutions to Eq. (A15) which are smaller than r_0 as subleading primary exponents. So the next largest primary exponent is

$$r_2 = -1 - \frac{\pi}{\pi - 2\varphi} = -2 - r_0 \tag{A35}$$

At this point the relation (A35) between r_2 and r_0 appears accidental. We will see later that this relation is necessary for a consistent definition of the anomalous dimension of the current operator. We also point out that the first descendant exponent

$$r_1 = r_0 - 2 \tag{A36}$$

satisfies $r_2 < r_1 < r_0$, which explains the labeling that we have chosen.

Coming back to Eq. (A30), by matching the coefficients of the terms y^{r_0}, $y^{r_0 - 2}$, y^{r_2}, appearing on the right and left hand sides we conclude that the coefficients g of the terms with the primary exponents are independent of x,

$$g_0(x) = g_0, \quad g_2(x) = g_2 \tag{A37}$$

while

$$g_1(x) = \left(-\frac{(1 + 2J(r_0))I(r_0 - 2)}{6(1 + I(r_0 - 2))} + \frac{1}{2}(x^2 + (1 - x)^2)J(r_0) \right) g_0 \tag{A38}$$

Moreover, by matching the coefficients of y^0 and y^{-2} we obtain the sum-rules,

$$\int_0^\mu dy \int_0^1 dx \frac{\gamma^-(x, y)}{\sqrt{x + y^2} + \sqrt{1 - x + y^2} - 2y} = a_0 \mu^{r_0 + 2} + a_1 \mu^{r_0} + a_2 \mu^{r_2 + 2} + \cdots \tag{A39}$$

$$\int_0^\mu dy \int_0^1 dx \frac{\gamma^-(x, y)}{\sqrt{1 + y^2}} = -\frac{\pi}{2 \sin 2\varphi} + b_0 \mu^{r_0} + b_1 \mu^{r_0 - 2} + b_2 \mu^{r_2} + \cdots \tag{A40}$$

57

with

$$a_0 = \frac{2}{r_0 + 2} g_0 \tag{A41}$$

$$a_1 = \frac{2J(r_0) + 1}{3r_0(1 + I(r_0 - 2))} g_0 \tag{A42}$$

$$a_2 = \frac{2}{r_2 + 2} g_2 \tag{A43}$$

$$b_0 = \frac{1}{r_0} g_0 \tag{A44}$$

$$b_1 = \frac{1}{r_0 - 2} \left(\frac{2J(r_0) - I(r_0 - 2)}{6(1 + I(r_0 - 2))} - \frac{1}{2} \right) g_0 \tag{A45}$$

$$b_2 = \frac{1}{r_2} g_2 \tag{A46}$$

The sum rule (A39) is crucial for the computation of the conductivity in Eq. (3.28). We note that we expect $g_0 \geq 0$ so that both $a_0 \geq 0$ and $a_1 \geq 0$.

Appendix B: Constant contribution to the conductivity in the rainbow approximation

In this appendix, we compute the constant contribution to the conductivity, Eq. (3.33). We work in the rainbow approximation and take the limit $N \to \infty$. To determine C_1, we must solve the integral equation, Eq. (3.18), for the current vertex Γ^- in the regime $p \sim \Lambda$. It will be sufficient to compute Γ^- to linear order in frequency. We expect,

$$\Gamma^-(\omega, \nu, p) = f_0(p/\Lambda) + \frac{\gamma\omega}{\Lambda^2} f_1(\nu/\omega, p/\Lambda) \tag{B1}$$

At zeroth order in frequency we obtain from (3.18) an equation for the static vertex f_0,

$$f_0(y) = 1 - \int_0^\infty dy' R(y, y') f_0(y') \tag{B2}$$

with the kernel,

$$R(y, y') = \frac{\sin 2\varphi}{\pi} \frac{y'}{1 + y'} \left(\frac{1}{(y' - y\cos 2\varphi)^2 + y^2 \sin^2 2\varphi} + \frac{1}{(y' + y\cos 2\varphi)^2 + y^2 \sin^2 2\varphi} \right) \tag{B3}$$

Next, expanding Eq. (3.18) to first order in frequency, after some algebra one finds,

$$f_1(x, y) = A(y) + (x^2 + (1 - x)^2 - \frac{2}{3}) B(y) \tag{B4}$$

Here, $B(y)$ is expressed in terms of the static vertex f_0,

$$B(y) = \frac{\sin^3 2\varphi}{2\pi} \int_0^\infty dy' \frac{y'}{1+y'} \left(\frac{1}{((y'-y\cos 2\varphi)^2 + y^2 \sin^2 2\varphi)^2} \right.$$
$$\left. + \frac{1}{((y'+y\cos 2\varphi)^2 + y^2 \sin^2 2\varphi)^2} \right) f_0(y') \tag{B5}$$

while $A(y)$ satisfies,

$$A(y) = C(y) - \int_0^\infty dy' R(y,y') A(y') \tag{B6}$$

and $C(y)$ is expressed in terms of f_0,

$$C(y) = \frac{2}{3} B(y) - \frac{1}{6} \int_0^\infty dy' \frac{1}{y'^2(1+y')} R(y,y') f_0(y') \tag{B7}$$

From Eqs. (A19), (A24), we expect the functions f_0, f_1 to have the following asymptotic behavior in the limit $y \to 0$,

$$f_0(y) \to g_0 y^{r_0}$$
$$f_1(x,y) \to g_1(x) y^{r_0-2} \tag{B8}$$

with $g_1(x)$ given by Eq. (A38).

We have numerically solved Eqs. (B2), (B6) for the functions $f_0(y)$, $A(y)$. Sample plots are shown in Fig. 23. The numerical solution is in good agreement with the asymptotic forms (B8) in the limit $p \ll \Lambda$.

Next, we proceed to the optical conductivity itself. Expanding the integrand in Eq. (3.27) to linear order in ω and using Eqs. (B1), (B2),

$$\Pi_{xx}^{\ell=1}(\omega) = \frac{1}{2} N^2 \omega C_1(\varphi) \tag{B9}$$

with

$$C_1(\varphi) = \frac{16N^2}{3\pi^2 \sin^2 \varphi} \left(\int_0^\infty dy \frac{y}{1+y} A(y) + \frac{1}{6} \int_0^\infty dy \frac{1}{y(1+y)^2} f_0(y) \right) \tag{B10}$$

Note that we have dropped a constant contribution in Eq. (B9) which renormalizes the Drude weight. Finally, performing a sum over hot spot index ℓ and going to real frequency, we obtain from (B9)

$$\mathrm{Re}\,\sigma_{ij}(\Omega) = N^2 C_1(\varphi) \delta_{ij} \tag{B11}$$

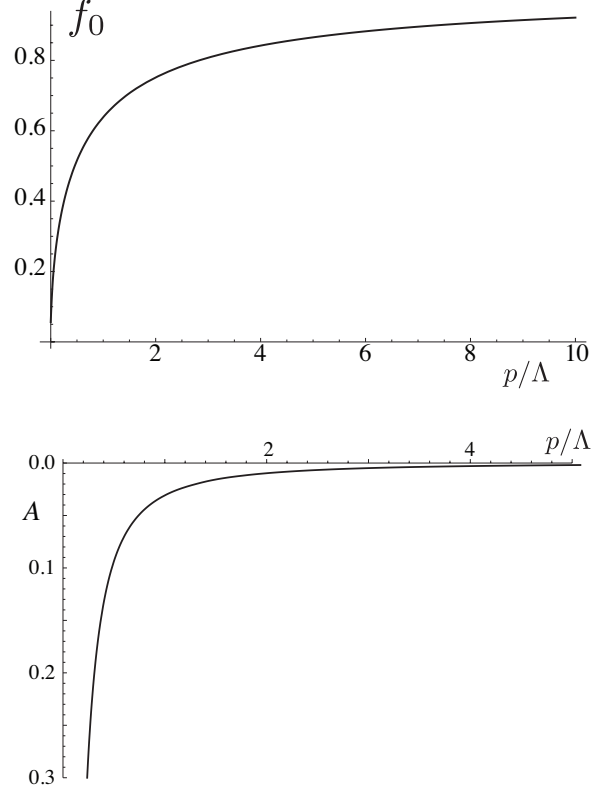We have performed the integral (B10) using the numerical solutions for f_0 and A. The result is shown in Fig. 8.

FIG. 23: Numerical solution for the current vertex in the rainbow approximation. Top: f_0 - current vertex in the static limit. Bottom: function A, Eq. (B4), which enters the first frequency dependent correction to the current vertex.

Appendix C: The correlation function $\langle \phi^2(x)\phi^2(0)\rangle$ in Hertz-Moriya-Millis theory

For completeness we calculate the two point function of the operator $O(x) = \vec{\phi}^2(x)$ in Hertz-Moriya-Millis theory. We start with the non-local action,

$$S = \frac{1}{2} \int \frac{d^2\vec{q}\,d\omega}{(2\pi)^3} (|\omega| + \frac{\vec{q}^2}{\gamma} + r)|\vec{\phi}(\vec{q},\omega)|^2 + \frac{u\gamma}{4} \int d^2\vec{x}\,d\tau(\vec{\phi}^2)^2 \tag{C1}$$

With our choice of normalizations, the coupling u is dimensionless, while γ has dimensions $\vec{q}^2/\omega$. Note that the normalization of ϕ differs here by a factor of $\sqrt{\gamma}$ compared to Eq. (2.14). We tune the coefficient r to the critical value. At the critical point, the theory requires the following renormalizations,

$$\gamma = Z_\gamma \gamma_r, \quad u = \frac{Z_u}{Z_\gamma}u_r, \quad [\vec{\phi}^2]_r = Z_2[\vec{\phi}^2] \tag{C2}$$

The field strength of $\vec{\phi}$ requires no renormalization. The renormalization constants Z_γ, Z_u and Z_2 are functions of Λ/μ and u_r only, with Λ - the UV cut-off and μ - the renormalization

60

scale. We define the β-functions and anomalous dimensions,

$$\beta(u_r) = \mu \frac{\delta u_r}{\delta \mu}|_{u,\gamma}, \quad b_\gamma(u_r) = -\mu \frac{\delta \log Z_\gamma}{\delta \mu}|_{u,\gamma}, \quad \eta_2 = \mu \frac{\delta \log Z_2}{\delta \mu}|_{u,\gamma} \tag{C3}$$

To leading order in u_r[55],

$$Z_u = 1 + \frac{11}{2\pi^2} u_r \log \Lambda/\mu, \quad Z_\gamma = 1 + \frac{5(12 - \pi^2)}{16\pi^4} u_r^2 \log \Lambda/\mu, \quad Z_2 = 1 + \frac{5}{2\pi^2} u_r \log \Lambda/\mu \tag{C4}$$

$$\beta(u_r) = c_u u_r^2, \quad b_\gamma = c_\gamma u_r^2, \quad \eta_2 = c_2 u_r \tag{C5}$$

$$c_u = \frac{11}{2\pi^2}, \quad c_\gamma = \frac{5(12 - \pi^2)}{16\pi^4}, \quad c_2 = -\frac{5}{2\pi^2} \tag{C6}$$

The two-point function C of the $\vec{\phi}^2$ operators requires an additional additive renormalization,

$$C(\vec{q}, \omega, u, \gamma, \Lambda) = Z_2^{-2} C_r(\vec{q}, \omega, u_r, \gamma_r, \Lambda) + B(\Lambda/\mu, u, \gamma) \tag{C7}$$

The renormalized two-point function C_r then satisfies the RG equation,

$$\left(\mu \frac{\delta}{\delta \mu} + \beta(u_r) \frac{\delta}{\delta u_r} + b_\gamma(u_r) \gamma_r \frac{\delta}{\delta \gamma_r} - 2\eta_2(u_r) \right) C_r(\omega, \vec{q}, u_r, \gamma_r, \mu) = \gamma_r X(u_r) \tag{C8}$$

where

$$\gamma_r X(u_r) = -Z_2^2 \mu \frac{\delta}{\delta \mu} B|_{u,\gamma} \tag{C9}$$

Solving the RG equation, we obtain,

$$C_r(\vec{q}, \omega, u_r, \gamma_r, \mu) = Z_2^{-2}(\lambda) C_r(\vec{q}, \omega, u_r(\lambda), Z_\gamma(\lambda) \gamma_r, \lambda\mu) - \gamma_r \int_1^\lambda \frac{d\lambda'}{\lambda'} Z_2^{-2}(\lambda') Z_\gamma(\lambda') X(u_r(\lambda')) \tag{C10}$$

$$\lambda \frac{du_r}{d\lambda} = \beta(u_r(\lambda)) \tag{C11}$$

$$\lambda \frac{d \log Z_2(\lambda)}{d\lambda} = \eta_2(u_r(\lambda)) \tag{C12}$$

$$\lambda \frac{d \log Z_\gamma(\lambda)}{d\lambda} = b_\gamma(u_r(\lambda)) \tag{C13}$$

By dimensional analysis,

$$C_r(\vec{q}, \omega, u_r, \gamma_r, \mu) = \gamma_r L(\frac{|\vec{q}|}{\mu}, \frac{\gamma_r |\omega|}{\mu^2}, u_r) \tag{C14}$$

So,

$$L(\tilde{q}, \tilde{\omega}, u_r) = Z_2^{-2}(\tilde{q})Z_\gamma(\tilde{q})L(1, Z_\gamma(\tilde{q})\frac{\tilde{\omega}}{\tilde{q}^2}, u_r(\tilde{q})) - \int_1^{\tilde{q}} \frac{d\lambda'}{\lambda'} Z_2^{-2}(\lambda')Z_\gamma(u_r(\lambda'))X(u_r(\lambda')) \quad \text{(C15)}$$

Now solving the flow equations using the leading order anomalous dimensions, we obtain,

$$u_r(\lambda) = \frac{u_r}{1 - c_u u_r \log \lambda} \tag{C16}$$

$$Z_2 = (1 - c_u u_r \log \lambda)^{-c_2/c_u} \tag{C17}$$

$$Z_\gamma = 1 + \frac{c_\gamma}{c_u} \frac{u_r^2 \log \lambda}{1 - u_r \log \lambda} \tag{C18}$$

Thus, for $\tilde{q} \to 0$ and to leading order in u_r,

$$L(\tilde{q}, \tilde{\omega}, u_r) \approx (c_u u_r |\log \tilde{q}|)^{2c_2/c_u} \left(L(1, \frac{\tilde{\omega}}{\tilde{q}^2}, 0) + \frac{X(0)}{c_u u_r} \right) + \frac{X(0)}{(2c_2/c_u + 1)c_u u_r} (c_u u_r |\log \tilde{q}|^{2c_2/c_u+1} - 1) \tag{C19}$$

We see that the second term Eq. (C19), which originates from the additive renormalization, dominates over the first term. In fact corrections to this second term coming from considering higher order contributions in u_r to η_2 and X are of the same order as the first term in Eq. (C19). Nevertheless, the first term contains the dependence on $\tilde{\omega}$ and this is the reason we have kept it.

To complete the calculation, we need to compute C in the non-interacting theory (Fig. 16),

$$C_0(\vec{q}, \omega) = 6 \int \frac{d^2\vec{l}dl_\tau}{(2\pi)^3} D(l)D(l+q) \tag{C20}$$

Using the Feynman trick,

$$
\begin{aligned}
C_0(\vec{q}, \omega) &= 6\gamma^2 \int_0^1 du \int \frac{d^2\vec{l}dl_\tau}{(2\pi)^3} \frac{1}{((\vec{l} - u\vec{q})^2 + \gamma(u|l_\tau| + (1-u)|l_\tau - \omega|) + u(1-u)\vec{q}^2)^2} \\
&= \frac{3\gamma^2}{(2\pi)^2} \int_0^1 du \int_{-\infty}^\infty dl_\tau \frac{1}{\gamma(u|l_\tau - \omega| + (1-u)|l_\tau|) + u(1-u)\vec{q}^2} \\
&= \frac{3\gamma}{2\pi^2} \int_0^1 du \left[\log \frac{\Lambda^2}{\gamma u|\omega| + u(1-u)\vec{q}^2} + \frac{1}{2(1-2u)} \log \frac{\gamma(1-u)|\omega| + u(1-u)\vec{q}^2}{\gamma u|\omega| + u(1-u)\vec{q}^2} \right]
\end{aligned}
\tag{C21}
$$

where we have cut-off the l_τ integral at $l_\tau = \gamma\Lambda^2$. Performing the u integral,

$$
\begin{aligned}
C_0(\vec{q},\omega) \;=\; \frac{3\gamma}{2\pi^2}\Bigg(&\log\frac{\Lambda^2}{\gamma|\omega|+\vec{q}^2} + \frac{\gamma|\omega|}{\vec{q}^2}\log\left(\frac{\gamma|\omega|}{\gamma|\omega|+\vec{q}^2}\right) \\
&-\frac{1}{2}\mathrm{Li}_2\left(\frac{\vec{q}^2}{2\gamma|\omega|+\vec{q}^2}\right) + \frac{1}{2}\mathrm{Li}_2\left(\frac{-\vec{q}^2}{2\gamma|\omega|+\vec{q}^2}\right)\Bigg)
\end{aligned}
\tag{C22}
$$

with Li_2 - the polylogarithm function. After renormalization,

$$
\begin{aligned}
C_{0r}(\vec{q},\omega) \;=\; \frac{3\gamma}{2\pi^2}\Bigg(&\log\frac{\mu^2}{\gamma|\omega|+\vec{q}^2} + \frac{\gamma|\omega|}{\vec{q}^2}\log\left(\frac{\gamma|\omega|}{\gamma|\omega|+\vec{q}^2}\right) \\
&-\frac{1}{2}\mathrm{Li}_2\left(\frac{\vec{q}^2}{2\gamma|\omega|+\vec{q}^2}\right) + \frac{1}{2}\mathrm{Li}_2\left(\frac{-\vec{q}^2}{2\gamma|\omega|+\vec{q}^2}\right)\Bigg)
\end{aligned}
\tag{C23}
$$

Giving the final result,

$$
\begin{aligned}
L(\tilde{q},\tilde{\omega},u_r) \;=\; \frac{33}{\pi^2}(c_u u_r)^{-10/11}&|\log\tilde{q}|^{1/11}\Bigg[1 + \frac{1}{22|\log\tilde{q}|}\left(\frac{|\tilde{\omega}|}{\tilde{q}^2}\log\frac{|\tilde{\omega}|}{\tilde{q}^2} - \left(1+\frac{|\tilde{\omega}|}{\tilde{q}^2}\right)\log\left(1+\frac{|\tilde{\omega}|}{\tilde{q}^2}\right)\right. \\
&\left.-\frac{1}{2}\mathrm{Li}_2\left(\frac{\tilde{q}^2}{2|\tilde{\omega}|+\tilde{q}^2}\right) + \frac{1}{2}\mathrm{Li}_2\left(\frac{-\tilde{q}^2}{2|\tilde{\omega}|+\tilde{q}^2}\right) + \frac{2}{c_u u_r}\right)\Bigg] - \frac{33}{\pi^2 c_u u_r}
\end{aligned}
\tag{C24}
$$

Appendix D: Self energy in the $2k_F$ channel (one-dimensional contribution)

In this section we compute the self energy in Fig. 17b). We take all the external and internal fermions to be lukewarm and use the fermion propagator 5.17. The self energy is given by,

$$
\begin{aligned}
\Sigma(p) \;=\; -42N\lambda^8 \int &\frac{d^3q}{(2\pi)^3}\frac{d^3l_1}{(2\pi)^3}\frac{d^3l_2}{(2\pi)^3}\frac{d^3l_3}{(2\pi)^3} D(p-l_1)D(l_1-l_2)D(l_2-l_3)D(l_3-p) \\
&\times G^{-1}(p-q)G^2(l_1)G^{-2}(l_1-q)G^1(l_2)G^{-1}(l_2-q)G^2(l_3)G^{-2}(l_3-q)
\end{aligned}
\tag{D1}
$$

We take the boson propagators to be static and ignore their dependence on fermion momenta perpendicular to the Fermi surface,

$$
\begin{aligned}
D(p-l_1) &\approx N^{-1}\sin^2 2\varphi\left((\hat{v}_2\cdot\vec{p})^2 + (\hat{v}_1\cdot\vec{l_1})^2 - 2\cos 2\varphi(\hat{v}_2\cdot\vec{p})(\hat{v}_1\cdot\vec{l_1})\right)^{-1} \\
D(l_1-l_2) &\approx N^{-1}\sin^2 2\varphi\left((\hat{v}_1\cdot\vec{l_1})^2 + (\hat{v}_2\cdot\vec{l_2})^2 - 2\cos 2\varphi(\hat{v}_1\cdot\vec{l_1})(\hat{v}_2\cdot\vec{l_2})\right)^{-1} \\
D(l_2-l_3) &\approx N^{-1}\sin^2 2\varphi\left((\hat{v}_2\cdot\vec{l_2})^2 + (\hat{v}_1\cdot\vec{l_3})^2 - 2\cos 2\varphi(\hat{v}_2\cdot\vec{l_2})(\hat{v}_1\cdot\vec{l_3})\right)^{-1} \\
D(p-l_3) &\approx N^{-1}\sin^2 2\varphi\left((\hat{v}_2\cdot\vec{p})^2 + (\hat{v}_1\cdot\vec{l_3})^2 - 2\cos 2\varphi(\hat{v}_2\cdot\vec{p})(\hat{v}_1\cdot\vec{l_3})\right)^{-1}
\end{aligned}
\tag{D2}
$$

Then integrals over $l_{i\tau}$ and components of $\vec{l}_i$ perpendicular to the Fermi surface in Eq. (D1) can be performed,

$$\int \frac{d^3l}{(2\pi)^3} G^a(l)G^{-a}(l-q) \approx -\frac{|\vec{v}|^2}{16\pi^2 v_x v_y} \int d(\hat{v}_{\bar{a}} \cdot \vec{l}) \frac{Z^2(\hat{v}_{\bar{a}} \cdot \vec{l})}{v^*(\hat{v}_{\bar{a}} \cdot \vec{l})} \log\left(\frac{\Lambda_{FL}^2(\hat{v}_{\bar{a}} \cdot \vec{l})}{q_\tau^2 + v^*(\hat{v}_{\bar{a}} \cdot \vec{l})^2(\hat{v}_a \cdot \vec{q})^2}\right) \tag{D3}$$

Here, $\Lambda_{FL}(l) \sim l^2/\gamma$ is the upper energy cut-off of the region where the rainbow propagator (2.16) has the quasiparticle form (5.17). Hence,

$$\begin{aligned}
\Sigma(\omega, \vec{p}) &= 42\lambda^8 N(8\pi^2 \sin 2\varphi v \Lambda)^{-3} \int \frac{d^3q\, d(\hat{v}_1 \cdot \vec{l}_1)d(\hat{v}_2 \cdot \vec{l}_2)d(\hat{v}_1 \cdot \vec{l}_3)}{(2\pi)^3} \\
&\quad D(p-l_1)D(l_1-l_2)D(l_2-l_3)D(l_3-p)|\hat{v}_1 \cdot \vec{l}_1||\hat{v}_2 \cdot \vec{l}_2||\hat{v}_1 \cdot \vec{l}_3| \\
&\quad \frac{Z(\hat{v}_2 \cdot \vec{p})}{i(\omega - q_\tau) + v^*(\hat{v}_2 \cdot \vec{p})\hat{v}_1 \cdot (\vec{p} - \vec{q})} \log\left(\frac{\Lambda_{FL}^2(\hat{v}_2 \cdot \vec{l}_2)}{q_\tau^2 + v^*(\hat{v}_2 \cdot \vec{l}_2)^2(\hat{v}_1 \cdot \vec{q})^2}\right) \\
&\quad \log\left(\frac{\Lambda_{FL}^2(\hat{v}_1 \cdot \vec{l}_1)}{q_\tau^2 + v^*(\hat{v}_1 \cdot \vec{l}_1)^2(\hat{v}_2 \cdot \vec{q})^2}\right) \log\left(\frac{\Lambda_{FL}^2(\hat{v}_1 \cdot \vec{l}_3)}{q_\tau^2 + v^*(\hat{v}_1 \cdot \vec{l}_3)^2(\hat{v}_2 \cdot \vec{q})^2}\right) \tag{D4}
\end{aligned}$$

The crucial observation is that the integrals over $\hat{v}_1 \cdot \vec{q}$ and $\hat{v}_2 \cdot \vec{q}$ in Eq. (D4) factorize. This is due to our treatment of the Fermi surfaces as flat. The leading contribution to the integral over $\hat{v}_2 \cdot \vec{q}$ comes from 2 and -2 fermions away from the Fermi surface and we may approximate,

$$\begin{aligned}
&\int d(\hat{v}_2 \cdot \vec{q}) \log\left(\frac{\Lambda_{FL}^2(\hat{v}_1 \cdot \vec{l}_1)}{q_\tau^2 + v^*(\hat{v}_1 \cdot \vec{l}_1)^2(\hat{v}_2 \cdot \vec{q})^2}\right) \log\left(\frac{\Lambda_{FL}^2(\hat{v}_1 \cdot \vec{l}_3)}{q_\tau^2 + v^*(\hat{v}_1 \cdot \vec{l}_3)^2(\hat{v}_2 \cdot \vec{q})^2}\right) \\
&\sim \min\left(\frac{\Lambda_{FL}(\hat{v}_1 \cdot \vec{l}_1)}{v^*(\hat{v}_1 \cdot \vec{l}_1)}, \frac{\Lambda_{FL}(\hat{v}_1 \cdot \vec{l}_3)}{v^*(\hat{v}_1 \cdot \vec{l}_3)}\right) \sim \frac{1}{N} \min(|\hat{v}_1 \cdot \vec{l}_1|, |\hat{v}_1 \cdot \vec{l}_3|), \tag{D5}
\end{aligned}$$

because the domain of integration is limited to the regime where the arguments of the logarithms are large. On the other hand, integration over $\hat{v}_1 \cdot \vec{q}$ and q_τ to logarithmic accuracy gives,

$$\begin{aligned}
&\int dq_\tau d(\hat{v}_1 \cdot \vec{q}) \frac{1}{i(\omega - q_\tau) - v^*(\hat{v}_2 \cdot \vec{p})\hat{v}_1 \cdot \vec{q}} \log\left(\frac{\Lambda_{FL}^2(\hat{v}_2 \cdot \vec{l}_2)}{q_\tau^2 + v^*(\hat{v}_2 \cdot \vec{l}_2)^2(\hat{v}_1 \cdot \vec{q})^2}\right) \\
&= -\frac{2\pi i\omega}{v^*(\hat{v}_2 \cdot \vec{l}_2) + v^*(\hat{v}_2 \cdot \vec{p})} \log\left(\frac{\Lambda_{FL}(\hat{v}_2 \cdot \vec{p})}{|\omega|}\right) \tag{D6}
\end{aligned}$$

Here for simplicity we have set the external momentum $\vec{p}$ to lie on the Fermi surface. We have also set the argument of Λ_{FL} inside the logarithm on the second line of Eq. (D6) to $\hat{v}_2 \cdot \vec{p}$. We will see shortly that all integrals over momenta along the Fermi surface are saturated at $l_\parallel \sim p_\parallel$, so to logarithmic accuracy the precise value of the argument is not important.

64

Combining Eqs. (D4),(D5), (D6),

$$\Sigma(\omega,\vec{p}) \sim -iN^3\gamma v\omega \int d(\hat{v}_1\cdot\vec{l}_1)d(\hat{v}_2\cdot\vec{l}_2)d(\hat{v}_1\cdot\vec{l}_3)D(p-l_1)D(l_1-l_2)D(l_2-l_3)D(l_3-p)$$

$$\times\ |\hat{v}_1\cdot\vec{l}_1||\hat{v}_2\cdot\vec{l}_2||\hat{v}_1\cdot\vec{l}_3|\min(|\hat{v}_1\cdot\vec{l}_1|,|\hat{v}_1\cdot\vec{l}_3|)\frac{|\hat{v}_2\cdot\vec{p}|}{|\hat{v}_2\cdot\vec{l}_2|+|\hat{v}_2\cdot\vec{p}|}\log\left(\frac{\Lambda_{FL}(\hat{v}_2\cdot\vec{p})}{|\omega|}\right)$$

$$(D7)$$

In the integrand, we can now count 7 powers of $\vec{l}$ in the numerator, and 4 powers in the denominator from 2 of the D functions; so the integral in Eq. (D7) is not singular for $\vec{l}\to 0$, which confirms our claim that the self energy in the $2k_F$ channel is not dominated by scattering off hot modes. The integral is saturated at $\hat{v}_1\cdot\vec{l}_1,\hat{v}_2\cdot\vec{l}_2,\hat{v}_1\cdot\vec{l}_3 \sim \hat{v}_2\cdot\vec{p}\sim p_\parallel$, and all the 4 D functions yield a contribution of $1/p_\parallel^2$ each; this leads to our estimate in Eq. (5.18).

Appendix E: The $2k_F$ correlation function (curvature saturated contribution)

We can first compute the 'tree level' lowest order contribution in figure 19. This is simply

$$C^{(0)}(m) = \int \frac{d^3t}{(2\pi)^3}G_2(m+t)G_{-2}(t)\,. \tag{E1}$$

As indicated in the main text, we work with the lukewarm propagators following from (2.18) and (2.12), together with an additional curvature term

$$G_{\pm 2}^{-1}(q) = \mp vq_\perp + \frac{3\gamma v}{16N}\frac{iq_\tau}{|q_\parallel|} - \kappa q_\parallel^2\,. \tag{E2}$$

Recall that the lukewarm regime is

$$t_\parallel \gg \sqrt{\gamma t_\tau}, Nt_\perp\,. \tag{E3}$$

We can restrict ourselves to this regime because we are looking to pick out a BCS-like logarithmic divergence that is cut off in the particle channel by curvature effects. Here we are defining parallel and perpendicular with respect to the $\ell = 1, a = 2$ hot spot Fermi surface.

Using (E2) it is possible to explicitly perform the integrals in (E1). One computes first the $t_\perp$ integral, followed by the t_τ integral. The t_τ integral is logarithmically UV sensitive, and the divergence is cut of by $t_\parallel^2/\gamma$. We noted in the main text that the self energy scaling determined by hot spot scaling is weak, $\Sigma \sim \omega^{5/2}$. Here we are interested in determining the effect of BCS-like contributions that will violate this scaling. We will be interested in

the upper limit of the remaining $t_\parallel$ integral and thus we are free to focus on

$$t_\parallel \gg \sqrt{\gamma m_\tau}, |\vec{m}| \,. \tag{E4}$$

In this regime we have

$$\frac{1}{(2\pi)^3} \int dt_\tau dt_\perp G_2(m+t) G_{-2}(t) = \frac{c_1}{2} X(t_\parallel, m_\tau, m_{\perp,2}) \,, \tag{E5}$$

where we introduced, also for future use,

$$X(t_\parallel, m_\tau, m_{\perp,2}) \equiv t_\parallel \log \frac{\gamma^2 m_\tau^2 + c_2^2 t_\parallel^2 \left(m_{\perp,2} + 2\kappa/vt_\parallel^2\right)^2}{4t_\parallel^4} \,. \tag{E6}$$

The notation $m_{\perp,2}$ refers to the component of m perpendicular to the ± 2 Fermi surfaces. The constants

$$c_1 = \frac{4N}{3\pi^2 \gamma v^2} \,, \qquad c_2 = \frac{16N}{3} \,. \tag{E7}$$

The remaining integral of (E6) over $t_\parallel$ can also be performed exactly. The most IR singular terms are found to be (we mean terms that are not saturating the UV cutoff scale and also that are not the IR terms with $C \sim m_\tau$ arising in the absence of Fermi surface curvature)

$$C^{(0)}(m) = -\frac{c_1}{2} \frac{(\gamma|m_\tau|)^{2/3}}{(c_2\kappa/v)^{2/3}} \sum_i \frac{3 + 2r^2 x_i + 4rx_i^2}{r^2 + 8rx_i + 12x_i^2} \log \frac{-x_i \kappa^2 (\gamma|m_\tau|)^{2/3}}{(c_2\kappa/v)^{2/3}} \,. \tag{E8}$$

Here r is the ratio

$$r = \frac{m_{\perp,2}}{(\gamma|m_\tau|)^{2/3}} \frac{c_2^{2/3}}{(\kappa/v)^{1/3}} \,, \tag{E9}$$

and the x_i are the three roots of the polynomial

$$4x^3 + 4rx^2 + r^2 x + 1 = 0 \,. \tag{E10}$$

In the main text, in section V B, we discuss the physical interpretation of this formula.

Considering the right hand graph in figure 19, we must incorporate the vertex corrections

$$\delta\Gamma(m,s) = \int \frac{d^3t}{(2\pi)^3} G_2(m+t) G_{-2}(t) D(t-s) \,, \tag{E11}$$

so that the diagram can be written

$$C(m) = \int \frac{d^3s}{(2\pi)^3} \delta\Gamma(m,s)^2 G_1(m+s) G_{-1}(s) \,. \tag{E12}$$

66

We used the fact that the boson propagator D is symmetric.

Nine integrals are required in principle to evaluate (E12). We are interested in isolating as strong a contribution as possible in order to lead to the strongest self energy and hence dissipative conductivity. We shall take cues from the computation of the density wave vertex correction in Ref. 21. The complication in the case at hand is that we have an additional external energy-momentum s as well as the spatial components $\vec{m}$.

The first lesson and simplification from Ref. 21 is that enhancement physics is dominated by lukewarm fermions. A second lesson that appeared already in the tree level computation we have just performed is that it is important to account for the effects of Fermi surface curvature. While the curvature is an irrelevant operator of the scaling theory, it will cut off the BCS-like logarithmic divergence and therefore sets an energy scale that will be saturated in the processes we are interested in.

Thus both the t and s integrals can be performed using the propagators (E2) in the lukewarm regime and additionally satisfying (E4). The momentum s of the integrals in (E12) however lives on the $+1$ rather than the $+2$ Fermi surface and we will therefore use $s_\parallel$ and $s_\perp$ to denote the components of s with respect to that $+1$ Fermi surface. In the lukewarm regime, the boson propagator (2.14) appearing in the vertex correction (E11) can be written

$$D(t-s) = D(t_\parallel, s_\parallel) = \frac{1}{t_\parallel^2 + s_\parallel^2 - 2t_\parallel s_\parallel \cos 2\varphi} \ . \tag{E13}$$

We can then perform the $s_\perp$ and s_τ integrals in (E12) in the same way as we did the $t_\perp$ and t_τ integrals above. We obtain

$$C(m) = c_1^3 \int_0^{\Lambda_\parallel} ds_\parallel X(s_\parallel, m_\tau, m_{\perp,1}) \left(\int_0^{\Lambda_\parallel} dt_\parallel D(t_\parallel, s_\parallel) X(t_\parallel, m_\tau, m_{\perp,2}) \right)^2 \ . \tag{E14}$$

The lower limits of the integrals are determined by (E4) but will not be important for isolating the most singular contribution. In particular, the lower limit of integration can be taken to zero for our purposes.

The dependence on the angle 2φ between the Fermi surfaces does not in fact appear in the final leading logarithmic result for these integrals. In order to keep the size of intermediate equations down, we will quote intermediate results with $\cos 2\varphi = 0$. The $t_\parallel$ integral can be evaluated explicitly in terms of logarithms and dilogarithms

$$\int_0^{\Lambda_\parallel} dt_\parallel D(t_\parallel, s_\parallel) X(t_\parallel, m_\tau, m_{\perp,2}) = \frac{1}{2} \log^2 \tilde{s}_\parallel^2 + \frac{1}{4} \log^2 \tilde{\Lambda}_\parallel^2 - \frac{1}{3} \log \gamma m_\tau (c_2 \kappa/v)^2 \log \frac{\tilde{s}_\parallel^2}{\tilde{\Lambda}_\parallel^2}$$

$$- \frac{1}{4} \sum_i \left(\log \frac{1}{\tilde{s}_\parallel^2 + x_i} \log \frac{(-x_i)^2}{\tilde{s}_\parallel^2 + x_i} + 2\mathrm{Li}_2 \frac{x_i}{\tilde{s}_\parallel^2 + x_i} \right) \ . \tag{E15}$$

Here we set

$$\tilde{s}_\parallel^2 = \frac{(c_2\kappa/v)^{2/3}}{(\gamma m_\tau)^{2/3}} s_\parallel^2 \,, \qquad \tilde{\Lambda}_\parallel^2 = \frac{(c_2\kappa/v)^{2/3}}{(\gamma m_\tau)^{2/3}} \Lambda_\parallel^2 \,, \tag{E16}$$

and the x_i are again the roots of the cubic polynomial (E10) above. We have only quoted the result to leading order in logarithms, i.e. order logarithm squared. There are additional constant terms and terms with single logarithms.

The remaining $s_\parallel$ integral in (E14) appears more challenging to compute exactly. It is however possible to extract the leading logarithmic behavior. Recall we are interested in the most singular behaviour as $m_\tau \to 0$. We are keeping the ratio (E9) fixed in taking this limit. In our result (E15) m_τ appears both explicitly and through the rescaled $s_\parallel$ and $\Lambda_\parallel$. We will rescale the $s_\parallel$ variable of integration and integrate instead over $\tilde{s}_\parallel$. After squaring our result (E15) there will be a term $\sim \frac{1}{81}\log^4 m_\tau$, from the m_τ in the $\tilde{\Lambda}_\parallel$ terms. This will contribute at leading order in logarithms of m_τ and therefore we need to integrate this term over the whole range of integration. The remaining terms can only compete with this term near the upper limit of the integral, where $\tilde{s}_\parallel \to \tilde{\Lambda}_\parallel$. Here extra powers of m_τ can appear. Both of these two contributions can be evaluated, in the latter case by expanding the integrand at large $\tilde{s}_\parallel$. The final result for the most singular contribution is

$$C(m) = c_1^3 \frac{(\gamma m_\tau)^{2/3}}{(c_2\kappa/v)^{2/3}} \log^2 \tilde{\Lambda}_\parallel^2 \tag{E17}$$

$$\times \left(\frac{1}{32}\log^2\left[(\gamma m_\tau)^{4/3}(c_2\kappa/v)^{8/3}\tilde{\Lambda}_\parallel^2\right] \sum_i \left(\log(-x_i)x_i - \log(-y_i)\frac{3 + 2\bar{r}^2 y_i + 4\bar{r}y_i^2}{\bar{r}^2 + 8\bar{r}y_i + 12y_i^2} \right) \right.$$

$$\left. + \frac{r+\bar{r}}{2160}\log\tilde{\Lambda}_\parallel^2 \left(40\log^2\gamma m_\tau(c_2\kappa/v)^2 + 75\log\gamma m_\tau(c_2\kappa/v)^2\log\tilde{\Lambda}_\parallel^2 + 36\log^2\tilde{\Lambda}_\parallel^2 \right) \right).$$

Here we introduced the analogous ratio to (E9) for the $+1$ Fermi surface

$$\bar{r} = \frac{m_{\perp,1}}{(\gamma|m_\tau|)^{2/3}} \frac{c_2^{2/3}}{(\kappa/v)^{1/3}} \,, \tag{E18}$$

and the y_i are now the three roots of the polynomial

$$4y^3 + 4\bar{r}y^2 + \bar{r}^2 y + 1 = 0 \,. \tag{E19}$$

Equation (E17) is the result to leading order in logarithms, i.e. keeping $\log^5$ terms, and with an overall scaling $m_\tau^{2/3}$. In one of these limits a power of logarithms is lost, but the result is still accurately captured by (E17) in this case. In the above expression we can note that

$$\sum_i \frac{3 + 2\bar{r}^2 y_i + 4\bar{r}y_i^2}{\bar{r}^2 + 8\bar{r}y_i + 12y_i^2} = \bar{r} \,, \qquad \sum_i x_i = -r \,. \tag{E20}$$

In the main text, equation (5.28), we dropped the last line of (E17) as it is linear in $r, \bar{r}$, which replace the overall frequency dependence $m_\tau^{2/3}$ with momenta $m_{\perp,2}$ and $m_{\perp,1}$.

1 M. Norman, "Fermi-surface reconstruction and the origin of high-temperature superconductivity," Physics **3**, 86 (2010).

2 M. Vojta, "Picking the cuprates' Fermi pockets," Physics **4**, 12 (2011).

3 S. Sachdev and B. Keimer, "Quantum Criticality," Physics Today **64**, no. 2, 29 (2011) [arXiv:1102.4628 [cond-mat.str-el]].

4 D. Haug et al., "Neutron scattering study of the magnetic phase diagram of underdoped $YBa_2Cu_3O_{6+x}$" New J. Phys. **12**, 105006 (2010) [arXiv:1008.4298 [cond-mat.str-el]].

5 Chenglin Zhang et al., "Spin excitations as a probe of itinerant electron and local moments in hole-doped $Ba_{0.67}K_{0.33}Fe_2As_2$ superconductor," arXiv:1012.4065 [cond-mat.super-con].

6 F. Laliberte et al. et al., "Fermi-surface reconstruction by stripe order in cuprate superconductors," arXiv:1102.0984 [cond-mat.supr-con].

7 M. V. Kartsovnik et al., "Fermi Surface of the Electron-doped Cuprate Superconductor $Nd_{2-x}Ce_xCuO_4$ Probed by High-Field Magnetotransport," New J. Phys. **13**, 015001 (2011) [arXiv:1104.1165 [cond-mat.supr-con]].

8 D. J. Scalapino, "A common thread," Physica C **470**, S1 (2010) [arXiv:1002.2413 [cond-mat.supr-con]].

9 Ar. Abanov, A. V. Chubukov, and A. M. Finkel'stein, "Coherent vs incoherent pairing in 2D systems near magnetic instability," Europhys. Lett. **54**, 488 (2001) [arXiv:cond-mat/9911445].

10 I. I. Mazin, D. J. Singh, M. D. Johannes, and M.-H. Du, "Unconventional sign-reversing superconductivity in $LaFeAsO_{1-x}F_x$" Phys. Rev. Lett. **101**, 057003 (2008) [arXiv:0803.2740 [cond-mat.supr-con]].

11 K. Kuroki, S. Onari, R. Arita, H. Usui, Y. Tanaka, H. Kontani, and H. Aoki, "Unconventional Pairing Originating from the Disconnected Fermi Surfaces of Superconducting $LaFeAsO_{1-x}F_x$," Phys. Rev. Lett. **101**, 087004 (2008) [arXiv:0803.3325 [cond-mat.supr-con]].

12 Kangjun Seo, B. A. Bernevig, and Jiangping Hu, "Pairing Symmetry in a Two-Orbital Exchange Coupling Model of Oxypnictides," Phys. Rev. Lett. **101**, 206404 (2008) [arXiv:0805.2958 [cond-mat.supr-con]].

13 M. A. Metlitski and S. Sachdev, "Instabilities near the onset of spin density wave order in metals," New J. Phys. **12**, 105007 (2010) [arXiv:1007.1968 [cond-mat.str-el]].

14 J. A. Hertz, "Quantum critical phenomena," Phys. Rev. B **14**, 1165 (1976);

15 T. Moriya, *Spin Fluctuations in Itinerant Electron Magnetism*, Springer-Verlag, Berlin (1985);

16 A. J. Millis, "Effect of a nonzero temperature on quantum critical points in itinerant fermion systems," Phys. Rev. B, **48**, 7183 (1993).

17 Ar. Abanov, A. V. Chubukov, J. Schmalian, "Quantum-critical theory of the spin-fermion model

and its application to cuprates: normal state analysis," Adv. Phys. **52**, 119 (2003) [arXiv:cond-mat/0107421].

[18] H. v. Löhneysen, A. Rosch, M. Vojta, and P. Wölfle, "Fermi-liquid instabilities at magnetic quantum phase transitions," Rev. Mod. Phys. **79**, 1015 (2007) [arXiv:cond-mat/0606317].

[19] S.-S. Lee, "Low-energy effective theory of Fermi surface coupled with U(1) gauge field in 2+1 dimensions," Phys. Rev. **B 80**, 165102 (2009) [arXiv:0905.4532 [cond-mat.str-el]].

[20] M. A. Metlitski and S. Sachdev, "Quantum phase transitions of metals in two spatial dimensions: I. Ising nematic order," Phys. Rev. B **82**, 075127 (2010) [arXiv:1001.1153 [cond-mat.str-el]].

[21] M. A. Metlitski and S. Sachdev, "Quantum phase transitions of metals in two spatial dimensions: II. Spin density wave order," Phys. Rev. B **82**, 075128 (2010) [arXiv:1005.1288 [cond-mat.str-el]].

[22] Ar. Abanov and A. V. Chubukov, "Anomalous Scaling at the Quantum Critical Point in Itinerant Antiferromagnets," Phys. Rev. Lett. **93**, 255702 (2004) [arXiv:cond-mat/0409601].

[23] R. Hlubina and T. M. Rice, "Resistivity as a function of temperature for models with hot spots on the Fermi surface," Phys. Rev. **B 51**, 9253 (1995) [arXiv:cond-mat/9501086].

[24] A. Rosch, "Interplay of disorder and spin fluctuations in the resistivity near a quantum critical point," Phys. Rev. Lett. **82**, 4280 (1999) [arXiv:cond-mat/9810260].

[25] Jie Lin and A. J. Millis, "Optical and Hall conductivities of a thermally disordered two-dimensional spin-density wave: two-particle response in the pseudogap regime of electron-doped high-T_c superconductors," arXiv:1011.3265 [cond-mat.str-el].

[26] A. Pelissetto, S. Sachdev and E. Vicari, " Nodal quasiparticles and the onset of spin density wave order in the cuprates," Phys. Rev. Lett. **101**, 027005 (2008) [arXiv:0802.0199 [cond-mat.str-el]].

[27] T. Moriya, Y. Takahashi, and K. Ueda, "Antiferromagnetic Spin Fluctuations and Superconductivity in Two-Dimensional Metals—A Possible Model for High T_c Oxides," J. Phys. Soc. Japan **59**, 2905 (1990).

[28] H. Maebashi and H. Fukuyama, "Electrical Conductivity of Interacting Fermions. I. General Formulation," J. Phys. Soc. Japan **66**, 3577 (1997).

[29] H. Maebashi and H. Fukuyama, "Electrical Conductivity of Interacting Fermions. II. Effects of Normal Scattering Processes in the Presence of Umklapp Scattering Processes," J. Phys. Soc. Japan **67**, 242 (1998).

[30] Y. Yanase, "Theory of Electric Transport in the Pseudogap State of High-T_c Cuprates," J. Phys. Soc. Japan **71**, 278 (2002) [arXiv:cond-mat/0111021].

[31] H. Kontani, "Anomalous transport phenomena in Fermi liquids with strong magnetic fluctuations," Rep. Prog. Phys. **71**, 026501 (2008) [arXiv:0711.1693 [cond-mat.str-el]].

[32] S. A. Hartnoll, P. K. Kovtun, M. Müller, and S. Sachdev, "Theory of the Nernst effect near quantum phase transitions in condensed matter, and in dyonic black holes," Phys. Rev. B **76**, 144502 (2007) [arXiv:0706.3215 [cond-mat.str-el]].

[33] D. van der Marel, H. J. A. Molegraaf, J. Zaanen, Z. Nussinov, F. Carbone, A. Damascelli,

H. Eisaki, M. Greven, P. H. Kes, and M. Li, "Powerlaw optical conductivity with a constant phase angle in high T_c superconductors," Nature **425**, 271 (2003) [arXiv:cond-mat/0309172].

34 D. van der Marel, F. Carbone, A.B. Kuzmenko, and E. Giannini, "Scaling properties of the optical conductivity of Bi-based cuprates," Annals of Physics, **321**, 1716 (2006) [arXiv:cond-mat/0604037].

35 D. Bergeron, B. Kyung, V. Hankevych, and A.-M. S. Tremblay, "Optical and DC conductivity of the two-dimensional Hubbard model in the pseudogap regime and across the antiferromagnetic quantum critical point, including vertex corrections," arXiv:1101.4037 [cond-mat.str-el].

36 C. Nayak and F. Wilczek, "Non-Fermi liquid fixed point in (2+1)-dimensions," Nucl. Phys. **B 417**, 359 (1994) [arXiv:cond-mat/9312086].

37 C. Nayak and F. Wilczek, "Renormalization group approach to low temperature prop- erties of a non-Fermi liquid metal," Nucl. Phys. **B 430**, 534 (1994) [arXiv:cond-mat/9408016] .

38 D. F. Mross, J. McGreevy, H. Liu and T. Senthil, "A controlled expansion for certain non-Fermi liquid metals," Phys. Rev. B **82**, 045121 (2010) [arXiv:1003.0894 [cond-mat.str-el]].

39 T. Faulkner, N. Iqbal, H. Liu, J. McGreevy, D. Vegh, "Holographic non-Fermi liquid fixed points," [arXiv:1101.0597 [hep-th]].

40 K. Goldstein, S. Kachru, S. Prakash, S. P. Trivedi, "Holography of Charged Dilaton Black Holes," JHEP **1008**, 078 (2010). [arXiv:0911.3586 [hep-th]].

41 S. A. Hartnoll and A. Tavanfar, "Electron stars for holographic metallic criticality," Phys. Rev. D **83**, 046003 (2011) [arXiv:1008.2828 [hep-th]].

42 A. Rosch and N. Andrei, "Conductivity of a clean one-dimensional wire," Phys. Rev. Lett. **85** 1092 (2000) [arXiv:cond-mat/0002306].

43 D. L. Maslov, V. I. Yudson, and A. V. Chubukov "Resistivity of a non-Galilean–invariant Fermi Liquid near Pomeranchuk Quantum Criticality," arXiv:1012.0069 [cond-mat.str-el].

44 Y. B. Kim, A. Furusaki, X-G. Wen and P. A. Lee, "Gauge-invariant response functions of fermions coupled to a gauge field," Phys. Rev. **B 50**, 17917 (1994) [arXiv:cond-mat/9405083].

45 J. Polchinski, "Low-energy dynamics of the spinon-gauge system," Nucl. Phys. **B 422**, 617 (1994) [arXiv:cond-mat/9303037].

46 B. L. Altshuler, L. B. Ioffe and A. J. Millis, "Low-energy properties of fermions with singular interactions," Phys. Rev. **B 50**, 14048 (1994) [arXiv:cond-mat/9406024].

47 M. Ossadnik, C. Honerkamp, T. M. Rice, and M. Sigrist, "Breakdown of Landau Theory in Overdoped Cuprates near the Onset of Superconductivity," Phys. Rev. Lett. **101**, 256405 (2008) [arXiv:0805.3489 [cond-mat.str-el]].

48 D. V. Livanov, G. Savona and A. A. Varlamov, "Strong compensation of the quantum fluctuation corrections in a clean superconductor," Phys. Rev. **B 62**, 8675 (2000) [arXiv:cond-mat/0001433]

49 A. Larkin and A. Varlamov, *Theory of Fluctuations in Superconductors*, Oxford University Press, Oxford (2005).

50 C. M. Varma, P. B. Littlewood, S. Schmitt-Rink, E. Abrahams and A. E. Ruckenstein, "Phe-

nomenology of the normal state of Cu-O high-temperature superconductors," Phys. Rev. Lett. **63**, 1996 (1989).

[51] T. Faulkner, N. Iqbal, H. Liu, J. McGreevy and D. Vegh, "Strange Metal Transport Realized by Gauge/Gravity Duality," Science **329**, 1043 (2010).

[52] S. Sachdev, "Holographic metals and the fractionalized Fermi liquid," Phys. Rev. Lett. **105**, 151602 (2010). [arXiv:1006.3794 [hep-th]].

[53] I. R. Klebanov, E. Witten, "AdS / CFT correspondence and symmetry breaking," Nucl. Phys. **B556**, 89-114 (1999). [hep-th/9905104].

[54] S. Kachru, X. Liu, M. Mulligan, "Gravity Duals of Lifshitz-like Fixed Points," Phys. Rev. **D78**, 106005 (2008). [arXiv:0808.1725 [hep-th]].

[55] S. Pankov, S. Florens, A. Georges, G. Kotliar, and S. Sachdev, "Non-Fermi liquid behavior from two-dimensional antiferromagnetic fluctuations: a renormalization-group and large-N analysis," Phys. Rev. B **69**, 054426 (2004) [arXiv:cond-mat/0304415].